CONSTRUCTION MATERIALS AND ENGINEERING

Pyrite and Pyrrhotite

Managing the Risks in Construction Materials and New Applications

Michael L.J. Maher

Editor

NOVA

Chapter 5

Concrete Deterioration from the Oxidation of Pyrrhotite: A State-of-the-Art Review

Dipayan Jana*
Construction Materials Consultants, Inc. and Applied Petrographic Services, Inc.,
Greensburg, PA, USA

Abstract

After pyrite, pyrrhotite is a common accessory mineral found in many igneous, sedimentary, and metamorphic rocks used as aggregates in concrete. In moist exposures, oxidation of pyrrhotite has caused distress ranging from minor cracking to extensive cracking, crumbling, and disintegration of concrete structures. In almost all cases, distress is found to be due to two-stage expansions associated with oxidation of pyrrhotite forming goethite, limonite, ferrihydrite, and other oxidation products in aggregates, followed by internal sulfate attacks in paste by reactions between the sulfates released from pyrrhotite oxidation with the aluminous phases in paste. Originally discovered in a concrete tunnel in Oslo, Norway, subsequently many other parts of the world showed similar distress, e.g., in numerous foundations in the Trois-Rivières area in Québec, Canada, in concrete dams in Central and Catalan Pyrenees in Spain, in a dam in Switzerland, in many houses in Penge, South Africa, 'mundic' problems of pyrite and pyrrhotite oxidation in many buildings in Cornwell and Devon, England, and in numerous residential concrete foundations across eastern Connecticut and Massachusetts in the USA. This chapter provides an overview of worldwide occurrences of pyrrhotite oxidation-related distress with special emphasis on the cases examined by the author, perhaps at the epicenter of such distress in the eastern US where an estimated 35,000 residential concrete foundations in Connecticut and 10,000 more in Massachusetts are in danger of potential collapse from slow and progressive cracking due to pyrrhotite oxidation in the crushed gneiss coarse aggregates. Time of occurrence varied from less than a year in Norway to 5 years in Canada to 20 years in the US. A detailed review is provided on various field and laboratory testing procedures, e.g., petrography, SEM-EDS, XRD, XRF, μXRF, chemical analyses for sulfur content, thermomagnetic susceptibility, oxygen consumption rate, mortar bar expansion, etc., for detection of pyrrhotite and measuring oxidation-related distress. Also discussed are mechanisms of distress, problems in detection of pyrrhotite in aggregates, factors influencing pyrrhotite oxidation, and various microstructural evidence of distress. Finally,

* Corresponding Author's Email: info@cmc-concrete.com.

In: Pyrite and Pyrrhotite
Editor: Michael L. J. Maher
ISBN: 979-8-88697-329-7

some multi-step laboratory testing protocols are discussed for effective screening of aggregates to prevent such occurrences in future construction.

Keywords: pyrrhotite, oxidation, ettringite, petrography, sulfate, iron sulfide, aggregate

Introduction

Pyrrhotite (pronounce *pir-uh-tahyt*, Greek *pyrrhos* i.e., flame-colored or redness, Deer et al., 2013) is a non-stoichiometric mineral of general formula $Fe_{1-x}S$, where 'x' varies from 0 (FeS, troilite) to 0.125 (Fe_7S_8). Pyrrhotite is commonly associated with pyrite as minor accessory minerals in many igneous, sedimentary, and metamorphic rocks, as major phases in sulfide ore bodies, and as a secondary mineral in high temperature hydrothermal and replacement veins often after pyrite, pentlandite [$(Fe,Ni)_9S_8$], marcasite (orthorhombic FeS_2), magnetite (Fe_3O_4) and chalcopyrite ($CuFeS_2$). Pyrite (FeS_2) is a cubic-structured isotropic mineral of fixed chemical composition (46.67% Fe and 53.33% S by weight) with a yellowish-white color in reflected light and a characteristic metallic luster. By contrast, pyrrhotite has variable chemical compositions and crystal structures, e.g., monoclinic (stable below 254°C) or hexagonal (stable above 254°C), anisotropic having various natural forms, e.g., Type 4C, 5C, 6C, 11C having respective ideal compositions of Fe_7S_8, Fe_9S_{10}, $Fe_{11}S_{12}$, and $Fe_{10}S_{11}$, and ideal weight percentage ranges of 60.38 to 61.49% Fe and 38.51 to 38.95% S (Duchesne et al., 2021). Pyrrhotite has a pink-cream or skin color in reflected light that has a metallic luster and bronze-brown, yellow, or reddish color. Pyrrhotite is distinguished by its bronze rather than brass color of pyrite, its lower hardness, decomposition in HCl with the evolution of H_2S, lower S/Fe atomic ratios (1 to 1.25 for unoxidized forms, as opposed to ~2 in pyrite), and its weakly magnetic nature (Type 4C is ferromagnetic, Types 5C, 6C, and 11C are antiferromagnetic, troilite is nonmagnetic, magnetism decreases with increasing iron content). Upon heating, pyrrhotite shows a characteristic drop of magnetic susceptibility across its Curie temperature (e.g., 310 to 325°C), which can be used to determine the pyrrhotite content. Powder X-ray diffraction studies also diagnose and quantify pyrrhotite and other sulfide species in aggregates. Pyrrhotite has four times higher solubility and a much faster rate of oxidation in the presence of oxygen and moisture than pyrite, which makes pyrrhotite a more serious candidate for oxidation-related distress than pyrite when present in aggregates used for concrete and exposed to moisture during service. Pyrrhotite oxidation has been studied extensively in acid mine drainage leading to acidification, ferric iron precipitation and an increased mobility of trace metals in drainage waters (Belzie et al., 1997, 2004; Johnson et al., 2000). Variable compositions, crystal structures (e.g., Fe vacancies in crystal lattice), specific surface areas, electrochemical reactions with other sulfide species in the pore solutions of concrete, and other factors not only influence but complicate oxidation of pyrrhotite in aggregates.

This chapter provides a review of various cases of concrete deterioration from expansion and unsoundness of pyrrhotite-bearing aggregates from oxidation of pyrrhotite in various igneous, sedimentary, and metamorphic aggregates, along with subsequent expansions in paste from sulfate ions released from pyrrhotite oxidation.

Reactions Involving Oxidation of Iron Sulfide Minerals and Subsequent Sulfate Attacks in Concrete

Figure 1 shows *oxidation reactions of pyrite and pyrrhotite*, and subsequent *internal sulfate attacks in concrete* by reactions between the dissolved sulfate ions of sulfuric acid generated from pyrite/pyrrhotite oxidation, and cement hydration products. Goethite [FeO(OH)], limonite [FeO(OH). nH_2O], and ferrihydrite [Fe_2O_3. $0.5(H_2O)$] are the common oxidation products, of which ferrihydrite is the most stable in the highly alkaline conditions of concrete. Products of internal sulfate attacks are (a) gypsum [$CaSO_4.2H_2O$] after reaction with portlandite $Ca(OH)_2$, (b) ettringite [$Ca_6Al_2(SO_4)_3(OH)_{12}.26H_2O$] from reactions with monosulfate and/or calcium aluminate hydrate, and (c) thaumasite [$CaSiO_3.CaCO_3.CaSO_4.15H_2O$] after reaction with carbonate aggregates, limestone fillers, or with the thin iron carbonate (siderite) coats on iron sulfides (e.g., as found in the Trois-Rivières area, Québec, Canada, Rodrigues et al., 2012).

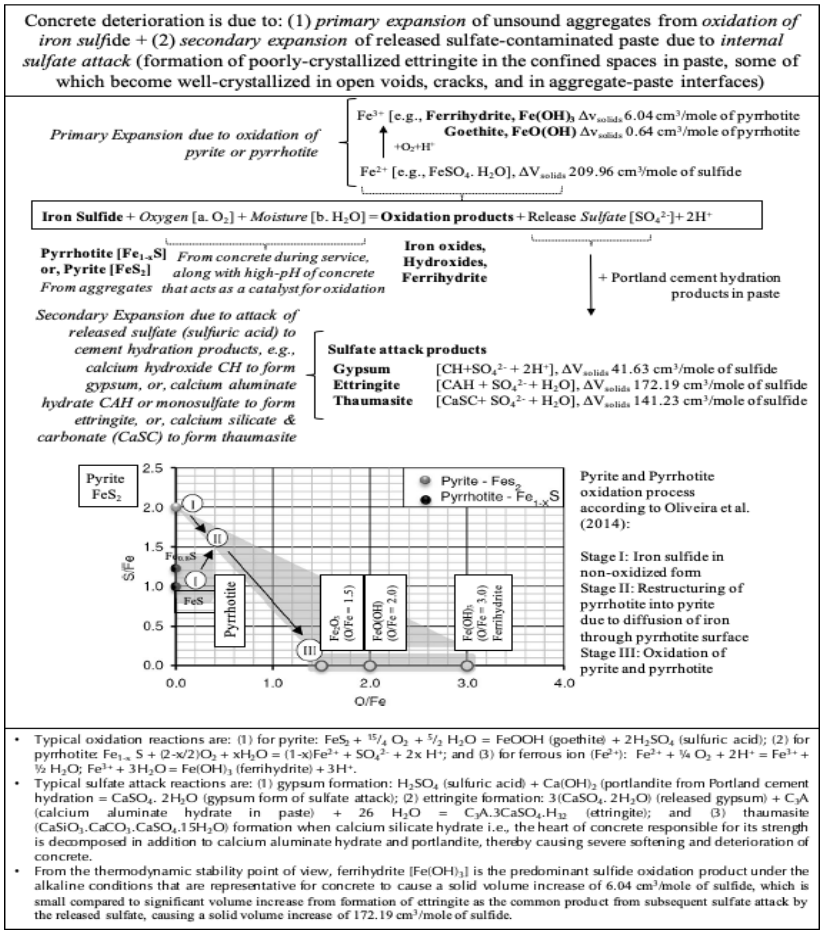

Figure 1. Mechanisms of concrete deterioration by oxidation of iron sulfide minerals in aggregates (from Jana, 2020). Increases in solid volumes ($\triangle V_{Solid}$) *from oxidation of pyrrhotite* to ferrihydrite through an intermediate state of Fe^{2+} ($FeSO_4.H_2O$) are compared with further solid volume increase from *internal sulfate attacks* of paste by reactions between the sulfates released from oxidation, and Portland cement hydration products, e.g., calcium hydroxide, monosulfate, and C-S-H, resulting in formation of calcium sulfate hydrate (gypsum), sulfoaluminate hydrate (ettringite), and silicate-carbonate hydrate (thaumasite) to cause severe deteriorations in concrete.

The latter eventually decomposes calcium silicate hydrate, the main strength-producing phase of concrete to cause noticeable softening and decomposition of paste as opposed to significant expansions occurring from gypsum or ettringite formation. Figure 2 shows the relative solid volume increases from oxidation reactions and sulfate attacks that are responsible for expansions and associated distress in concrete.

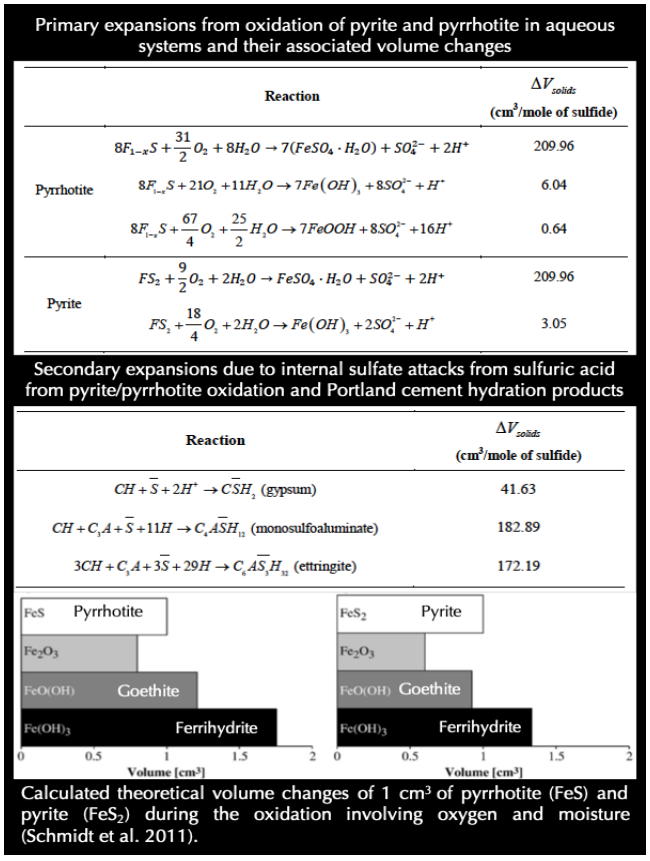

Figure 2. Typical reactions of oxidation of pyrrhotite, internal sulfate attack in paste from sulfates released from oxidation and associated solid volume increase ($\triangle V_{Solid}$) from oxidation and internal sulfate attack (Wille and Zhong, 2016). Oxidation of pyrite, or pyrrhotite in the presence of hydroxyl ion in excess of the normal concentration in water causes the formation of ferrous sulfate [$FeSO_4.H_2O$], ferric oxyhydroxides [goethite, FeO(OH) and ferrihydrite ($Fe(OH)_3$), and sulfuric acid as a preliminary step, followed by hydrolysis of the ferrous sulfate to ferric hydroxide and sulfuric acid. Interaction of the sulfuric acid with the calcium hydroxide component of Portland cement hydration in concrete produces calcium sulfate, which, in turn, produces calcium sulfoaluminate by reaction with calcium aluminate phases in the cement paste. The resulting substantial increase in solid volume in the system causes expansion with accompanying cracking and popout formation on the concrete. Some authors proposed the solid volume increase from pyrrhotite oxidation being the main mechanism of expansion and associated distress in concrete, whereas others proposed sulfate attack from the sulfate byproduct of oxidation, or both mechanisms combined being the main contributing factor to concrete distress. Steger (1982) has shown that the oxidation of pyrrhotite presents two pathways to form goethite and ferric sulfate. According to Grattan-Bellew and Eden (1975) and Shayan (1988), the sulfuric acid generated through this process reacts with the solids of the cement paste, particularly with the portlandite ($Ca(OH)_2$), to form gypsum ($CaSO_4 \cdot 2H_2O$) and ettringite ($Ca_6Al_2(SO_4)_3(OH)_{12} \cdot 26H_2O$). According to Casanova et al. (1996), the reaction of pyrrhotite oxidation forming iron sulfate may generate volume change in the order of 187 cm^3 per mole of sulfide (maximum expansion at reaction completion), and volume changes of 42, 183, and 172 cm^3 per mole of sulfide for gypsum, calcium aluminate monosulfate and ettringite, respectively.

Worldwide Occurrences of Pyrrhotite Oxidation-Related Deterioration of Concrete

Table 1 (adapted from Jana, 2020) provides a concise treatise on world-wide occurrences of pyrrhotite oxidation-related distress in concrete, which are described below.

Oslo, Norway

One of the earliest records of pyrrhotite oxidation-related distress came from Oslo, Norway, which was reported by Moum and Rosenqvist (1959). Oxidation of *monoclinic pyrrhotite in alum shale sedimentary rock* used as concrete aggregate caused swelling of shale and subsequent complete deterioration of a concrete water tunnel in a very short time. The ground water associated with the alum shales carried the ferrous sulfate from pyrrhotite oxidation, which produced severe sulfate attack and the precipitation of ferric iron compounds in concrete structures made with ordinary Portland cement. Cements of low tricalcium aluminate content, although they resisted the sulfate attack, were subjected to attack by acid solutions produced when the ferrous sulfate was oxidized. Microscopical examinations of unweathered shale showed pyrrhotite mostly occurred in minute grains often in direct contact with pyrite. Since both minerals are electrical conductors, their mixed association in moist shale or pore solutions of concrete has caused more severe and faster oxidation of both minerals than that of a single sulfide mineral.

In the case study in Norway, (Moum and Rosenqvist, 1959), it became apparent that concrete damage was more severe in cases where pyrrhotite was present in association with pyrite in shale than the ones where shale aggregate was free from pyrrhotite. Concrete prisms prepared with alum shale aggregate and placed deep in tunnel water below the low water level, showed more severe distress in 3 to 4 years with extensive cracking and formation of secondary ettringite (except the prisms made with sulfate-resistant cement) than the prisms left between the low and high-water levels, which remained sound.

More recent extensive work by the Nordic Workshop (2018) in connection with the railway tunnel project at the Follo line, near Oslo found many pyrrhotite-bearing aggregates in Norway (Jensen, 2018), however, without any known reported pyrrhotite oxidation-related distress in concrete. Jensen (2018), and Haugen and Lindgard (2018) provided results, which showed that several commercial quarries in Norway that produce crushed rock aggregates for concrete are exhibiting results above the critical limits of sulfur (0.1%), indicating the presence of pyrrhotite. It was discussed that one reason for not observing any deleterious damage so far in Norway could be the fact that up to now mainly natural sand and gravel have been used as concrete aggregates where sulfide minerals have already been oxidized. With an increased use of freshly crushed concrete aggregates, both as coarse aggregates and as manufactured sand, the situation could be different.

Table 1. Case studies of concrete deterioration around the world due to oxidation of pyrrhotite and pyrite in unsound aggregates (expanded from the original Table by Jana, 2020)

• Locality • (Reference)	• Pyrrhotite-containing rocks • Associated sulfide minerals • Products of oxidation and subsequent sulfate attacks	• Average sulfur content in aggregate, and, • Pyrrhotite content in aggregate	• Structure affected • Type of Damage • Time taken to manifest the damage	Proposed Mechanisms of Distress
Pyrrhotite-related deteriorations				
• *Oslo, Norway* • (Moum and Rosenqvist, 1959)	• Sedimentary rocks (alum shales, some with slight metamorphism) • Pyrite was associated with pyrrhotite • Gypsum formation from sulfates released from pyrrhotite oxidation	• 6% (highly variable), all shales that weathered 'explosively' due to oxidation contained more than 0.2% sulfur as monoclinic pyrrhotite. • Pyrrhotite content is related to rate of alteration of pyrite and rate of weathering of shale	• Foundation • Upheaval of foundation, cracking, crumbling, yellowish deposit of jarosite [$KFe_3(OH)_6(SO_4)_2$] and brown-iron oxide (Fe_2O_3. nH_2O) on weathered shales. • Within 9 months	Swelling of shale due to oxidation of pyrrhotite and internal sulfate attack from released sulfate; reactivity of alum shale and resultant damage increased with increasing pyrrhotite content with no occurrence of damage when alum shale was free of pyrrhotite; acidic and sulfate-rich water percolated through alum shale has caused acid attack and internal sulfate attack in concrete.
• *Trois-Rivières area, Québec, Canada* • (Tagnit-Hamou, et.al., 2005; Rodrigues, et.al., 2012, 2013, 2014, 2015, 2016; Duchesne et al., 2018, 2021; Duchesne and Fournier, 2011, 2013)	• Quarried intrusive igneous rock, anorthositic gabbro (norite) with different degrees of metamorphism. • Pyrrhotite and pyrite with minor amounts of chalcopyrite and pentlandite, only pyrrhotite was oxidized while pyrite and other sulfides were not. • Pyrrhotite oxidation products are iron oxide/hydroxide/oxyhydroxide • Products of internal sulfate attack are gypsum and ettringite • A thin coating of iron carbonate (siderite) on sulfides provided carbonates to promote thaumasite form of attack	• As low as 0.30% to 2.92% total sulfur by mass of aggregate in pyrrhotite-bearing coarse aggregates that have caused damage, all damaged concrete exceeded the European limit of 0.1% sulfur in aggregate when pyrrhotite is present by 3 times to as high as 30 times. • Less than 5 to 10% total sulfide minerals by volume, average 75% of sulfide minerals were pyrrhotite and lesser pyrite and chalcopyrite from a study of 223 house basements containing varying amounts of iron sulfide in gabbro coarse aggregate	• Residential foundations and commercial buildings. • Map cracking (cracks up to 40 mm in width) and yellowish or brownish staining), pop outs of oxidized pyrrhotite with white rim of secondary reaction products, and open cracks more pronounced at the corners of the foundation blocks • More than 1000 to as high as estimated 4000 residential and commercial buildings were affected within 3 to 5 years after construction	Oxidation of sulfide minerals (mainly pyrrhotite) in anorthositic gabbro coarse aggregate in concrete has: (a) formed various "rust" minerals (e.g., ferric oxyhydroxides such as goethite FeO(OH), limonite, and ferrihydrite) and (b) released sulfuric acid/sulfates, which then reacted with cement hydration products resulting in further expansive formation of gypsum, ettringite, and thaumasite in concrete. Oxidation of pyrrhotite, followed by internal sulfate attack of cement paste are the main mechanisms of concrete deterioration.

• Locality • (Reference)	• Pyrrhotite-containing rocks • Associated sulfide minerals • Products of oxidation and subsequent sulfate attacks	• Average sulfur content in aggregate, and, • Pyrrhotite content in aggregate	• Structure affected • Type of Damage • Time taken to manifest the damage	Proposed Mechanisms of Distress
• *Northeastern Connecticut, USA* • (Wille and Zhong, 2016; Zhong and Wille, 2018; Jana 2018 a, b, 2019 a, b, c, 2020, 2022)	• Foliated schist and gneissic metamorphic rocks, granofels, foliated quartz diorite in a hydrothermally altered vein from a particular quarry in Willington, Connecticut (Becker's quarry). • Pyrrhotite as the predominant iron sulfide mineral present in metamorphic rocks containing quartz, plagioclase feldspar, biotite and muscovite micas, and pyrope garnet, pyrite was not detected • Oxidation products of pyrrhotite are ferrihydrite • Sulfate attack in paste produced ettringite	• Average 2.54% sulfur in pyrrhotite-bearing quarry aggregate • Pyrrhotite was not detected in XRD analysis of quarry aggregate by Wille and Zhong (2016) due to possible presence below the detection limit of XRD	• Residential foundations. • Map cracking, crumbling, deformation of walls, reddish-brown discoloration, whitish formation of secondary ettringite and thaumasite in the vicinity of surface cracks. Cores from foundation walls of houses showed noticeably lower compressive strengths (some no strength due to complete crumbling) compared to the cores from slabs, indicating possible effect of more oxidation in walls than slabs and hence more damage in walls than slabs • 10 to 20 years after construction, estimated 34,000 homes are at risk	Primary expansion due to oxidation of pyrrhotite, followed by secondary expansion due to internal sulfate attack by the released sulfates.
• *Catalan Pyrenees, Spain* • (Araujo et al., 2008)	• Schist containing quartz, muscovite mica, chlorite and non-expansive illitic clay. • Pyrite and Pyrrhotite	• 2% sulfur (as SO_3 from XRF) in schist. • Predominantly pyrrhotite (S/Fe ratio 0.62 as opposed to 1.15 of pyrite) but XRD also detected some pyrite	• Tórán Dam • Map cracking and non-recoverable movements, more dramatic expansion in the downstream face of the dam responsible for upstream displacement of the crest	Oxidation of pyrite and pyrrhotite forming surface stains of greyish brown iron hydroxides (goethite) and lighter-green potassium iron sulfates (jarosite), gypsum efflorescence from sulfate attack; and causing expansions, e.g., 6.04 cm^3/mol from primary expansion from oxidation of iron sulfides followed by 172.19 cm^3/mol from internal sulfate attack by reaction between released sulfates and cement phases

Table 1. (Continued)

• Locality • (Reference)	• Pyrrhotite-containing rocks • Associated sulfide minerals • Products of oxidation and subsequent sulfate attacks	• Average sulfur content in aggregate, and, • Pyrrhotite content in aggregate	• Structure affected • Type of Damage • Time taken to manifest the damage	Proposed Mechanisms of Distress
• *Central Pyrenees, Spain* • (Ayora et al., 1998; Oliveira et al., 2014)	• Schist containing bands of pyrrhotite that created planes of weakness and present cracks that serve as preferential paths for entrance of oxygen thus aggregates containing pyrrhotite bands with cracks showed much more pronounced oxidation than the aggregates without cracks. • Pyrite	• Median sulfur (SO_3) content of 1.42% for rocks from a quarry that are known to cause severe damage when used as aggregate in dams	• Graus and Tavascan Dams • Map cracking, damage in downstream face and galleries of the Graus Dam due to severe cracking and movement	Alteration from acidic solution produced by weathering and oxidation of pyrrhotite in aggregates followed by expansion due to internal sulfate attack and formation of ettringite and gypsum. Characteristic ratios of 2.44 for the Fe/O ratio and of 2.63 for the S/O ratio in pyrrhotite marked critical limits that produced the activation and acceleration of pyrrhotite oxidation leading to an increase of expansive reactions and risk of structural damage.
Pyrite-related deteriorations				
• *Ottawa, Québec City, Matane, and Montreal, Canada* • (Quigley and Vogan, 1970; Berard, 1970; Bérubé et al., 1986; Penner et al., 1972) • *Ireland* • *Wales* (Hawkins and Pinches, 1987) • *Marcellus Shale, USA* (Hoover and Lehmann, 2009) • *Chattanooga Shale, Kentucky, USA* (Anderson, 2008)	• Black shale containing pyrite (not pyrrhotite). Pyrite was most common in shale as either a primary mineral or a fine, widespread impregnation of subsequent origin. • Pyrite is frequently found in association with coal and shale deposits • Mundic (mine waste) concrete blocks used in the foundations of thousands of 20th century homes in SW England, blocks were prepared using mine waste rocks as aggregates containing pyrite that has caused serious damage (Mundic decay) in foundations	• The minimum amount of pyrite that has caused heaving problems was not known with certainty. Some reports described difficulties with pyrite contents as low as 0.1% by weight. In the Ottawa area, heaving problems have been encountered only in rock formations with much higher pyrite contents, although a systematic sampling program has not been carried out. Pyrite weathering is a chemical-micro-biological oxidation process; some of the oxidation reactions are solely chemical, others are	• Foundations, basement floors above weathered pyritic substrate. Pyrite weathering was identified as early as 1950 as a major foundation problem in the U.S.A. in buildings dating back to 1920. • Pyrite oxidation in the Chattanooga Shale has caused serious foundation problems in numerous buildings and structures in Estill County, KY.	Oxidation of pyrite in shale or coal has caused formation of *gypsum* from reactions between (a) sulfates or sulfuric acid released from pyrite oxidation and calcium hydroxide component of cement hydration (if pyritic rock is used as aggregate in concrete), and/or (b) between sulfuric acid from oxidation and associated calcite in pyritic rocks cause heaving and associated volume changes. When calcite converts to gypsum, the volume increases by a factor of 2, but of greater importance is the force associated with the growth of gypsum crystals, which can be very high.

• Locality • (Reference)	• Pyrrhotite-containing rocks • Associated sulfide minerals • Products of oxidation and subsequent sulfate attacks	• Average sulfur content in aggregate, and, • Pyrrhotite content in aggregate	• Structure affected • Type of Damage • Time taken to manifest the damage	Proposed Mechanisms of Distress
• SW England in Cornwall and Devon		attributed to autotrophic bacteria of the ferrobacillus-thiobacillus group, and still others are both chemical and micro- biological.	• Heaving of pyritic substrate causes cracking, lifting of concrete floor slabs; differences in levels across floor slabs; cracking, buckling, lifting of elements resting on the concrete floor slabs, doors, stairs, fixtures; cracking, bulging, movement of internal or external walls. • Blistering and de-bonding of vinyl tile from concrete floor is reported due to oxidation of pyritic aggregates at the surface of a concrete floor (Shayan, 1988)	When gypsum grows in rock under buildings it tends to form needle-like crystals that force the layers apart, resulting in much greater heave than would occur with simple volume expansion during formation. Another oxidation product found in all weathered pyritic materials is jarosite, $KFe_3(SO_4)_2(OH)_6$, recognized by its bright yellow-brown color. The calculated volume increase from pyrite to jarosite is 115%, which was another main contributor to volume increase and heaving.

Trois-Rivières Area in Québec, Canada

Severe deterioration of numerous concrete foundations from pyrrhotite oxidation have been reported from the Trois-Rivières area in Québec, Canada, from pyrrhotite in *anorthositic gabbro coarse aggregate*, e.g., by Tagnit-Hamou et al. (2005), and mainly the group from Université Laval in Québec, e.g., Rodrigues et al. (2012a, b, 2013, 2014, 2015, 2016a, b), Duchesne and Fournier (2011, 2013), and Duchesne et al. (2018, 2021).

Early work of Tagnit-Hamou et al. (2005) by petrography, XRD, and SEM-EDS studies of concrete cores from deteriorated foundations discovered severe concrete distress in many foundations within 2 years after construction due to oxidation of the pyrrhotite in the anorthosite aggregates used to produce the concrete. The oxidation process led to the precipitation of iron hydroxides having a higher volume than the original pyrrhotite. The presence of mica (biotite) close to the pyrrhotite seemed to have promoted and accelerated the oxidation process. Their XRD and petrographic work detected pyrrhotite in close association with biotite, globular masses of goethite in SEM, 'glittering' sound pyrrhotite in sound aggregates as opposed to 'rusty' oxidized pyrrhotite in the cracked aggregates, weathered feldspar in unsound aggregate, extensive cracking through unsound aggregate and paste, and secondary ettringite filling air voids around weathered aggregate in cement paste, and higher paste porosities in the vicinity of weathered aggregates in optical microscopy.

Along with the typical oxidation products of pyrrhotite, e.g., goethite, limonite, and ferrihydrite, and subsequent sulfate attack products of secondary gypsum and ettringite, Rodrigues et al. (2012a, 2013) detected thaumasite and some thin layers of iron carbonate (siderite) on some iron sulfide minerals in the unsound coarse-grained, dark-colored dense anorthositic (hypersthene) gabbro/norite aggregates of anorthite feldspar-biotite-pyroxene silicates where along with pyrrhotite, the predominant form of iron sulfide, in close association with subordinate pyrite, some minor finely disseminated chalcopyrite and pentlandite, were also present. The amount of sulfide minerals was less than 5 to 10% by volume. Pyrrhotite was oxidized in the presence of water and oxygen forming 'rust' stains of ferric oxyhydroxides, e.g., goethite, limonite, and sulfuric acid, whereas pyrite was not, due to the faster rate of oxidation of pyrrhotite than pyrite.

In a comprehensive study of 223 house basements in Trois-Rivières that were built with varying amounts of iron sulfides in gabbro coarse aggregates, pyrrhotite content was on average 75% of the sulfide with lesser amounts of pyrite and chalcopyrite, where damage occurred within 3 to 9 years by preferential oxidation of pyrrhotite compared to other sulfides (Rodrigues et al., 2012a). Pyrrhotite content in coarse aggregate causing visual damage in concrete was between 0.23% (0.30% total sulfur by mass) and up to 3.69% (4.81% total sulfur by mass), all of which have exceeded the European limit of 0.1% S in the aggregate (when pyrrhotite is present) by 3 times to as much as close to 30 times.

The extensive petrographic, XRD, and SEM-EDS work of Rodrigues et al. (2012a, 2013) on the concrete cores drilled through the deteriorated foundation walls of several houses showed severe cracking through and around the unsound aggregates and paste with the above-mentioned products. Full core-length (i.e., foundation wall-thickness) showed extension of deterioration with more pronounced distress at the exposed ends due to increased exposure to moisture, where expansions from oxidation of pyrrhotite along with subsequent internal sulfate attack in paste, and, additional softening and disintegration of paste by thaumasite formation are found to be the main mechanisms of concrete deterioration. Cracked foundations displayed

map cracking, yellowish surface coloration, pop-outs and open cracks reaching up to 4 cm in width, which were more pronounced at the corners of the foundation blocks.

In a separate investigation of damage in a two-story apartment building in the Trois-Rivières area where concrete used the same unsound anorthositic gabbro aggregate, Rodrigues et al. (2014) found that a higher strength (32 MPa) concrete developed significantly more deterioration with map cracking, large opened-crack network, brownish discoloration of concrete surface and localized disintegration of concrete, whereas the adjacent lower strength (15-20 MPa) foundation showed only localized cracking and no traces of rust, which indicates strength of concrete alone cannot be a measure to prevent pyrrhotite oxidation-related damage. Their attempt to quantify the damage by using the popular damage rating index (DRI) used in quantification of ASR-related damage was inconclusive due to the microstructural features and corresponding weighting factors used in DRI calculations which are very different between ASR (cracks in reactive aggregates and paste, reaction rim, reaction gel) and pyrrhotite oxidation (weathered aggregates, oxidized sulfides, cracks in aggregates and paste, internal sulfate attack in paste, etc.). In addition, gradual disintegration of certain portions of pyrrhotite-bearing aggregates from oxidation, makes it impossible to clearly distinguish cracking in unsound particles.

Central and Catalan Pyrenees, Spain

Deterioration of concrete dams in Central and Catalan Pyrenees, Spain have been attributed to similar mechanisms of pyrrhotite oxidation followed by internal sulfate attacks in concrete dams by Araujo et al. (2008); Chinchón et al. (1995); Chinchón-Paya (2012); Ayora et al. (1998); and Oliveira et al. (2014), where pyrrhotite bands in *schist aggregate* have caused the distress.

XRF studies of schist aggregate used in the Toran dam by Araujo et al. (2008) showed 2% sulfur (as SO_3) from pyrite and pyrrhotite. In the presence of oxygen, the primary oxidant and moisture in the Toran dam caused oxidation of iron sulfides to form hydroxide ion (goethite), iron sulfate (potassium iron sulfate, jarosite), and sulfuric acid (to cause further sulfate attack, and formation of acicular efflorescent salts of gypsum), where the oxidation and sulfate attack products were determined from XRD. Additionally, increase in temperature in the dam concrete led to a major increase in the extent of oxidation of pyrrhotite.

Ayora et al. (1998) studied pyrrhotite-related concrete deterioration of the Graus and Tabescan dams in central Pyrenees, Spain, where cement paste was altered to ettringite and gypsum from the acidic solution produced by weathering of pyrrhotite contained in the aggregate fragments.

Chinchón-Paya et al. (2012) used micro-XRF and X-ray photoelectron spectroscopy (XPS) techniques on iron sulfides from central Pyrenees dams and found micro-XRF determines the total sulfur without separating different sulfide species, but XPS can distinguish the sulfide types and 0.1% by mass of sulfur can be detected if the aggregates contain pyrrhotite.

Chinchón et al. (1995) studied weathering reactions in aggregates extracted from the Mont Palau quarry in Barcelona, Spain. They found that the host rock lithologies enclosing the iron sulfides play an important role in controlling the progress of weathering and oxidation of pyrrhotite and pyrite, e.g., whilst expansive hydrated Fe-sulfates characteristic of acidic

environments formed in the black shales, the neutralizing capacity of calcite dissolution prevents the formation of these harmful mineral phases in the limestones.

Oliveira et al. (2014) studied pyrrhotite oxidation in Graus dam concrete in Spain. They studied three aspects that may affect the oxidation process of pyrrhotite particles inside the aggregate: (a) the shape and the integrity of the particle, (b) the existence of preferential paths for the entrance of oxygen, and (c) the conversion process of the chemical elements involved in the reaction. Their study showed that the pyrrhotite appearing as bands in schist host rock created planes of weakness and presented cracks that served as preferential paths for the entrance of oxygen to cause oxidation (formation of goethite) and subsequent internal sulfate attack in concrete. Sulfur (as SO_3) contents of schists from XRF showed values from 0.28 to 1.72%. They used elemental mapping of iron, sulfur, and oxygen in SEM-EDS to analyze pyrrhotite oxidation and detect zones of non-oxidized (high S/Fe, low O/Fe atomic ratios) and oxidized (high O/Fe and low S/Fe atomic ratios) pyrrhotite. It was also found that characteristic ratios of 2.44 for the Fe/O ratio and of 2.63 for the S/O ratio, mark critical limits that produce the activation and acceleration of the pyrrhotite oxidation. This is described in further detail in the SEM-EDS section under Methodologies.

Concrete Dam in Switzerland

Schmidt et al. (2011) studied a 1970s deteriorated concrete dam and the quarried aggregate used in the concrete from Switzerland where oxidation of iron sulfide grains (containing 80% pyrrhotite and 20% pyrite by volume) in foliated quartz-feldspar-biotite-muscovite schist aggregates have caused significant cracking from unsound aggregate to paste, rust staining, and abundant secondary ettringite formation in cement paste. Rust deposits of iron oxides and hydroxides were reported as well as a smell of sulfurous compounds in the inspection galleries of the dam. The dam suffered from steady expansion since the early 1980s, eventually reaching about 0.025% expansion in the upper part of the dam. Sulfide grains near the surface regions of aggregates, with easy availability of oxygen and moisture, showed higher oxidation than the ones from the interior, but a similar increase in oxidation of aggregates situated near the surface of the dam was not noticed. Image analyses of micrographs of polished and thin sections have revealed that only about 30% to 40% by volume of the total iron sulfides of the extracted aggregates reacted after more than 40 years in the concrete dam. Iron sulfides were randomly dispersed within the aggregate particles, with pyrite/marcasite (80%) and pyrrhotite (20%) representing about 0.3% to 0.4% by volume. The size of the ore inclusions was in the range of about 30 to 200 μm and minor amounts of ilmenite ($FeTiO_3$) were also noticed. The concrete was made using an ordinary Portland cement (equivalent to present day CEM I 32.5), using a water-to-cement ratio in the range of 0.5 to 0.6. Pyrrhotite grains showed oxidation of about 60% by volume as opposed to oxidation of only about 4% by volume of pyrite, indicating a significantly higher rate of oxidation in the alkaline environment and expansion potential of pyrrhotite especially at the earlier stages of concrete distress, than pyrite. Cores were extracted from the downstream face and the inspection galleries of the 40-year-old structure. Their investigations indicated that the deterioration process of the iron sulfide particles was similar but not uniform in the various concrete samples. The oxidation or degradation process of both pyrite/marcasite and pyrrhotite usually started from the surface of the particle forming a layer of oxidation products, which were darker than the unreacted iron sulfide. From the chemical

microanalyses, the iron sulfide particles seem to react to form iron oxide [Fe_2O_3] and then iron hydroxides [FeO(OH), $Fe(OH)_3$]. The concrete samples showed significant cracking originating from the iron sulfide-containing regions within the aggregate particles, and then extended into the cement paste. Thus, the degradation would be directly linked to the reaction of iron sulfides, leading to an increase in volume within the aggregate particles that, in turn, cause cracking and expansion of the concrete. The formation of secondary ettringite, from released sulfates, was observed, but there were no clear signs of expansion associated with the extra sulfate. It was not clear to the authors as to what extent sulfate attack may have contributed to the expansion observed. It was found that pyrrhotite reacted much faster than pyrite in the alkaline concrete environments.

Penge, South Africa

In the 1980s, serious problems affecting concrete houses in the mining town of Penge, South Africa were reported by Oberholster et al. (1984). The affected elements (slabs and bricks) were constructed with a carbonaceous, sulfide-bearing, cummingtonite slate aggregate. The main iron sulfide present was pyrrhotite, but pyrite and chalcopyrite were also present at subordinate amounts. Examination of the concrete bricks revealed a white powdery material around the black carbonaceous aggregate particles that corresponds to thaumasite.

Mundic Problem in Cornwall and Devon, England

Many buildings in Cornwall and Devon, England, constructed with concrete blocks containing pyrite and other iron sulfide-bearing aggregates (called Mundic rocks) during 1900 to 1950 developed deterioration. Mundic is a Cornish word for chemical pyrites embedded in the mine waste rock used as aggregate, which turn to sulfuric acid when water penetrates the concrete. The acid then causes the concrete to crumble. The term is now widely used to describe concrete distress resulting from the decomposition of not only pyrite but pyrrhotite and other forms of sulfides present in the aggregates. To address the Mundic problem, in 1985 the Royal Institute of Chartered Surveyors (www.rics.org) set up a committee to investigate the problem and developed a detailed guideline to use chemical and petrographic methods for identification of the ‘mundic’ concrete. A subsequent addition to the guideline implemented an experimental program to measure unrestrained linear expansion of concrete cores extracted from the ‘problematic’ houses.

Eastern Connecticut and Massachusetts, USA

Most of the pyrrhotite-related concrete deteriorations in the United States are recorded in northeastern Connecticut and Massachusetts (Gourley, 2018, Figure 3), where distresses are mostly related to the use of a pyrrhotite-bearing *crushed quartz-feldspar-biotite-garnet gneiss coarse aggregate* mined during 1983 through 2015 from one square-shaped quarry (called Becker’s quarry) located in Willington, Connecticut that sits in a weathered hydrothermal vein

of significant pyrrhotite mineralization. The geology in the vicinity of the quarry is made up of metamorphic rocks mapped as Ordovician Brimfield Schist consisting predominantly of gray, rusty brown to orange-yellow weathered, medium to coarse grained, interlayered foliated schist and gneiss, granofels, and foliated quartz diorite. Quartz, plagioclase or oligoclase are primary minerals with micas, garnet and pyrrhotite present as common accessory minerals. Case studies of cracking, spalling, and crumbling of residential concrete foundations in Connecticut from oxidation of pyrrhotite have been investigated by Wille and Zhang (2016), Zhong and Wille (2018), and, most extensively by Jana (2018 a, b; 2019 a, b; 2020; 2022). A recent map of potential distribution of pyrrhotite in the continental US compiled by the United States Geological Survey (Jeffrey, 2020; Mauk et al., 2020, Figure 3; O'Neill, 2018) showed intense localization along a narrow, elongated belt following the Appalachian Mountains in the eastern US, and some isolated patches in the Western US. This map was built from the data available on rock units in which pyrrhotite had been reported, rock units containing sulfide minerals, and rocks moderately to highly metamorphosed.

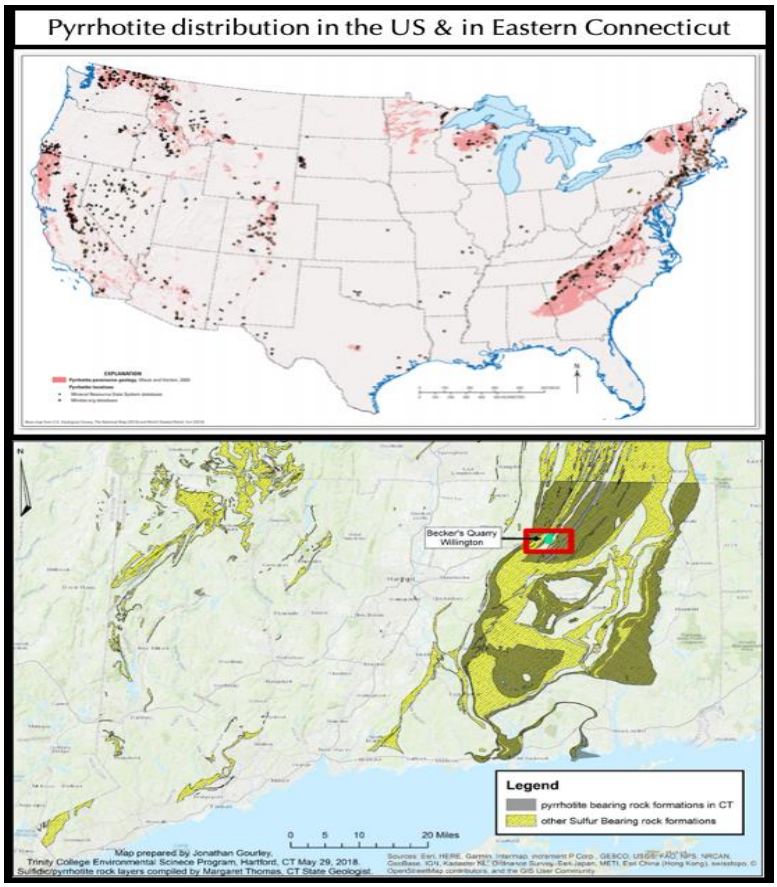

Figure 3. Maps showing potential distribution of pyrrhotite across the continental US as black dots in the top map (Jeffrey, 2020; Mauk et al., 2020; O'Neill, 2018; Jana, 2022), and, in the eastern Connecticut region as dark shaded areas in the bottom map (Gourley, 2018; Jana, 2022). The top map prepared by USGS shows a narrow, elongated belt of potential pyrrhotite crystallization in the metamorphic rocks of the Appalachian Mountains along the east coast. The square in the bottom map shows the location of the Becker's quarry, which has supplied the coarse aggregates for concretes through the 1980s in the entire shaded areas showing pyrrhotite-oxidation-related distress.

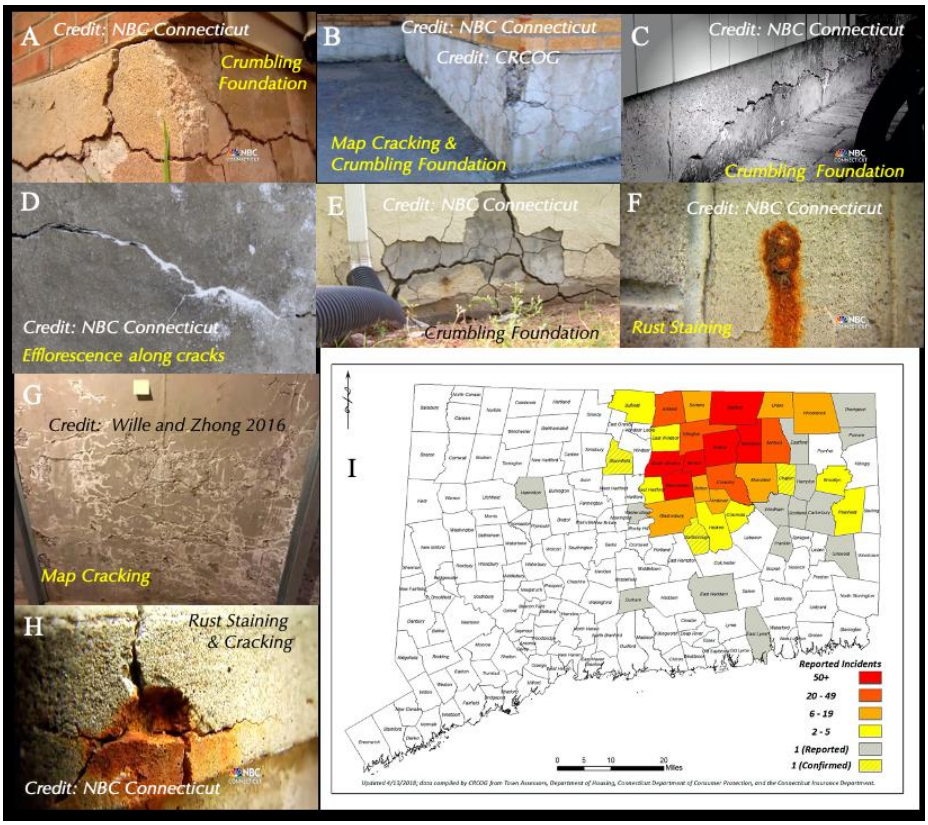

Figure 4. Field photos showing cracking in residential foundations from eastern Connecticut due to pyrrhotite oxidation-related deterioration of concrete. Photo credits: NBC Connecticut for photos A, B, C, D, F, and H, Wille and Zhong (2016) for photo G, and Capitol Region Council of Governments (CRCOG) for photo E. Photo I shows a map of northeastern Connecticut compiled at the time of preparation of this article by CRCOG from Town Assessors, Department of Housing, Connecticut Department of Consumer Protection, and Connecticut Insurance Department where townships having very high incidences (50+) of pyrrhotite-related distress, as well as the ones having high (20-49), medium (6-19), and low (2-5) incidences of distress, are shown in various shades of colors.

In light of this known problem of pyrrhotite oxidation and resultant distress, and its discovery in the crushed gneiss coarse aggregate particles in many residential foundations in northeastern Connecticut, which are all reportedly quarried from the Becker's quarry in Connecticut, for the past ten years the author's laboratories have been involved in extensive investigation of numerous concrete cores. These have been drilled from distressed concrete across many residential and school foundations in Ellington, Mansfield, and Tolland areas of eastern Connecticut, which are all situated within the known area of the 'pyrrhotite epidemic'. Figure 4 shows typical distress noted in the field, and a map of northeastern Connecticut showing very high (>50), medium (6 to 19) and low (2 to 5) incidences of distress.

Cases of Pyrite Oxidation

Similar distresses from oxidation of pyrite have been reported from Canada by Quigley and Vogan (1970), Berard (1970), Bérubé et al. (1986), and Penner et al. (1972); from Wales by

Hawkins (1987), and USA by Hoover and Lehmann (2009), Anderson (2008), and Shayan, (1988). Many of these pyrite oxidation cases are briefly described in Table 1.

Mechanisms of Deterioration

In all these studies, mechanisms of concrete deterioration have been attributed to oxidation of pyrrhotite (or pyrite) present rather as a minor constituent in concrete aggregates in the presence of moisture and oxygen during service. Most studies have proposed a two-stage expansion scenario due to (a) oxidation of pyrrhotite (or pyrite) in the presence of oxygen, moisture, and high pH in concrete, to form various forms of ferric oxy-hydroxides, e.g., goethite [FeO(OH)], more commonly ferrihydrite [$Fe(OH)_3$], limonite etc., causing staining, pop-outs, or cracking of concrete from the unsound aggregates, which is then followed by (b) internal sulfate attacks of cement paste by the sulfates released from oxidation of iron sulfide grains forming gypsum, ettringite, and/or thaumasite with further cracking. Dissolved sulfate salts (e.g., gypsum, thenardite) of reaction products are also found as efflorescence deposits along the cracks.

Timing of Occurrence, Total Sulfur, and Pyrrhotite Contents

Damage from pyrrhotite-oxidation has occurred as fast as within 9 months of construction in Oslo, Norway to within 3 to 5 years in Canada to as long as after 10 to 20 years in the eastern US. Average median sulfur contents in unsound aggregates varied from 6% in Norway to as low as 0.3 to 2.9% in Canada, 1.5 to 2% in Spain to 2.5% in the US. Pyrrhotite contents in the unsound aggregates showed even more variation, e.g., from less than 5% to higher than 75% by volume of all iron sulfides.

Forms of Distress

Typical manifestations of visual deterioration are in the form of: (a) map cracking of concrete, (b) pop-outs of near-surface unsound aggregates from oxidation of near-surface pyrite or pyrrhotite grains, (c) reddish-brown discoloration of concrete surface as rust stains from leaching of iron oxides and oxy-hydroxides, (d) whitish formation of efflorescence salts of sulfates (thenardite, mirabilite, gypsum, ettringite, and thaumasite), and carbonates (calcite, aragonite) in the vicinity of surface cracking, (e) spalling of large chunks of concrete from wider cracks, and, in severe cases (f) extensive cracking and crumbling of foundations to the point of imminent threat to the structures as found in many residential homes and a school in eastern Connecticut (Wille and Zhang, 2016; Jana, 2018 a, b, 2019 a, b, 2020, 2022).

Methodologies

The following sections describe various methods for: (a) detection of pyrrhotite in deteriorated concrete either during field survey or during various subsequent laboratory examinations, e.g.,

by optical and electron microscopy; X-ray diffraction (XRD); X-ray fluorescence (XRF); micro-XRF; X-ray photoelectron spectroscopy (XPS); thermal analysis; NMR relaxometry; magnetic susceptibility; chemical methods such as total sulfur content by IR combustion; acid leaching, etc.; and (b) laboratory tests of expansion potentials of pyrrhotite-bearing aggregates from accelerated oxidation tests to accelerated mortar bar tests at various temperatures, relative humidity, and, wetting-drying conditions.

Field Investigation

A detailed field investigation of a distressed concrete structure is the first step to determine the forms, location, timing, and extent of distress, as well as for selection of locations to be sampled for subsequent laboratory investigations. In the eastern US, many concrete foundations showing closed polygonal-shaped map cracks or random cracks, spalling, rust staining, white efflorescence deposits along cracks from three decades of oxidation of pyrrhotite in crushed schist and gneiss coarse aggregates in concrete were selected as the prime candidates to be sampled for laboratory investigation. Approximately 4 in. (100 mm) to 6 in. (150 mm) diameter concrete cores, or saw-cut sections, or simply chunks from demolished foundations were collected from the distressed locations. Cores were drilled through the entire thickness of foundation walls, often from over the visible surface cracks after collecting any white secondary deposits on the surface, if noted, before wet drilling. Fragments that were disintegrated from the core barrel after retrieval from severely distressed foundations were also collected as samples of extreme distress.

Duchesne et al. (2018) followed a sampling strategy of collecting five (1 m × 1 m × 0.225 m size) sectioned concrete blocks per house showing different levels of distress across a house that were visually ranked from level 0 (i.e., no visible cracking) to level 3 (i.e., high damage with crack openings of 2 to 12 mm) across numerous houses prior to their demolition in the Trois-Rivières area (Québec, Canada). Sections were then placed in an outdoor exposure site and instrumented on site with metal studs inserted in a 500-mm grid pattern to perform annual monitoring of expansion, and measurement of cracking index (mm/m), and cracking density where cracks with a width >0.05 mm were measured using a crack meter, which is a plastic transparent card with lines of different thickness for monitoring continuous opening of cracks. A mapping of the crack paths was carried out by tracing each visible crack on a plastic film fixed to the surface of the concrete block. The layers thus produced were digitized in order to determine the surface density of cracking (total length of crack per evaluated surface). Mapping of cracks was performed at the same time as the crack index measurements, i.e., by drawing the new cracks with a different color at each measurement to monitor the evolution of the cracking. Additionally, *in situ* temperature and relative humidity measurements were done with respective probes at three levels (e.g., above-ground, at 30 cm below ground, and at the base of the house foundation) on each of eight residential foundations showing varying levels of damage (level 0 to 3); more than 300 cores were also extracted from those three levels from eight foundations for laboratory tests, including petrography, and chemical analyses (total sulfur contents). A good correlation was observed between the monitoring of cracks and the development of expansion in concrete foundation walls of different initial damage degrees. Deterioration was also found to be largely influenced by the exposure conditions and relative humidity (RH) conditions within the concrete. However, significant variability was observed

in total sulfur contents measured on different core samples from the same foundation. Similar approaches of *in situ* measurements of temperature, RH, crack pattern, and expansion, by installing metal studs can be done on other concrete foundations underdoing expansion from pyrrhotite oxidation.

Sample Preparation for Laboratory Investigation of Distressed Concrete

The following paragraphs provide a detailed comprehensive overview of various sample preparation steps exercised by the author. Samples collected from the field are first photographed and well-documented by describing the following: (a) the degree of damage and resultant overall condition of the core from an assigned level of damage rating, e.g., from 0 for no visible distress to 1 through 4 for increasing extent and widths of cracking to 5 for complete fragmentation of retrieved sample; (b) tracing of visible cracks on the cylindrical core surface to depict the extent of cracking, and, measurement of crack widths; (c) the type of aggregates present especially marking the ones responsible for distress; (d) variation in rock types, mineralogies, and textures of aggregates; (e) appearance of interstitial mortar fraction; and (f) secondary deposits seen on the cracks. Samples are then assigned for testing and sectioned into multiple portions for various tests. The sample preparation methods are described below.

a) A drilled core or a saw-cut concrete specimen is first sectioned with water, or with a light mineral oil-cooled continuous or segmented rim diamond slab saw, into multiple longitudinal slices, preferably traversing the entire length of the sample, i.e., to encompass both the exposed face to opposite ends of a foundation wall represented in the sample. One sectioned longitudinal slice is then dried in an oven (at <60°C) to a constant mass to remove all inherent moisture, as well as moisture introduced from sectioning, making sure paste or any secondary deposit is not decomposed from the drying temperatures. The oven-dried slice is then encapsulated with a very low-viscosity (<100 centipoise) fluorescent dye-mixed epoxy, under vacuum (i) to improve the overall integrity of the slice during lapping, especially if it is of a cracked or crumbled concrete; and (ii) to highlight the crack patterns across the sample by observing the polished slice in an ultraviolet light. Two opposite parallel sectioned sides of the epoxy-encapsulated concrete slice are then ground with successively finer diamond abrasives on a horizontal lapping plate with water/oil coolant, to obtain smooth polished surfaces for detailed examinations in a low-power stereomicroscope.
b) Another sectioned slice is similarly oven-dried and impregnated with a colored (e.g., blue) or fluorescent dye-mixed low viscosity (<100 centipoise) epoxy to highlight cracks, air voids, and porous areas in the paste. This second slice is used for the subsequent thin-sectioning process where multiple portions of the slice through depth are trimmed to obtain one or multiple large-area (50 × 75 mm) thin sections. Microstructural and microchemical analyses of unsound aggregates and affected paste are performed on thin section first by optical microscopy and subsequently by SEM-EDS. For thin section preparation, epoxy-encapsulated blocks are (i) first polished to a smooth perfectly flat surface; (ii) then glued to a frosted glass slide with a UV-cured epoxy; (iii) then sectioned down to 1 mm thickness with a micrometer-controlled precision sectioning saw of thin-sectioning equipment; (iv) then further ground down

to 100 micron thickness with a micrometer-controlled precision grinding wheel of the thin-sectioning equipment; and (v) then finally ground down to 25-30 micron thickness by hand on a glass plate with 10-15 micron alumina abrasive slurry. Thin sections thus prepared are then (vi) polished on a polishing cloth with submicron (0.3 to 0.05 μm) size diamond abrasive paste in a polishing machine to produce a shiny finish suitable for observations in reflected light mode in an optical (ore) microscope, followed by examinations of specific areas of interest selected during optical microscopy in a scanning electron microscope for microstructural and microanalytical studies. Details of thin sectioning procedures and other petrographic sample preparation steps are described in Jana (2006).

c) Both lapped sections and thin sections are scanned on a flatbed scanner where along with normal scanning of lapped sections, the entire fluorescent epoxy-impregnated lapped section is also scanned in UV light to highlight the cracks. Thin sections are scanned on a flatbed film scanner with one or two perpendicular sheets of polarizing filters to respectively, recreate plane or cross polarized light views of the entire thin section.

d) Another longitudinal thin slice of core is sectioned at various depths from the exposed end and pulverized down to fine powder of less than 45-micron particle size in a rock pulverizer for X-ray diffraction (XRD) to determine mineralogical compositions of the concrete and to search for the products of oxidation and sulfate attack.

e) An aliquot of the pulverized concrete is used for preparation of a pressed pellet for energy-dispersive (ED-XRF) X-ray fluorescence spectroscopy, or fused bead for wavelength-dispersive (WD-XRF) spectroscopy. Both these techniques determine the chemical composition of concrete including the total sulfur content expressed as SO_3 in the case of ED-XRF, or, additionally, speciation of sulfide sulfur and sulfate sulfur forms in the case of WD-XRF. Less than a gram of the pulverized mass is also used for measurement of total sulfur content by the combustion IR (Leco) method in an induction furnace. Other wet chemical (gravimetric) and instrumental methods, e.g., inductively-coupled plasma spectroscopy (ICP) can also be used for determination of sulfur and other components of a sample.

f) Potentially unsound pyrrhotite-bearing aggregates are then extracted from a cross sectional slice of core after examining the cross section in a stereomicroscope to mark the aggregates to be removed. Aggregates are then carefully extracted with a hammer and flat chisel or a thin trim saw, cleaned of all adhering paste, oven-dried, and subsequently pulverized down to finer than 45 microns size for XRD, XRF, thermogravimetric analysis (TGA), and other tests (e.g., IC or accelerated oxidation).

g) Pyrrhotite-bearing aggregates on a lapped cross section are also drilled with a benchtop drill press to collect fine drill dust of the aggregate (often moistened with alcohol to collect with a syringe or pipette) for XRD studies on a zero-background sample holder where oxidation products of pyrrhotite are best identified. Stereo-microscopical examinations of aggregates detect the pyrrhotite grains, especially the grains showing evidence of oxidation, e.g., fine striations and reddish-brown stains around the grains, which are marked and drilled with a fine-tipped micro drill for collection of the small amount of drill dust moistened in alcohol for transfer with a pipette to a zero-background holder.

h) An aliquot of a pulverized portion of extracted concrete, as mentioned in Step ‘e’ or aggregate in Steps ‘f’ or ‘g’, is used for determining total sulfur content by combustion (Leco) method.
i) Aliquots of pulverized portions of extracted aggregates are immersed in a strong oxidant solution (e.g., 35% hydrogen peroxide solution) for several days to release sulfates from the aggregate to be analyzed by ion chromatography.

Petrographic Examinations of Distressed Concrete

A detailed petrographic examination of quarried aggregates in accordance with the procedures of ASTM C 295, and of the distressed concrete in accordance with ASTM C 856 remain at the heart of investigation of pyrrhotite-related deterioration in concrete. These techniques allow the detection of the abundance and distribution of pyrrhotite in aggregates to its oxidation products, as well as the abundance and distribution of pyrrhotite-bearing, potentially unsound aggregates in distressed concrete. They can also provide evidence and products of oxidation and sulfate attack in paste and allow detection of the extent of deterioration.

Petrographic examination was used extensively for investigation of pyrrhotite oxidation-related distress, e.g., (a) in Québec, Canada by Tagnit-Hamou et al. (2005); Rodrigues et al. (2012, 2013, 2014); Duchesne et al. (2021) for the Trois-Rivières area; (b) Schmidt et al. (2011) for a concrete dam in Switzerland; and (c) Jana (2018 a, b, 2019 a, b, c, 2020, 2022) for eastern Connecticut.

Jana (2006, 2020, 2022) described various steps followed during petrographic examinations of a deteriorated concrete to maximize the information obtained, which include:

a) Visual examinations of distressed concrete to trace the extent of cracking;
b) Collection of any secondary deposits on the exposed surfaces for examination in an oil immersion mount, or in thin section, or XRD to identify the exposed efflorescence deposits, or underside crypto(sub)-fluorescent salts formed beneath the exposed surface depicting telltale evidence of distress;
c) Detection of potentially unsound pyrrhotite-bearing coarse aggregates on lapped cross sections and thin sections scanned on a flatbed/film scanner, followed by estimation of the abundance and distribution of such particles by image analysis;
d) Tracing the crack pattern and crack frequency by digital image analysis (e.g., using Image J from https://imagej.nih.gov) from the scanned images of lapped cross sections collected with a flatbed scanner;
e) Stereo-microscopical examinations of lapped cross section, and examination in a reflected-light (ore) microscope of polished cross section to detect the extent of cracking, tracing the crack paths, air contents and air-void systems, depths of carbonation, size, frequency and nature of distribution of pyrrhotite grains in aggregates, occurrences of ‘oxidized’ pyrrhotite grains from the characteristic fine striations, and reddish-brown stains of oxidation products;
f) UV light observations of fluorescent epoxy-impregnated lapped sections and thin sections in a dark room and with a stereomicroscope to trace the crack patterns and record the extent of cracking;

g) Examinations of blue or fluorescent dye-mixed epoxy-impregnated thin sections of concrete in a petrographic microscope to detect the composition, mineralogy, and texture of the host unsound aggregates as well as abundance and distribution of potentially unsound iron sulfide minerals in those aggregates;
h) Examination of interstitial paste fractions of distressed concrete in thin sections for microstructures of pyrrhotite-oxidation-related distress in unsound aggregates, e.g., from macro and microcracking of unsound particles to resultant oxidation products, as well as the products of sulfate attack in paste often occurring as gypsum, or fine acicular crystals of ettringite, or, in extreme cases of paste decomposition as thaumasite in the presence of carbonates – all from sulfates released from pyrrhotite oxidation.
i) In severe cases of deterioration, fine fibrous crystals of ettringite are found intricately intermixed with the hydration products of Portland cement, especially in relatively porous areas of paste where ettringite infestation in paste is well documented at high magnifications of a petrographic microscope. Such formation of ettringite in the confined spaces in paste is directly responsible for paste expansion and associated distress in concrete. Moisture absorption by microcrystalline, gelatinous, or semi-amorphous forms of ettringite often documented by some authors (Mehta, 1973) can also introduce deleterious expansion.

Scanning Electron Microscopy and Energy-Dispersive X-Ray Microanalysis (SEM-EDS)

A common step to follow after optical microscopy is in-depth examinations of oxidized pyrrhotite and its oxidation products, and compositional and microstructural investigations of the affected interstitial paste fractions in a scanning electron microscope equipped with secondary electron and backscatter electron detectors, and energy-dispersive X-ray spectrometer (SEM-EDS), by following the procedures of ASTM C 1723. Features to be examined in SEM are usually marked across multiple areas of thin sections with a conductive marker pen during optical microscopy. After optical microscopy, polished thin sections are coated with a thin film of conductive gold-palladium alloy for observations in SEM-EDS.

Features that can be obtained from an SEM-EDS study include:

a) Backscatter and secondary electron images of microstructures of distressed concrete where micro and macrocracks from pyrrhotite oxidation-related distress in unsound aggregates, can be obtained. The unsound pyrrhotite grains can be highlighted;
b) S/Fe and O/Fe atomic ratios of pyrrhotite grains where many pyrrhotite grains show irregular veins of oxidized iron in a pyrrhotite matrix, or parallel bands of Fe-S-rich and Fe-O-rich veins;
c) Microcracking in pyrrhotite grains from oxidation often extending into the host aggregate;
d) Elemental maps of iron and sulfur distribution in pyrrhotite grains and surrounding minerals of the host aggregate; and,
e) Microstructures and compositions of various products of sulfate attack in paste of which ettringite is the most common product, followed by gypsum and thaumasite in

some cases. Backscatter and secondary electron images can show formation of these products in air voids, cracks, paste, and along aggregate-paste interfaces. SEM-EDS chemical analysis can be performed, where ettringite is identified by its characteristic Ca-S-Al-O peaks, gypsum by Ca-S-O peaks, and thaumasite by Ca-S-Si-C-O peaks.

To explain the iron sulfides oxidation process from SEM-EDS data of oxidized pyrrhotite, Schmidt et al. (2009) used a graph of the atomic ratio between sulfur and iron (S/Fe) in the Y-axis against the atomic ratio between oxygen and iron (O/Fe) in the X-axis where a rather simplified evolution of pyrite and pyrrhotite oxidation reaction was depicted. In their representation, the authors used the results obtained in zones of the iron sulfide particles that are either clearly oxidized, or not. As a result, there was a concentration of points either near the Y-axis indicating the iron sulfide after the oxidation process, or near the X-axis showing the oxidation products. There are no dots indicating the conversion or the movement between the axes.

Thus, a more detailed description of the iron sulfides oxidation conversion, required analysis of a greater amount of points in the 'transition zone' between the oxidized and the non-oxidized iron sulfide in the S/Fe vs. O/Fe plot, which was subsequently done by Oliveira et al. (2014) on quarried aggregates (with 1.42% median SO_3 content) adjacent to a concrete dam built in Lladorre (Spain) in 1971. The dam was 91 m long and 9 m high and was severely affected by internal sulfate attack. The pyrrhotite oxidation was studied by SEM-EDS point analysis to determine the elemental contents of iron, sulfur, and oxygen. The pyrite oxidation path of conversion is identical to that for pyrrhotite, with the difference being that the degradation process usually starts with an S/Fe atomic ratio slightly higher, since S/Fe is equal to 2 for pyrite and between 1 and 1.25 for pyrrhotite. They found two zones, one of oxidized pyrrhotite preferentially concentrated along the cracks due to migration of oxygen along the cracks to cause oxidation, which showed greater dispersion in S/Fe and O/Fe values and another of unoxidized pyrrhotite between the cracks with much tighter placement at the S/Fe axis. It was also found that characteristic ratios of 2.44 for the Fe/O ratio and of 2.63 for the S/O ratio in the Fe/O vs S/O atomic ratios in logarithmic scale, mark critical limits that produce the activation and acceleration of the pyrrhotite oxidation. For Fe/O less than 2.44 and S/O less than 2.63, the analyzed points are close to the representative atomic ratios of the iron oxides (Fe_2O_3) and hydroxides ($FeO(OH)$, $Fe(OH)_3$). This should lead to an increase of the expansive reactions and, consequently, of the risk of structural damage. It was confirmed that the cracks mark a preferential path for the entry of the oxidizing agent (oxygen). Thus, the analyzed aggregates that present pyrrhotite bands with cracks show a degree of oxidation much more pronounced than the aggregates without cracks. They found that the oxidation of pyrrhotite goes through three distinct stages: (a) first, the pyrrhotite is in the non-oxidized form, representing a very low or no presence of oxygen (Stage I); (b) then, oxidation starts and restructuring of the pyrrhotite into pyrite occurs due to the diffusion of iron through the pyrrhotite surface (Stage II); and (c) finally, the products of the pyrrhotite oxidation are formed (Stage III). All these stages in their proposed oxidation scheme in S/Fe vs O/Fe atomic ratio space are shown in Figure 1.

X-Ray Diffraction (XRD)

X-ray diffraction (XRD) is a rapid and powerful analytical technique used to identify various iron sulfide minerals in aggregates as well as their oxidation products. One limitation of XRD is the detection limit of pyrrhotite, which is approximately 2 to 5% by mass (Janzen et al., 2000), which exceeds the potentially harmful limits in concrete that according to some experts could be as low as 0.3%. Rietveld refinement is a whole-pattern fitting approach for the quantification of crystalline compounds using good quality XRD patterns (ASTM C 1365). Jana (2020, 2022) used this technique to analyze concrete and extracted aggregate samples from Connecticut. Tagnit-Hamou et al. (2005) and Rodrigues et al. (2012a, 2013) used XRD to analyze anorthosite gabbro aggregates and concretes from the Trois-Rivières area in Québec, Canada. For aggregate or concrete samples, a large volume of material should be ground and mixed well to obtain a representative sample. As with petrography, several samples are needed to estimate the actual distribution of pyrrhotite. High-resolution X-ray diffraction with synchrotron radiation can lower the detection limit to as low as 0.1% or less by mass on a very fine micronized powder sample (<45 μm). Some latest silicon drift XRD detectors can detect pyrrhotite at levels as low as 0.05% by mass.

XRD studies are done on a variety of samples, with some examples described below:

a) On bulk concrete, e.g., sectioned as a thin slice through the entire recovered length of a core from a foundation wall, and pulverized, reduced in size by coning and quartering, then re-pulverized down to finer than 45-micron size for qualitative detection of pyrrhotite and its products of oxidation as well as the products of sulfate attack in concrete;
b) On the pyrrhotite-bearing aggregate particles extracted from concrete for quantitative determination of pyrrhotite, and other iron sulfides, as well as products of oxidation and subsequent sulfate attack;
c) On paste fractions removed from concrete after screening the aggregates for detection of the products of sulfate attack;
d) On drill dust of aggregates selectively collected from over the lapped cross sections of cores to determine the oxidation products and variations in aggregate mineralogies across the lapped section; and
e) On white secondary (e.g., efflorescence) deposits of sulfate salts collected from the field or from a deteriorated core.

X-Ray Fluorescence Spectroscopy (XRF)

Apart from the bulk chemical (oxide percent) compositions, XRF analysis is used for determination of sulfur content (expressed as SO_3) of concrete where the measured 'sulfur' incorporates (i) sulfate from cement, (ii) oxidized sulfate from the sulfide phases of aggregate, as well as (iii) unoxidized sulfide phases in aggregate.

For XRF analyses, concrete as well as aggregate particles extracted from concrete are pulverized down to finer than 45-micron particle sizes and either (a) mixed with a resin to prepare pressed pellets for energy-dispersive XRF (ED-XRF) or wavelength dispersive XRF (WD-XRF), or, mixed with a flux to be fused into glass beads for WD-XRF. Instruments for

both techniques are calibrated with carefully selected standards covering the speciation and concentration ranges of sulfide and sulfate compounds anticipated in the samples.

Modern high-resolution analyzer crystals in sequential WD-XRF make analyses of the different chemical compounds of sulfur possible from their characteristic peak shifts, which can be used to separate both sulfur compounds, sulfate (SO_4^{2-}) and sulfide (S^{2-}) and determine their relative concentrations. The outer electrons of lighter elements up to atomic number 18 are present in the atomic shells, which are important for the emission of X-ray fluorescence lines. Sulfur has 6 valence electrons in the M-Shell. Any change in the oxidation state and therefore in the number of electrons in this shell will affect the Kß line of sulfur. In Portland cement, there are two sulfur species present, sulfide (S^{2-}) and sulfate (SO_4^{2-}), both calculated as SO_3 in cement. Sulfide has 8 electrons in total in the M-shell, whereas sulfate has no electron left in the important outer shell. This difference leads to changes in the energy spectrum, which can be used for the speciation of the sulfur compounds, e.g., (a) X-ray line shifts (chemical shift) - both the Ka and Kß lines show a shift of the line position; the physical reason is a shift of the energy levels caused by the chemical bonding influence; (b) additional X-ray lines appear (satellite lines) - there is a significant difference concerning the presence of an additional line on the low energy side of the Kß line of sulfate, but not for sulfide; and (c) changes in the ratio between Ka and Kß - the sulfide/sulfate ratio can be calculated based in the Ka/Kß ratio with respect to the total sulfur concentration.

For example, in Bruker's WD-XRF units (e.g., S8 Tiger Series 2), the S Kß line is measured by using the fine collimator with an opening of 0.23° and the high-resolution curved crystal XS-Ge-C (Bruker Lab Report XRF 145). The curved crystal provides a higher resolution and increased sensitivity for sulfur in comparison to traditional crystals, leading to a better analytical performance. The absolute precision of the goniometer positioning is vital for the accurate determination of the sulfur species. In both spectra, the effects of the chemical bonding on the spectrum can be seen. The S Kß line shows a clear peak shift of about 0.2° (2Θ). This difference is typically too small for a routine determination of the two compounds. The intensity of the S Kß line is determined by the emission of sulfide and sulfate. But sulfate in addition has a satellite line on the low energy side, the so-called S Kß SX line. The difference of the peak positions is about 0.68° (2Θ), which can be clearly resolved. The total sulfide concentration can then be analyzed using the Kß line. The part from sulfate is subtracted by defining a line overlay correction based on the satellite line S Kß SX. Instrument calibration is done using a set of 8 cement samples with varying concentrations of sulfide and sulfate.

Chubarov et al. (2016) described determination of total sulfur and sulfide in sulfide ores by WD-XRF, where the $SK\alpha_{1,2}$ line was used to determine total sulfur, and the ratio between sulfide and total sulfur was measured by the ratio of satellite $SK\beta'$ and $SK\beta_{1,3}$ line intensities. The samples were prepared as pressed powder pellets on boric acid substrates. The total relative standard deviation (SD) of the measurements and preparation repeatability was less than 2%. To determine total sulfur, the calibration curve was obtained from the samples of certified reference materials of gold-bearing sulfide-containing ores. The accuracy was verified by comparison with a gravimetric method. The relative SD was 6% for sulfur concentrations from 1 to 8 wt.%. The calibration curve was defined using pure reagents to determine sulfide. The ore was analyzed by a gravimetric procedure with a relative SD of 6.5% for the sulfide concentration from 1 to 6 wt.%.

Gazulla et al. (2008) also used WD-XRF for analysis of sulfur in geological samples by preparing pressed pellets as well as fused beads and using corresponding calibration curves of

standards of beads and pellets. For pellets, calibration curves have different slopes depending on the form in which sulfur occurs, as there are significant mineralogical structure and matrix effects. Pressed pellets can therefore only be used if the form of sulfur present in the sample is known beforehand, and appropriate reference materials are also available for calibration and validation. For beads, a BaO additive was introduced in a quantity at least twice that of barium stoichiometrically required for all the sulfur present in the sample to form $BaSO_4$ to prevent any loss of volatile sulfur during bead preparation. They also analyzed sulfur by combustion and IT detection, where due to the high temperatures (2000°C) used in the combustion process, sulfur reached the detector in the form of SO_2, so the types of compounds formed by sulfur had no influence on the sulfur response.

Cruz-Hernandez et al. (2020) proposed a similar WD-XRF method to determine individual sulfur species, i.e., sulfide (S^{2-}) from iron sulfide bearing aggregates, and sulfate $(SO_4)^{2-}$ from cement and sulfate phases in aggregates from Connecticut, USA. Total sulfur is determined either by a standard addition method using WD-XRF, or, by an infrared combustion (e.g., Leco) elemental analyzer, and the concentration is used to quantify total sulfide and total sulfate in concrete. The sulfide sulfur content of aggregate is then estimated by subtracting the sulfate introduced by Portland cement. The authors reported that for a $[S_T]$ content of 1%, $[S^{2-}]$ can be detected down to 0.037% by weight. This method, however, uses a calibration curve that can be influenced by the matrix effect, and, as with other sulfur analysis methods, it cannot identify the presence of pyrrhotite, especially if other sulfide phases (e.g., pentlandite) are present with pyrrhotite.

Micro X-ray Fluorescence Spectroscopy (μXRF)

Micro-XRF is a method for mapping elemental distributions of samples. From the combined Fe and S elemental maps, this technique characterizes and quantifies the iron sulfides present in the aggregates without differentiating between pyrite and pyrrhotite minerals (Chinchón-Paya et al., 2015). These authors examined concrete core samples with aggregates containing iron sulfide minerals. The combination of elemental chemical distribution images facilitated the identification of mineral phases. Quantification was carried out using image analysis. Micro-XRF allows elemental mapping of an area up to 15 cm^2 with a minimum beam size of 20 μm. For investigation of polished solid sections or large-area thin sections that are too large to insert in the SEM sample chamber, μ-XRF is a promising technique where along with elemental mapping of the entire section, detection of pyrrhotite and related oxidation products can be highlighted.

Total Sulfur Content of Aggregate from Infrared Combustion, Acid Solution-Gravimetry, and XRF

Total sulfur content $[S_T]$ measures both sulfate $[S^{6+}]$ and mono/di-sulfide $[S^{2-}]$ sulfur contents including any organic sulfur. Determination of S_T is commonly done by carbon/sulfur elemental analyzers based on combustion technology, which ignite the sample in an oxygen stream and determine the released SO_2 gases with infrared cells. Size reduction is the only

sample preparation needed. The advantage of this method is that the elemental content of sulfur can be determined to be in the ppm range up to 100%. The disadvantage is that only the S_T content is determined without determining the contributions from different sulfide and sulfate phases.

Vlisidis (1966) proposed a method for the determination of sulfate and sulfide sulfur that occur together in rocks or minerals where all the sulfate sulfur is converted to barium sulfate in an inert atmosphere to prevent oxidation of any sulfide sulfur. Cadmium chloride is added to precipitate any sulfide ion that may be liberated. The sulfate sulfur is then measured indirectly by the determination of the barium and is therefore unaffected by any subsequent oxidation of the sulfide sulfur. Total sulfur is determined on a separate sample, and sulfide sulfur is calculated by difference.

Nagashima et al. (1972) proposed a method for the determination of minute amounts of sulfide and sulfate sulfur in igneous rocks where the rock is dissolved by heating with tin (II)-strong phosphoric acid where total sulfur is evolved as hydrogen sulfide, or in strong phosphoric acid, where sulfide-sulfur (not sulfate) is evolved as hydrogen sulfide. The evolved hydrogen sulfide is fixed as zinc sulfide and then determined by the photometric method, using mercuric thiocyanate and ferric iron.

Mahanta et al. (2017) used ICP-OES for the determination of total sulfur and sulfate sulfur in rocks, soils, and sediments where samples are decomposed with potassium carbonate in the presence of MgO, leached with water, and acidified with perchloric acid. Then most of the salt is removed by filtration and analyzed for total sulfur by ICP-OES. Another aliquot of the sample is leached with HCl for the determination of sulfate sulfur. The quantity of flux and MgO, combinations of fluxes, temperature, and duration of fusion for complete attack and recovery were evaluated and optimized. The salt content of the sample solution was reduced by precipitating potassium as perchlorate. Interference effects of matrix elements were investigated, and the emission line of 181.978 nm was used for analysis under nitrogen purging. The method is relatively simple, does not involve acid fuming or require a special apparatus for sample decomposition.

Besides an elemental analyzer, the alternate method of determination of total sulfur is conventional wet chemical acid solution-gravimetry (after fusion with alkali flux or acid digestion) viz. gravimetry, turbidimetry, and titrimetry. Jensen (2018) analyzed 300 Norwegian aggregate samples for total sulfur by wet chemical method, which showed a reasonable (R^2 = 0.802) correlation to the results obtained from IR combustion. Jensen (2018) analyzed 35 commercial quarries which contained pyrrhotite and did not fulfil the requirement for $S_T \leq$ 0.10%. Rock types containing pyrrhotite with $S_T > 0.10\%$ are mafic rock (gabbro, amphibolite, and greenstone), gneiss, granite, greywacke, sandstone, siltstone, claystone, limestone, felspathic rock (rhomb porphyry), and volcanic rock (rhyolite). Nevertheless, according to Jensen (2018), cases of concrete deterioration due to pyrrhotite have not yet been reported in Norway.

As mentioned before under the section on XRF, Chuvarov et al. (2016) described determination of total sulfur and sulfide sulfur in sulfide ores by WD-XRF where the $SK\alpha_{1,2}$ line was used to determine total sulfur, and the ratio between sulfide and total sulfur was measured by the ratio of satellite $SK\beta'$ and $SK\beta_{1,3}$ line intensities. Gazulla et al. (2008) and Cruz-Hernandez et al. (2020), mentioned under the XRF section, also used WD-XRF for the determination of total sulfur as well as separate sulfide and sulfate sulfur.

The European Standard for chemical analyses of aggregates, BS and NS-EN 1744-1 clause 11 mentions two methods for analyzing total sulfur: (a) Clause 11.1 (reference method) for acid solution and gravimetry; and (b) Clause 11.2 (alternative method) for the combustion method (e.g., Leco method). Norwegian testing agencies have used both methods simultaneously for several years for commercial testing of total sulfur.

Haugen and Lindgård (2018) used the reference method in the Norwegian Standard NS-EN 1744-1 for determination of S_T in Norwegian aggregates (crushed stones, and natural sand and gravel), which is the wet chemical method where the samples were treated with hydrogen peroxide, hydrochloric acid, and a solution of ammonia, in order to convert the sulfur components to sulphate. Thereafter, barium chloride is added. The sulfates will then precipitate as barium sulphate. The requirements in the aggregate standard NS-EN 12620 with respect to maximum allowed content of total sulfur (as S_T) is 1% S_T if pyrite is the only ore mineral present, and 0.1% S_T if pyrrhotite is present. In their study, 14% of the 235 analyzed samples had S_T higher than 0.14%, of which 58% (19 samples from 8 different rock quarries) contained pyrrhotite, which were not acceptable by the standard but were still used in concrete. Rock quarries that showed a pyrrhotite content above the critical acceptance limit consisted of limestone, gabbro, amphibolite, or a combination of gneiss/granite rocks.

The CSA Technical Committee on Concrete Materials and Construction (CSA A23.1/ A23.2, 2019) devised a test method to determine the sulfide sulfur content of aggregates, where:

a) The total weight percentage of sulfur (S_T, to the nearest 0.01%), is determined either by *high temperature combustion analysis*, or, by *powder x-ray fluorescence spectrometry*. In high temperature combustion, an aliquot of the sample is subjected to a minimum operating temperature of 1,350°C in a stream of oxygen, where the high temperature combustion analyzer is equipped with either an acid base detection or infrared absorption detection system. Alternately, an X-ray fluorescence spectrometer calibrated for sulfur using properly matrix matched calibration standards can be used to determine S_T.
b) The weight percentage of the sulfate sulfur (S_S, to the nearest 0.01%) is determined by *gravimetry* by (i) first digestion of 2 to 5 g of pulverized aggregate (M_1) in 50 ml hydrochloric acid (2:3) for 30 min in a boiling condition, (ii) then vacuum filtration of filtrate through a tared glass frit to use the filtrate for determination of sulfate sulfur gravimetrically by (iii) further diluting the filtrate to 250 ml with distilled water, (iv) heat to boiling, (v) adding 10 ml hot barium chloride solution and continue boiling until formation of precipitate, (vi) digestion of solution for 12 to 24 hours at a temperature below boiling, (vii) keeping the solution volume between 225 and 260 ml by adding distilled water if needed, (viii) then filter and wash the precipitate with hot water, (ix) ignite the precipitate in filter paper in a tared particular crucible (M_4) at 800 to 900°C, and (x) weigh the ignited residue with crucible (M_5), where $S_S = [(S_{M5}\text{-}S_{M4})\text{-}(B_{M5}\text{-}B_{M4})]/M_1 \times 13.74$ (which is the molar ratio of S to $BaSO_4 \times 100$), where S/B_{M5} and S/B_{M4} are sample/blank ignited residue plus crucible weight in grams, and sample/blank tared crucible weight, in grams, respectively, where a blank determination is needed following the same procedure and using the same amount of reagents as the test sample; finally,
c) The weight percentage of the sulfide sulfur, S_O, is obtained by calculating the difference from the above two results, $S_T\text{-}S_S$ to the nearest 0.01%.

Acid Leaching Method

Marcelino et al. (2016) described an acid leaching procedure to evaluate the amount of pyrrhotite in sulfide-bearing concrete samples based on a methodology developed by Lorenzen (1995). An aggregate sample was first ground to a particle size finer than 0.15 mm. One gram of ground sample was then agitated for 1 h in 100 ml of HCl at 60°C. Finally, the sample was filtered, washed, and oven-dried at 40°C for 24 h. The total sulfur content was measured on a solid sample from which the pyrite content was calculated. The difference between the total sulfur content of the aggregate and the pyrite content indicated the pyrrhotite content. The result was verified by leaching pyrite in the residual solid using aqua regia (75% HCl, 25% HNO_3). Their results showed that the amount of pyrite in their tested sulfide-bearing rocks has remained virtually constant over time in different exposure conditions, which indicates that sulfur limits in aggregates should be set according to the type of iron sulfide present, and not solely by the total amount of sulfur.

Raman Spectroscopy

Along with determination of pyrrhotite content in their sulfide-bearing rocks by hydrochloric acid leaching, Marcelino et al. (2016) also used Raman spectroscopy to determine the pyrite and pyrrhotite contents, where higher abundance of pyrrhotite (average 1.42%) compared to pyrite (average 0.6%) was not only detected but also confirmed by subsequent direct combustion methods.

X-Ray Photoelectron Spectroscopy (XPS)

XPS is a surface-sensitive quantitative spectroscopic technique that can distinguish sulfide types. XPS provides information about the element oxidation state and concentration with a detection limit in the parts per million (ppm) range. XPS easily detects small amounts of pyrrhotite, e.g., below 0.1% by mass of total S can be detected if the aggregates contain pyrrhotite (Chinchón-Paya et al., 2015). However, XPS analysis requires ultra-high vacuum conditions, and the sample size is limited to a length of up to 5 cm. Jones et al. (1992) used XPS and XRD to study oxidation of ground pyrrhotite surfaces exposed to air, water, and perchloric acid oxidant.

Auger Electron Spectroscopy (AES)

Based on a study of depth profiling with AES (Auger Electron Spectroscopy), Mycroft et al. (1995) and Pratt et al. (1994) have proposed a mechanism of oxidation of pyrrhotite where they determined the chemical composition profile of the pyrrhotite surface. The authors noted that the deepest layer of the particle beyond 35Å is composed of unreacted pyrrhotite (S/Fe = 1.14); the second layer between 5 and 35 Å is a mixture of Fe_2S_3 and Fe_7S_8 (S/Fe = 1.5 to 1.14), while the next layer between 2 and 5 Å is pyrrhotite with a stoichiometry approaching that of pyrite

(FeS_2; S/Fe = 2). Finally, the external layer (pyrrhotite surface) between 0 and 2 Å is composed of iron oxyhydroxide [Fe(III)-O, S/Fe ~ ∞] resulting from the oxidation process. To justify the profile, Mycroft et al. (1995) and Pratt et al. (1994) considered that the pyrrhotite oxidation causes iron to diffuse from inside to outside the particle. This displacement of iron results in an enrichment of sulfur in the zone below and promotes the formation of disulfide bonds and the reorganization of the pyrrhotite structure towards marcasite (FeS_2) or a disordered pyrite structure (Jones et al., 1992; Belzile et al., 2004; Legrand et al., 2005; Oliveira et al., 2011).

Thermal Analysis

Differential thermal analysis (DTA) and thermogravimetric analysis (TGA) provide two types of results: (a) indication of pyrite when one endothermic peak is detected, and (b) indication of pyrrhotite or a combination of different types of sulfides when two peaks are detected (Jensen, 2018). Type of sulfide is determined by DTA when total sulfur content is >0.1% (Haugen and Lindgard, 2018). Thermal reactions of pyrite, or pyrrhotite are combinations of (i) oxidation (exothermic, e.g., FeS_2 +7.5 O_2 = Fe_2O_3 +4SO_3, peaks between 400 and 500°C), (ii) disproportion (endothermic, e.g., FeS_2 = FeS + S peaks between 600 and 700°C in N_2 atmosphere), and (iii) thermal dissociation (endothermic, dissociation of iron sulfate to Fe_2O_3 and SO_3). These reactions overlap each other partly or completely.

Magnetic Susceptibility (χ)

Thermomagnetic analysis measures the change in magnetic susceptibility, χ, during controlled heating, where χ indicates the degree of magnetization of a material in an external magnetic field. Given the inherent magnetic nature of pyrrhotite, and the change in susceptibilities due to variations in Fe-vacancies in its structure during heating, Geiss and Gourley (2019) undertook thermomagnetic studies in an attempt to quantify the pyrrhotite content in an aggregate and the risk of concrete deterioration due to pyrrhotite oxidation. In these studies, magnetic susceptibility, χ was monitored as the sample was heated from room temperature to 700°C for: (a) magnetite (Fe_3O_4), (b) Fe-rich pyrrhotite (hexagonal, from x = 0, i.e., FeS troilite to x < 0.1 of $Fe_{1-x}S$, where Fe-vacancies in the lattice are arranged in several superstructures), (c) Fe-poor pyrrhotite (monoclinic, up to Fe_7S_8 for x=0.125 having higher concentration of Fe-vacancies in the crystal lattice) showing relative changes in magnetic susceptibility, χ, normalized to the room-temperature susceptibility ($\chi^{20°C}$), (d) mass-normalized χ of a commercial pyrrhotite-free Quikrete mix containing magnetite; and, (e) a field concrete powder from a distressed foundation in Connecticut containing mixtures of Fe-rich and Fe-poor pyrrhotites and magnetite.

Since pyrrhotite is a strongly ferrimagnetic mineral with a Curie-temperature (T_C) of 325°C and several diagnostic phase transitions, the variation in magnetic susceptibilities between room-temperature and 700°C was measured, which served as a rapid and sensitive semi-quantitative indicator of pyrrhotite in aggregate or concrete samples.

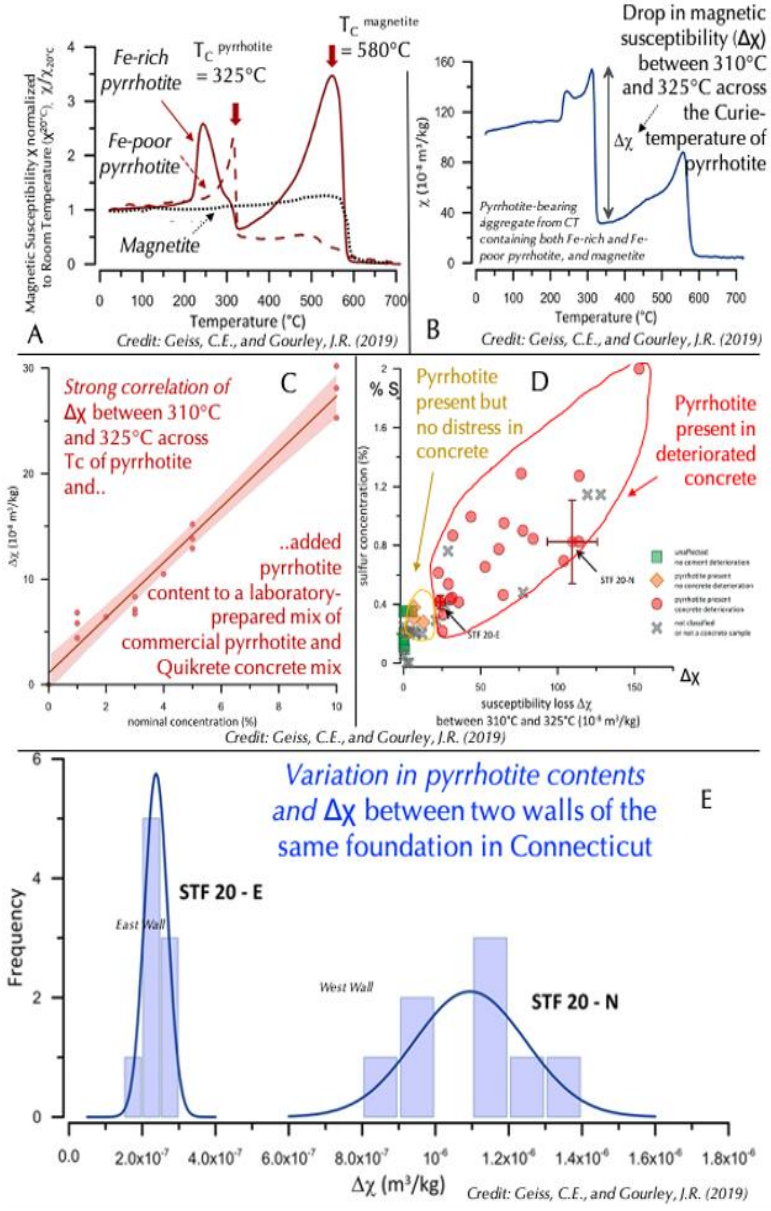

Figure 5. Thermomagnetic studies of Geiss and Gourley (2019) on: (a) the sharp drops in magnetic susceptibility (χ) of Fe-rich and Fe-poor pyrrhotites across their Curie-temperatures (T_C) at 325°C after reorganizations of their Fe vacancies to cause a sharp increase in their room temperature-normalized χ values before reaching the T_C (Plot A); (b) strong correlation of the magnitude of this drop of χ across 325°C (Δχ) to the pyrrhotite content in a series of controlled mixtures of pyrrhotite and proprietary sand-cement grout (Plot C); (c) similar drop in χ of a field concrete from Connecticut containing both Fe-rich and Fe-poor pyrrhotite and magnetite in Plot B, where Δχ can be used as a semi-quantitative measure of pyrrhotite abundance, e.g., from calibration of Δχs with different pyrrhotite contents mixed to a proprietary grout mix as shown in Plot C as long as pyrrhotite of similar crystallographic properties is used; or (d) correlation of Δχs with sulfur content in aggregate as shown for field samples from Connecticut in Plot D. Plot E shows variations in calculated pyrrhotite contents from Δχ across two walls of the same foundation indicating inherent variations in pyrrhotite contents in aggregates from high content-low scatter at the east wall to low content-high scatter at the west wall.

The results of Geiss and Gourley's (2019) studies showed the following:

a) For magnetite (dotted black line in Figure 5, Plot A from Geiss and Gourley, 2019), the magnetic susceptibility χ remains relatively constant until the sample reaches T_C at 580°C (demarking the loss of permanent magnetic properties) after which χ decreases sharply and is near zero for $T > T_C$. Fe-rich pyrrhotite (solid red line in Figure 5, Plot A) displays constant χ until about 240°C and then undergoes a reorganization of Fe-vacancies (the λ-transition), which increases χ until the newly formed phase undergoes further reordering and phase transition at 265°C. The final T_C is reached at 325°C with a sharp drop in χ. In Fe-poor pyrrhotite (dashed red line in Figure 5, Plot A), reorganization of Fe-vacancies leads to a progressive non-reversible increase in χ between 260°C and 310°C and then displays a sharp drop in χ at $T_C \approx 325$°C. At higher temperatures, the Fe-rich pyrrhotite is chemically more unstable than the Fe-poor variety and converts to magnetite with $T_C \approx 580$°C.
b) The thermomagnetic curve of a pyrrhotite-bearing aggregate from a distressed concrete in Connecticut displayed the clear pyrrhotite signal (Figure 5, Plot B). χ is relatively constant at $T < 220$°C, when it increases sharply to reach a peak at $T \approx 240$°C, and an even higher peak at $T \approx 310$°C. Both increases are irreversible at the heating rates due to a re-ordering of Fe-vacancies and a corresponding change in ferrimagnetic properties. χ then decreases sharply between 310 and 325°C. Upon further heating, χ rises gradually due to the formation of magnetite to a peak at $T \approx 560$°C and then drops sharply to near zero by $T_C \approx 580$°C, the Curie temperature of magnetite. The pyrrhotite present in this sample is a mixture of Fe-poor and Fe-rich varieties, and the resulting thermomagnetic curve is a mixture of the two pyrrhotite curves.
c) The drop in magnetic susceptibility ($\Delta\chi$) between 310°C and 325°C across the T_C of pyrrhotite can be used as a semi-quantitative measure of the pyrrhotite abundance, if the investigated pyrrhotites have similar chemical compositions and crystallographic superstructures as the ones used for calibration of $\Delta\chi$ versus pyrrhotite content, e.g., as the one shown in Figure 5, Plot C. This is for a series of laboratory-prepared mixtures from a pyrrhotite-free control Quikrete concrete mix with various dosages of a commercial pyrrhotite sample, which showed an excellent correlation ($r^2 = 0.96$, $n = 15$).
d) For pyrrhotite-bearing aggregates in Connecticut, such abundance estimates, however, are semi-quantitative at best, since the susceptibility of pyrrhotite depends on several factors including chemical purity, crystal size and shape, and the ordering of Fe-vacancies across basal layers, which can introduce wide variations in susceptibilities from different localities unless aggregate samples are taken from the same location. Even for the same foundation, however, $\Delta\chi$ and the resultant pyrrhotite abundance can vary as shown for pyrrhotite-aggregates from two walls of a foundation in Connecticut in the histograms in Figure 5, Plot E, showing less pyrrhotite (at lower $\Delta\chi$) but less variability from the east wall as opposed to higher pyrrhotite (larger $\Delta\chi$) and more variability (larger spread in $\Delta\chi$) for samples from the west wall.
e) Due to inherent variations in pyrrhotite contents between aggregates, along with variations in magnetic susceptibility of pyrrhotite with its own compositional and structural variations, when $\Delta\chi$ across the T_C of pyrrhotite is plotted with the total sulfur content for 50 concrete and natural samples, the data displayed considerable scatter (r^2

= 0.754, n = 44) in Figure 5, Plot D. Green squares denote samples that show neither signs of concrete deterioration or evidence of pyrrhotite. Red circles denote samples that show distinct signs of concrete deterioration and do contain pyrrhotite. Orange diamonds denote samples that do contain pyrrhotite as deduced from thermomagnetic data but, at this point, do not show any signs of concrete deterioration. Gray crosses denote samples for which no information on concrete deterioration is available. Despite these variations between individual walls and between subsamples from the same core, pyrrhotite was clearly identified in every thermomagnetic curve. Given the variability of sulfur and pyrrhotite concentrations within a foundation, it is recommended that more than one core is analyzed per structure.

f) In combination with measurements of total sulfur concentrations, pyrrhotite concentrations as low as 0.1% can be detected. The analysis can aid in the quantification of risk of internal sulfate attack due to the presence of pyrrhotite. However, the calibration curve is valid for pyrrhotites with similar chemical compositions and crystallographic superstructures. In the case studied, this method was used to determine the amount of pyrrhotite in deteriorated concrete from Connecticut.

Nuclear Magnetic Resonance (NMR) Relaxation

Bastow and Hill (2018) reported detection of pyrrhotite (Fe_7S_8) in mining of iron sulfide ores by ^{57}Fe NMR spectroscopy in zero applied field using two different methods, with both yielding a peak signal at 42.03MHz. NMR relaxometry is considered as a robust and resilient nondestructive tool for detecting pyrrhotite and identifying pyrrhotite-related degradation (Balachandra, 2020).

Staining and Chemical Analysis

Besides XRF, sulfate content in concrete can also be determined from conventional wet chemistry, e.g., according to the procedures of ASTM C 114, or other instrumental techniques, such as atomic absorption spectroscopy (AAS) or inductively coupled plasma atomic emission spectroscopy (ICP-AES). Alternately, concrete sulfate content can be estimated from the sulfate content of the Portland cement (typically 3% SO_3) and the usual cement dosage (15% by mass of normal weight concrete) used for residential foundations, when the only source of sulfur in the aggregate is from sulfide minerals.

Mielenz (1963) mentioned two staining procedures for detection of potentially deleterious iron sulfide phases in aggregates, e.g., a qualitative chemical test by Midgley (1958), and a semi-quantitative chemical test by Seaton (1948). The Midgley procedure is very rapid, involving the immersion of suspected particles in saturated lime water and observation for the formation of blue-green ferrous sulfides that turn brown on exposure to air. The reactions are completed within 30 min. According to Midgley, lack of such reactions in 30 min. indicates that the ferrous sulfides are absent or are not potentially deleteriously reactive in concrete. Mielenz has applied this test to numerous samples of pyritiferous dolomites, limestones, diabases, and metamorphic rocks where none proved to be reactive by these criteria, whereas

pyrite in a shale particle taken from an iron-oxide-stained pop-out in concrete proved to be reactive. The Seaton procedure involves exposure of a portion of the aggregate in a steam bath for 16 hours, after which the degree of staining resulting from the liberation of iron compounds is noted and the proportion of such compounds is determined by partial chemical analysis.

Ramos et al. (2015) described a series of attempts to define the most accurate staining method by testing the efficiency of ASTM C 641 and the Midgley test, but also by optimizing them, namely by using different oxidizing reagents. The use of 6% bleach was able to correctly identify the oxidation potential of the investigated aggregates when used as reagent in the Midgley test.

Oxygen Consumption, Oxidation Rate, and Oxidation Potential Tests

Elberling et al. (1994) devised an oxygen consumption test to evaluate sulfide oxidation rates, where sealed columns containing a mixture of quartz sand and pyrrhotite and overlain with varying thicknesses and grain sizes of a nonreactive layer, were subjected to oxygen flux. The overall rate of oxidation of pyrrhotite was reduced when a fine-grained layer was used due to the high water saturation condition of the fine grain sizes. Total sulfate produced in water over time from oxidation was also measured.

Rodrigues et al. (2012b) hand-picked several pyrrhotite-bearing grains of 2.5 to 5 mm particle size from crushed anorthositic gabbro collected from a quarry near Trois-Rivières (where pyrrhotite was associated with inclusions of chalcopyrite and pentlandite), along with pure pyrite, magnetic pyrrhotite, and chalcopyrite minerals and each with their associated other sulfide inclusions. Grains were first examined in epoxy-encapsulated polished sections in an ore microscope, which detected the main and associated sulfide phases and their characteristic textures, then separate grains were mounted on a thin layer of epoxy resin. This was subjected to different conditions of temperature (4°C, 38°C and 60°C), relative humidity (60% and 80%), and wet/dry cycles in two oxidizing solutions (bleach (pH 11) and hydrogen peroxide (pH:6). After four months of reaction, all samples were examined by stereomicroscope and SEM-EDS in order to identify the generated oxidation products. The oxidation rate was found to be dependent on the temperature and relative humidity conditions. At 60°C, surfaces of the sulfide minerals are much more oxidized and huge amounts of rust (secondary reaction products) were observed. At 4°C, almost no sign of rust was observed on sulfide surfaces. SEM/EDS analysis confirmed the near absence of products resulting from oxidation reaction. The use of oxidizing agents promoted oxidation of sulfides. In their experiment, sodium hypochlorite was the most effective oxidizing agent due to its alkaline pH (near 11). Because oxidation reactions were favored in high pH conditions, the high pH of pore solutions of concrete were judged to be favorable for sulfide oxidation.

As an extension of the approach of Elberling et al. (1996), Rodrigues et al. (2016) proposed an oxygen consumption test to assess the oxidation potential of pyrrhotite-bearing aggregate, where seven sulfide-bearing aggregates, one iron sulfide mineral, and three control aggregates of no or trace sulfide, were used to determine the test parameters that can effectively discriminate sulfide aggregates from their oxygen consumption rate. A compacted layer of finely ground sulfide-bearing aggregate was exposed to oxygen (O_2) in a hermetically sealed plexiglass column (200 mm high, 141.7 mm ID) sealed with a plexiglass cap in the upper part allowing a head/air space above the ground material to act as a reservoir for oxygen. The O_2

consumption was monitored with a galvanic-cell type oxygen sensor capable of measuring 0-100% oxygen in the air space. The determined optimized parameters all of which showed strong influence on oxygen consumption rate included: (i) a 10 cm compacted layer of ground aggregate with 50% porosity; (ii) a particle size <150-μm: the smaller the particle size tested the higher was the oxygen consumption values due to increased surface area exposed to oxidation, which is consistent with the findings of Divet and Davy (1996) and Janzen et al. (2000); (iii) a 40% saturation degree: oxygen consumption was very low at a higher tested saturation degree of 60% for development of a water film on the ground material within 30 min. of initiation of the test; with (iv) a 10-cm headspace (air volume) left at the top of the cell; and (v) a test period of oxygen consumption monitoring in the headspace of over 3-hours (after 30 minutes of probe initialization) at 22°C. The test was able to effectively discriminate the eight sulfide-bearing samples from the three control aggregates when a threshold limit of 5% oxygen consumption was used. In general, the highest values of oxygen consumption were obtained for the aggregates with the highest total sulfur contents.

Guirguis and Shehata (2017) described a screening test for oxidation potential of coarse aggregates in concrete, which involved submerging an aggregate in an oxidizing agent and measuring the mass loss. From 30 aggregates tested, samples with no known oxidizable sulfides showed a mass loss of < 1.0% after one week of testing at room temperature. Samples of oxidizable sulfides showed a mass loss higher than 3.5% and changes in the color of the test solution. It is proposed that aggregates which achieve a mass loss of less than 0.50% and no color change in the test solution be accepted.

Marcelino et al. (2020) developed a testing procedure to evaluate how reactive is a sulfide-bearing aggregate for use in concrete. The test aggregates were produced from iron sulfide rocks that had at least 1.5% of sulfur determined by a direct combustion test. Particle sizes between 0.15 and 4.80 mm were selected, and the exposed surface of each sulfide-bearing aggregate was calculated using an SEM connected to an automated image analysis system (Mineral Liberation Analyzer). Samples were also immersed in an H_2O_2 solution, and the released sulfate (from the sulfide oxidation) was quantified. The results showed that the larger the exposed sulfide surface and the smaller the particle size, the more effective its oxidation and consequently the more reactive the aggregate.

Wille and Zhong (2016) submerged pyrrhotite-bearing aggregates quarried from eastern Connecticut in 40% hydrogen peroxide solution to accelerate the oxidation process. The aggregate-soaked oxidizing solution was collected twice a week for a period of 30 days. Each aliquot was diluted ten times with deionized water (to improve the sulfate signal) and tested by ion chromatography (IC) to determine the evolution of sulfate concentration due to progressive oxidation of pyrrhotite. In their test, sulfate concentration normalized to aggregate weight (to eliminate any influence of aggregate size) showed a significant increase during the 30-day test period, e.g., from 0 to 15 ppm/g, whereas sulfate release from a control aggregate containing no iron sulfide minerals remained negligible during the entire test period.

Jana (2020, 2022) hand-picked several unsound pyrrhotite-bearing aggregates from lapped cross sections of concrete cores after determining suitable candidates of pyrrhotite-bearing crushed gneiss aggregates from reflected-light microscopy depicting various degrees of oxidation of pyrrhotite. The degrees of oxidation ranged from the finely disseminated non-oxidized forms to the ones in association with biotite showing fine striations and the banded nature of oxidized and non-oxidized bands of pyrrhotite. Pyrrhotite-bearing crushed gneiss coarse aggregate particles were either separated from saw-cut sections and cleared of all

adhering paste or drilled out with a benchtop drill press with fine-tip diamond drills from various particles across a lapped cross section. Ground aggregates were digested in 35% hydrogen peroxide solution, filtered out at various days for a total test period of 21 days. The filtrates were diluted 10 times and measured by ion chromatography for sample weight-normalized sulfate concentrations. Released sulfate levels from all aggregates selected were higher than those of Wille and Zhong's (2016) tests on quarried aggregates, with variations in sulfate release between the aggregate types, e.g., sulfates released from light brown muscovite-biotite-gneiss were noticeably higher than those released from dark gray gneiss particles. A control crushed gneiss aggregate without any pyrrhotite showed no release of sulfate during the test period.

Length Change Measurements of Mortar Bars and Concrete Specimens

Various authors have investigated the expansion potential of pyrrhotite-bearing aggregates using length change measurements of mortar bars and concrete according to ASTM C 157, containing both control and potentially unsound aggregates, subjected to various test conditions, some of which are presented here chronologically since the 1950s.

Having noticed some concrete deterioration problems involving sulfide-bearing aggregates in Sweden in the early 1950s, Hagerman and Roosaar (1955) described a method where aggregate was incorporated in concrete beams fitted with terminal gage studs. The beams were subjected to laboratory testing or outside storage for periods of up to several months, during which time the dynamic modulus of elasticity and length change were measured. To determine the maximum tolerable pyrrhotite content in concrete aggregates, they used aggregates from Pengfors (pyrrhotite contents of 4% and 14%), Norrforsen (21% of pyrrhotite), and Stockholm (control non sulfide-bearing granite). They manufactured a series of concrete beams, 80 × 15 × 10 cm and 40 × 15 × 10 cm in size, which they subjected to a range of test conditions, including weekly cycles consisting of 3 days in warm water and 4 days of air storage at 75°C, 3 days in water and 4 days in air both at room temperature, or continuous outdoor exposure. Alternatively, some beams were subjected to steam curing in an autoclave at 225°C for 5 h. The specimens were then allowed to cool to 100°C in the autoclave, and then exposed to warm water to progressively bring their temperature down to 23°C. This treatment was repeated four times at approximately 1-week intervals. Between autoclaving sessions, the specimens were stored in air at room temperature. After 7 months of testing, the series of beams (80 × 15 × 10 cm) made with aggregates incorporating a higher percentage of pyrrhotite (Pengfors 14% and Norrforsen 21%) and stored in warm water for 3 days followed by 4 days of air exposure at 75°C, showed the presence of rust, cracks and bending. The examination of broken surfaces of the beams made with the Norrforsen rocks revealed more damage at the end of testing and also that the rusty aggregate particles were limited to the first 10 mm from the surface. Further petrographic examination of thin sections confirmed the presence of sulfide oxidation, together with staining in the cracks. Ettringite was not observed. Beams in which the aggregate contained 14% of pyrrhotite expanded about 0.6% in outside exposure during a period of 2½ months.

Berard et al. (1975) investigated oxidation reactions of sulfide-bearing shale in coarse aggregates in Montreal, Canada, containing 4.5% pyrrhotite. Prisms were prepared by using shale aggregates and were subjected to the wetting cycle in a moist room for 1 week and then

switched to a dry-room for the drying cycle. They prepared 10 concrete prisms with different proportions of shale particles recycled from the deteriorated concrete elements (maximum aggregate particle size of 2 cm), and 10 companion prisms with shale particles obtained from the original quarry (maximum aggregate particle size of 4 cm). They then subjected the concrete prisms to cycles of wetting in a moist room at 23°C for a certain period of time and drying in air in the laboratory for an equal period of time. Results showed that the prims expanded with the presence of cracking and rusting near the surface at 46 weeks. All specimens suffered shrinkage, while one specimen showed a longitudinal crack with iron oxide seeping through the crack. Although the test was unable to reproduce the distress observed in the field (expansion/cracking), the deleterious properties of the shale were somewhat highlighted since some shale particles near the surface of the test prisms generated pop-outs through the oxidation of pyrrhotite mainly visible along bedding planes. In addition, five blocks/cubes, with an initial length of 4 cm and cut from the shale, were subjected to different test conditions and their expansion perpendicular to bedding was monitored over time. Two test cubes immersed in water expanded by more than 0.2% in less than 100 days. Two other test cubes kept outdoors expanded only slightly and less than the first two cubes. A fifth specimen, kept indoors at room temperature, showed slight shrinkage. Oxidation of sulfides was visible in all the specimens and was concentrated along the bedding planes.

Oberholster et al. (1984) investigated the conditions responsible for the deterioration of concrete houses in Penge, South Africa by cutting various sets of test prisms from deteriorating bricks, as well as casting blocks using the same aggregate from Penge. For the latter, two mix designs were used, namely aggregate-to-cement ratios of 5:1 and 10:1, and these were combined with two manufacturing processes, i.e., well compacted, and poorly compacted. Some prisms were stored at 38°C, either under water or above water in sealed containers. The test prisms that were cut from the bricks and stored under water expanded approximately 0.40% after 1,000 days, although the amount of expansion was much less than for those stored above water, i.e., more than 1% after 1,000 days. Some manufactured prisms stored above water started expanding at a high rate after 22 months, while those stored under water did not expand even after 3 years. Also, in the case of laboratory-made concrete prisms, only those incorporating low cement contents (i.e., aggregate: cement ratio of 10: 1) expanded, while well-compacted prisms expanded at a higher rate than poorly compacted ones. The presence of ettringite was reported in the laboratory-made prisms that expanded.

Chinchón et al. (1990) reported results of a study aimed at evaluating phase changes in cement-based mortars incorporating sulfide-bearing rocks. Two sets of mortars were made, consisting of 85% limestone (with 4.2% hexagonal pyrrhotite and 0.7% pyrite), or shale (with values of pyrrhotite and pyrite unknown), 15% P 450 Portland cement and 20% water (by mass). A series of 15g mortar specimens were thus separated into porcelain capsules and maintained at 20°C and 97% R.H. for a 140-day period. A reduction in the pyrrhotite and pyrite contents, along with a large production of ettringite was noted over that period. The appearance of ettringite was slower in the mortars incorporating limestone aggregate. The authors have concluded that the formation of ettringite resulting from the reactions between iron sulfide oxidation products and cement paste hydration products caused the observed mortar deterioration.

To investigate the ‘mundic’ problem of pyrite oxidation in Cornwall and Devon, England, Lugg and Probert (1996) did experiments by subjecting concrete cores to 100% RH at 38°C for 250 days. Cores showing an average expansion upon wetting exceeding 0.075% at 7 days were

considered to have failed the test; on the other hand, if the expansion was less than the above limit, the test had to be pursued for up to 250 days. It was concluded that core specimens showing an expansion lower than 0.025% over the remaining part of the 250-day test period were likely to remain stable under ambient conditions for many years provided that normal levels of care were maintained.

Gomides (2009) in Brazil investigated the performance of concretes incorporating sulfide-bearing aggregates and five types of cements. In Stage 1 of the experimental program, concrete mixtures with a fixed water-cement ratio of 0.45 were prepared with a quartz–muscovite–schist aggregate containing 3.89% of sulfides, i.e., 3.40% pyrrhotite, 0.31% pyrite and 0.17% marcasite. Three types of cements were used, i.e., a reference cement (CP II-F-32) and two cements resulting from the partial replacement of CP II-F-32 by 40% (CP40) and 60% (CP60) of ground granulated blast-furnace slag. In Stage 2, the same aggregate, but with 0.56% of sulfides, was used with three types of cements, specifically: CP II-F-32, CP III-40-RS (sulfate resistant cement) and CP IV-32 (having in its composition pozzolanic binder (25% to 40%) and 38% of fly ash). The aggregate used in Stage 2 was the same as used in Stage 1, but it was stored outdoors in steel drums, i.e., subject to all kinds of weathering conditions, during a period of 2 years. After those 2 years of storage, the aggregate in question had lost approximately 86% of its sulfide content due to an oxidation process, with a remaining/residual sulfide content of 0.56%, i.e., 0.29% pyrrhotite and 0.27% pyrite. Concrete specimens cast in the study consisted of prisms (75 mm × 75 mm × 285 mm in size) and cylinders (100 mm in diameter × 200 mm in height). After casting, all specimens were stored in a humid chamber at 23 ± 2°C and relative humidity ≥ 90% for a period of about 5 years. The results showed that pyrrhotite was the most reactive sulfide in the system. In the specimens from Stage 1, external spots of rust, white efflorescence, scaling and disintegration of aggregate particles containing high levels of sulfides were observed. These features of deterioration resulted from the oxidation of sulfides and were more pronounced in the concretes containing higher proportions of ground granulated blast-furnace slag (CP40 and CP60). The concretes prepared in Stage 2 showed no visible signs of distress. In general, the concrete showed the presence of typical deleterious products of sulfate attack, i.e., ettringite and gypsum, with higher concentrations of these products being observed in CP40 and CP60 concretes. No information was given about the concentration of ettringite and gypsum observed in the Stage 2 specimens. The expansion values calculated after five and a half years of testing reached a maximum value of 0.052% for the CP60 mix, and a maximum value of 0.041% for the CPIII mix after four and a half years of testing, suggesting that the higher the concentration of sulfides and aluminate ions present in the system, the greater the expansion or the observed levels of deterioration.

To recreate the deterioration mechanism responsible for the damage in a concrete dam in Switzerland, constructed in the beginning of the 1970s, Schmidt et al. (2011) prepared concrete prisms, 70 × 70 × 280 mm in size with the same aggregate that was utilized in the dam construction. The cement utilized was an ordinary Portland cement (CEM I 42.5), with a water-to-cement ratio of 0.50, with a cement content of 280 kg/m^3 and an aggregate content of about 1,900 kg/m^3. The prisms were stored in water for 5 years at 60°C. Unfortunately, the degree of expansion could not be assessed accurately; however, petrographic and SEM/EDS analyses were performed on the prisms after 4 years of storage. The laboratory concrete specimens had the same appearance and pattern of the reaction as the dam concrete, but the extent of reaction of the iron sulfides was much lower. The reaction products observed were the same in both specimens, i.e., iron oxide, iron hydroxides and ettringite. These observations clearly indicated

a very slow reaction rate of the iron sulfide inclusions under the immersion conditions used for testing, and the difficulties in identifying the right conditions to reproduce the specific iron sulfide degradation in the laboratory.

Rodrigues et al. (2015) conducted accelerated mortar bar tests (modified ASTM C 1260 method) where mortar bars (w/c of 0.65) 25 by 25 by 285 mm in size were subjected to different conditions of temperature, relative humidity, immersion in bleach and drying cycles and by storing at 23°C, 38°C, 60°C, and 80°C with 60% and 80% RH, then submersing in the oxidizing solution for 3 hours followed by air drying for 3 hours. This cycle was repeated 1 and 2 times a week for 12 weeks or 90 days. Bars containing iron sulfide bearing aggregates showed signs of distress, whereas bars without iron sulfide did not show any distress. Their two-phase mortar bar protocol consisted of: (a) 90 days of storage at 80°C/80% RH, with two 3 h wetting cycles per week in a 6% sodium hypochlorite (bleach) solution at 23°C (Phase I) to promote oxidation-related expansion, which was then followed by (b) up to 90 days of storage at 4°C/100% RH again with two wetting cycles in a 6% bleach solution (Phase II) to recreate thaumasite formation-related deterioration observed in the concrete structures of the Trois-Rivières area. This requires a low temperature and a carbonate source. Aggregates with oxidation potential presented an expansion of over 0.15% at 90 days during Phase I, while thaumasite formation potential at low temperature (from thin iron carbonate coats on iron sulfide minerals in anorthositic gabbro host) was detected by rapid regain of expansion, followed by destruction of the samples during Phase II. The control aggregates without sulfide mineral did not show any signs of deterioration in both phases of the testing program.

Guirguis et al. (2018) investigated the effects of supplementary cementitious materials (SCMs) on the expansion of mortars containing iron sulfide-bearing aggregates. In their oxidation mortar bar test, cementing systems containing low-calcium fly ash, metakaolin, slag, high-sulfate resisting Portland cement, or a Portland cement of low heat of hydration, showed a reduction in expansion by 50–85%. Mechanisms behind the reduced expansion are suggested to be the more refined pore structure of samples with SCMs, and the reduced C_3A in Portland cement of low heat of hydration. The refined pore structure reduces the permeation of the oxidizing solution into the samples. The similarity of this to penetration of oxygen into concrete under field exposure needs to be determined. For samples containing reactive alumina in SCMs, such as metakaolin, soaking the samples for greater than 3 h in the oxidizing agent produced excessive expansion, which was unrelated to oxidation of iron sulfide phases.

Marcelino et al. (2019) evaluated long-term behavior of mortar bars produced with ground aggregates (1: 2.25 by weight of cement: aggregate, and w/c of 0.47) containing pyrite and pyrrhotite from the Irapé Hydroelectric Power Plant area in Minas Gerais, Brazil. The plant was built in a geological site having sulfide concentrations of at least 3% with a predominance of pyrrhotite. During the almost 1,300 day long tests, mortar bars were subjected to three different exposure conditions: (a) 23° ± 2°C and 95 to 100% RH; (b) submerged in calcium hydroxide solution diluted in water, for almost 850 days and then kept in water up to 1,300 days, both at room temperature; and (c) submerged in calcium hydroxide solution diluted in water at 50°C for almost 850 days and then kept in water (at 50°C) for up to 1,300 days. The expansion caused by the iron sulfide oxidation, as well as the content of each sulfide were evaluated over time. The presence and amount of pyrrhotite were obtained from a leaching process of the material (aggregate or mortar) in a solution of hydrochloric acid (Marcelino et al., 2016). This procedure also allowed the evaluation of the pyrite content over time. The results showed that the calcium hydroxide solution speeds up the expansion process just like

temperature. It was also observed that the amount of pyrite remained virtually constant over time in the three exposure situations. This finding indicates that sulfur limits in aggregates should be set according to the type of iron sulfide present and not only by the total amount of sulfur.

To further accelerate the test, Saengsoy et al. (2020) considered other factors, e.g., aggregate size (0.15 to 4.75 mm), storage temperatures (50°C, 60°C, and 80°C) and number of wet-dry cycles (4 cycles per week, and 7 cycles per two weeks) that can accelerate the oxidation reaction of iron sulfides. In their studies of mortar bars made using pure pyrrhotite (PR), pure pyrite (PY), aggregate with pyrite (CB), and a control limestone aggregate without sulfide mineral (NA), the pyrite-bearing aggregate bar showed maximum expansion, even more than that of pure pyrrhotite.

Laboratory Studies of Deteriorated Concrete Foundations from Eastern Connecticut, USA

Petrographic Examinations

The most devastating occurrence of pyrrhotite oxidation-related deterioration has occurred as extensive cracking and crumbling of numerous concrete foundations in the eastern US where as many as 35,000 residential concrete foundations in eastern Connecticut and 10,000 more in Massachusetts are in danger of potential collapse from slow and progressive cracking due to pyrrhotite oxidation in the crushed gneiss coarse aggregates. The author's laboratories have been at the forefront of extensive investigation of pyrrhotite oxidation-related distress in many residential concrete foundations across various counties in eastern Connecticut that are within the 'epicenter' of pyrrhotite distress in the US (Figure 4). In most cases, cores were drilled horizontally through concrete foundation walls with variable distresses, traversing the full wall thickness, i.e., from the exposed face in the basement interior to the exterior face situated above or below external grade. Concrete floor slabs are reportedly less affected than the walls (Wille and Zhong, 2016).

Figure 6 shows the typical appearance of a cracked foundation wall (many others shown on Figure 4) and a core drilled over a visible crack where almost the entire length of the core is cracked extensively, sometimes to the extent of turning a core into rubble. Figure 7 shows fluorescent epoxy-impregnated lapped cross sections of a core scanned on a flatbed scanner, where prior to scanning both macro and microcracks were highlighted in red marker while observing in a stereo microscope (Photo A). This is followed by observing the section with a UV light (395 nm wavelength) in a dark room to preferentially highlight all cracks and voids that are filled with the fluorescent epoxy (Photo B). A companion saw-cut section cut parallel to the lapped section is then selected for preparation of two large-area (50 mm by 75 mm) thin sections from opposite ends of the core section, marked (Photo C) for trimming, grinding, gluing to a frosted glass slide, followed by precision sectioning and grinding in the thin sectioning steps (Jana, 2006). Two final blue dye-mixed epoxy-impregnated thin sections are shown in Photo D. All these steps are followed during petrographic examinations of any sample collected from distressed foundations. Figure 8 shows the extent of cracking throughout the depth of distressed cores where crack paths are traced with a red marker along with potentially

unsound crushed gneiss coarse aggregate particles after examining the section on a stereomicroscope.

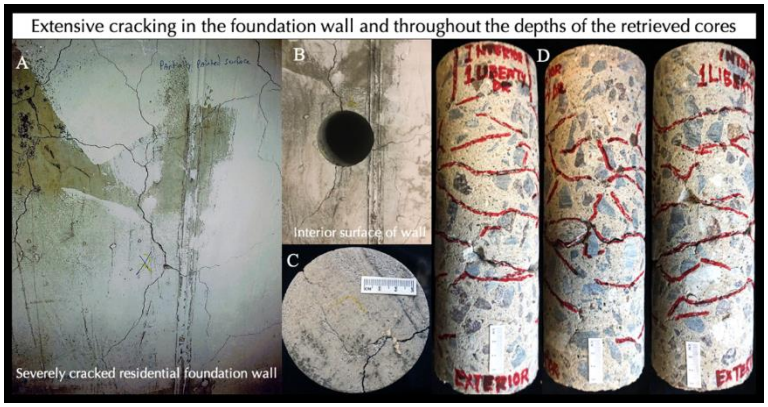

Figure 6. A typical investigation starts with field survey of cracks on the concrete structure as shown in Photo A, from a cracked concrete foundation wall in eastern Connecticut. A suitable location shown in Photo B, preferably at the intersection of cracks, is then selected for wet-drilling a 4-in. (100-mm) diameter core through the entire thickness of the wall. Surface cracks in the foundation wall are present on the core top as shown in Photo C from which longitudinal cross sections perpendicular to the top exposed end are made. Cores retrieved from severely cracked foundation walls are first examined to trace all visible cracks on the cylindrical surfaces as shown in Photo D. In severely distressed locations, cracks are usually present through the entire thickness of the wall as seen in Photo D. Unlike ASR-related distress, where many cracks are preferentially located at the exposed surface regions as tensile cracks due to internal expansion of concrete, cracks from pyrrhotite oxidation-related distress, however, can occur both at the surface ends, as well as in interior concrete without any preferential location as seen in Photo D.

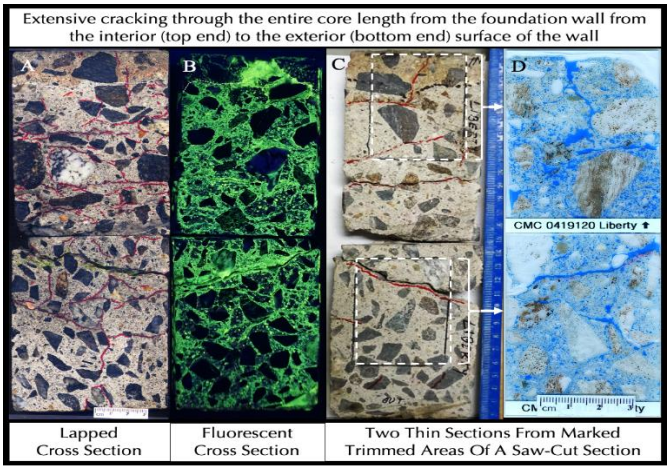

Figure 7. Longitudinal cross section of a core from a distressed foundation wall in eastern Connecticut (Jana, 2022) showing (from left to right): (a) extensive cracking throughout the entire depth, with cracks marked in red, and, depth of carbonation from the interior wall surface, which is marked with a white dashed line at the top (Photo A); (b) low-viscosity fluorescent dye-mixed epoxy-impregnated lapped cross section seen in UV light where the carbonated zone is dark due to densification of paste, and aggregates are also dark due to their inherent dense nature, whereas fluorescent epoxy-filled paste, air voids, and cracks are illuminated in UV light (Photo B); (c) two rectangular areas selected on a saw-cut section in Photo C for trimming and preparation of blue dye-mixed epoxy-impregnated thin sections, which are shown in Photo D; where (d) cracks, air voids, and porous areas in paste are highlighted by the blue epoxy due to preferential absorption of epoxy in those locations compared to aggregates and denser regions of paste.

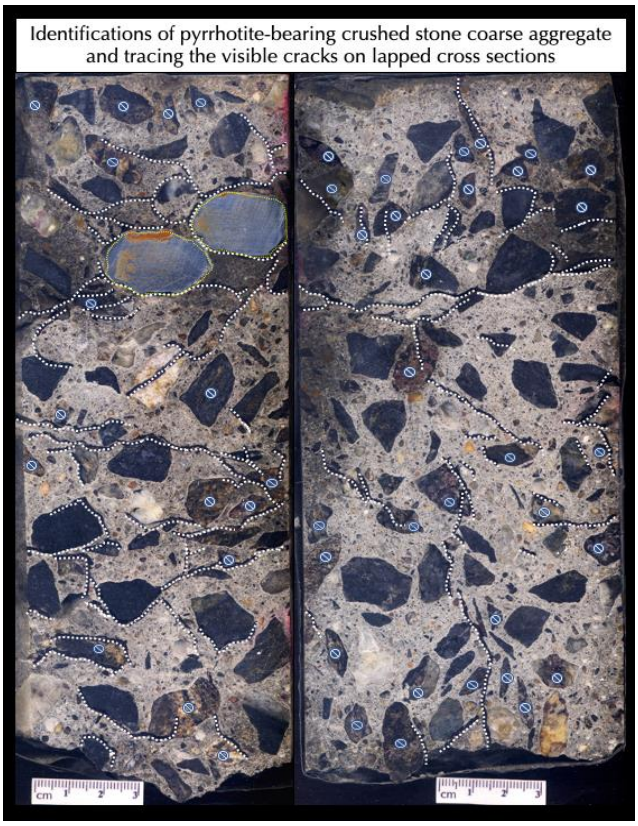

Figure 8. Lapped cross sections from a core from a distressed foundation in eastern Connecticut are examined in a low-power stereomicroscope to trace all visible cracks (shown in white dotted lines) as well as the pyrrhotite-bearing potentially unsound crushed stone coarse aggregate particles where particles with known detection of pyrrhotite from stereomicroscopical examinations are marked for further examination.

Examinations in a Stereomicroscope

Stereomicroscopical examinations of lapped cross sections showed fine striations on oxidized pyrrhotite grains (Figures 9 and 10) along with reddish-brown oxidation products around many oxidized grains and sometimes migration of oxidation products along the crack paths (Figure 11). Further examinations detected mixtures of three different color tones of crushed stone coarse aggregate particles consisting of: (a) dominant dark gray to black crushed gneiss consisting of parallel alignment of quartz, albite feldspar, biotite mica, and occasional pyrope garnet porphyroblasts, anhedral to subhedral equigranular to gneissose arrangement of minerals; (b) subordinate light to medium brown crushed granite gneiss of quartz, albite feldspar, garnet, biotite mica and occasional pyroxene (augite) grains; and (c) minor white crushed granite gneiss with quartzo-feldspathic minerals and black specks of mica flakes in parallel alternate (gneissose) arrangements. Coarse aggregates belong to the Ordovician Brimfield Schist formation and came from a quarry on a hydrothermal vein of significant pyrrhotite crystallization. The geology in the vicinity of the quarry is made up of metamorphic rocks of Brimfield Schist consisting predominantly of gray, rusty brown to orange-yellow weathered, medium to coarse grained, interlayered foliated schist and gneiss, granofels, and foliated quartz diorite. Quartz, plagioclase or oligoclase are primary minerals with micas, garnet

and pyrrhotite as common accessory minerals. Brown and dark gray gneiss usually contain more iron sulfide and iron oxide minerals than the minor white granite gneiss. All particles are angular, dense, hard, and medium to dark gray to brown, schistose to gneissose-textured, equidimensional to elongated, variably altered, uncoated, and variably cracked. Coarse aggregate particles are well-graded and well-distributed. There is no evidence of alkali-aggregate reactions of coarse aggregates in concretes that have shown pyrrhotite oxidation-related distress. Similar to the predominant dark gray to brown pyrrhotite-bearing gneiss that has shown pyrrhotite oxidation and distress, some dark gray to brown unsound pyrrhotite-bearing garnetiferous quartzo-feldspathic gneiss particles are also detected in many other residential foundations in eastern Connecticut compared to the lighter colored (white with black specks of mica) granite gneiss, which contained the disseminated unsound pyrrhotite grains (Figure 12) that cause extensive micro and macrocracking.

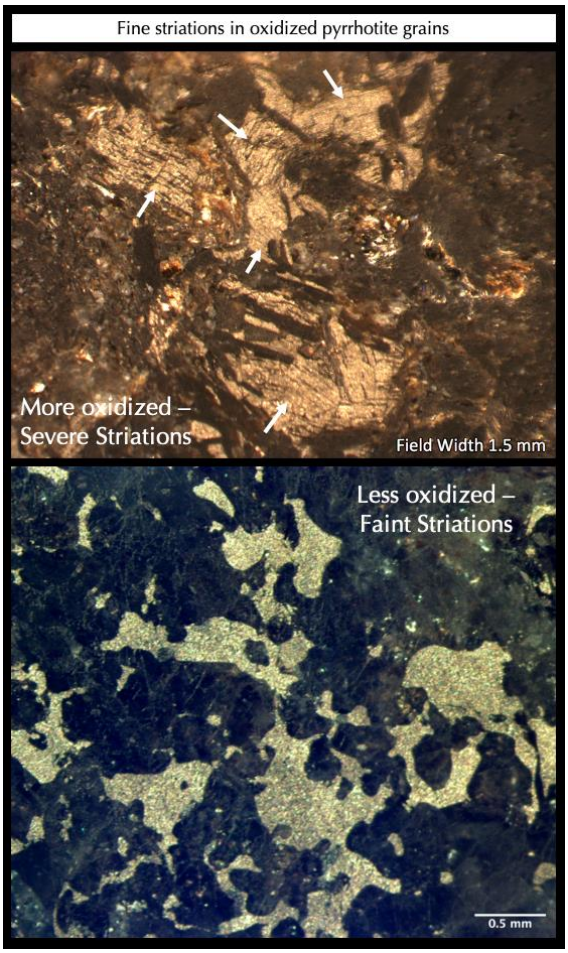

Figure 9. Typical striated appearance of oxidized pyrrhotite grains when seen on lapped cross sections in a stereomicroscope. Striations often appear as very fine parallel lines (marked with white arrows) often in intersecting patterns or sets of parallel lines formed along crystallographic orientations. Unlike air voids that are best seen at very low-angle incident illumination, pyrrhotite grains are best seen at near-vertical illumination of reflected light. From finely disseminated grains to isolated irregular-shaped ones, following the overall gneissose textural arrangements of quartzo-feldspathic grains, pyrrhotite grains occur in many different shapes, sizes, and orientations.

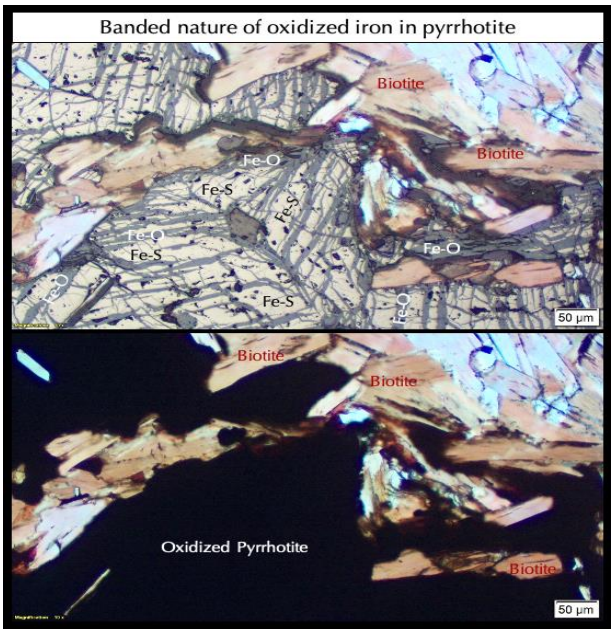

Figure 10. Typical striated appearance of oxidized pyrrhotite grains when seen on thin sections in a petrographic microscope equipped with reflected and transmitted polarized light (Jana, 2022). The bottom photo shows the typical opaque appearance of pyrrhotite when viewed only through the transmitted polarized light. The top photo reveals the grey iron oxide bands or veins in the brighter pyrrhotite body when viewed through both transmitted and reflected polarized light modes. Scale bars are 50 microns.

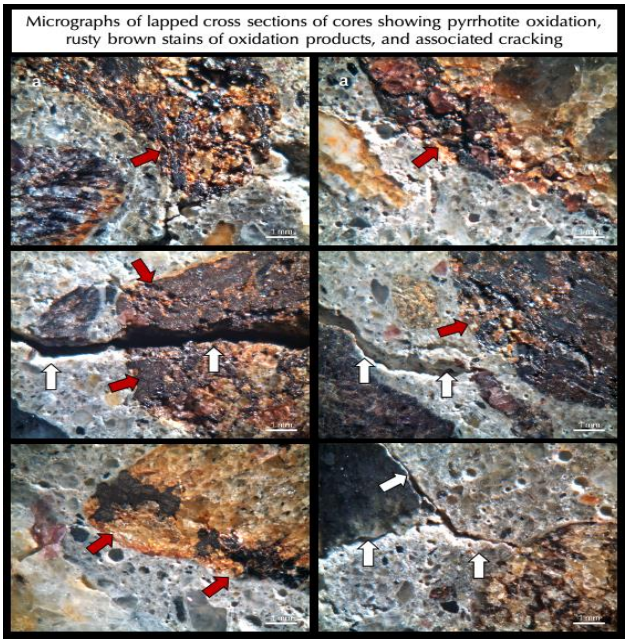

Figure 11. First major evidence of pyrrhotite oxidation comes during stereomicroscopical examinations of lapped cross sections when along with fine striations, oxidized pyrrhotite grains show rusty reddish-brown oxidation products of goethite and ferrihydrite (marked in red arrows) and associated cracking (white arrows) in aggregates, sometimes extending into the paste. Scale bars are 1 mm.

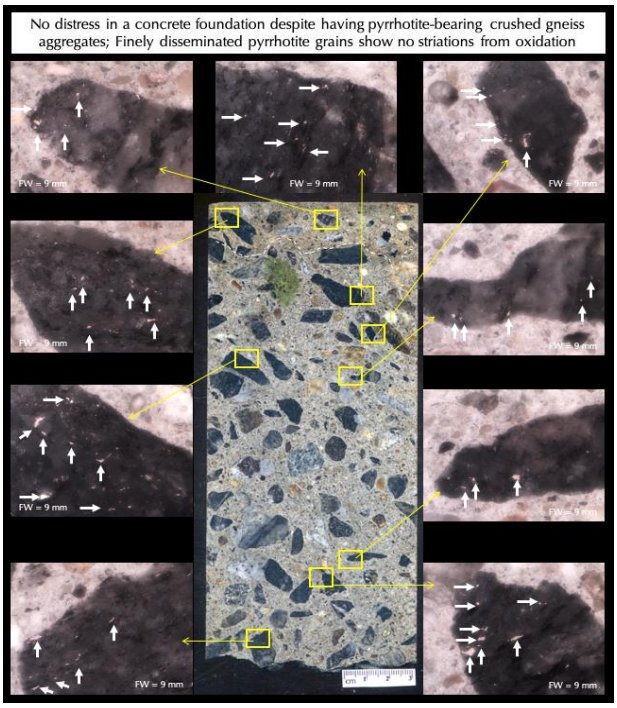

Figure 12. Micrographs of lapped cross section of a core from a sound foundation (Jana, 2019 b), where despite the presence of pyrrhotite in the same crushed gneiss coarse aggregate as present in other distressed foundations, no visible distress was noticed, which is judged to be mainly due to (i) the finely disseminated forms of pyrrhotite (many are marked by arrows), and (ii) the lack of availability of oxygen and moisture in the foundation to initiate and sustain the oxidation reactions. The exposed surface of this foundation has a 1-mm thick, dense, cementitious protective coating well-bonded to the concrete, which has prevented penetration of moisture into the concrete during service. Field widths of micrographs are 9 mm.

In all samples from eastern Connecticut, pyrrhotite is the major iron sulfide phase detected in the crushed gneiss coarse aggregates of deteriorated concretes, sometimes associated with traces of pentlandite and chalcopyrite (Wille and Zhong, 2016), or iron-titanium oxide (ilmenite) but no pyrite was found. This is contrary to the unsound pyrrhotite-bearing anorthositic gabbro in Trois-Rivières, which showed not only the presence of pyrite but also its deleterious electrochemical effect to enhance oxidation of pyrrhotite (Duchesne et al., 2021).

Assessment of Damage Rating Index (DRI)

The Damage Rating Index (DRI) is a petrographic method originally developed by Dunbar and Grattan-Bellew (1995) and subsequently used by other researchers (e.g., Shrimer, 2006; Rivard et al., 2002; Power and Shrimer, 2007) to evaluate the extent of damage in concrete caused primarily by alkali-silica reactivity (ASR). Rodrigues et al. (2014) attempted application of this method to evaluate the extent of damage in an apartment building from pyrrhotite oxidation in the Trois-Rivières area in Québec, Canada. The DRI provides a readily understandable numeric index of the amount of damage in concrete on a scale in which low DRI values indicate little or negligible defects, whereas higher DRI values correspond with a greater number of defects, typically also associated with damage of increasing concern. The DRI can also indicate the likelihood of further expansion, as well as the degree of such expansion. Traditionally, the method is used on lapped cross sections during stereomicroscopical examinations by traversing

across the entire section by a stepper motor-controlled XY stage and stopping at regular intervals to record various petrographic features of interest. Recorded defects include:

Damage Rating Index (DRI): A Useful Petrographic Tool For Determining Damage Caused by Pyrrhotite Oxidation in Concrete

Features	Best Seen In	Abbreviations	Weighing Factor
Cracks in Coarse Aggregate	Lapped Cross Section	CCA	× 0.5
Cracks in Coarse Aggregate + Pyrrhotite	Lapped Cross Section	CCAP	× 2.0
Cracks in Coarse Aggregate + Rust Stain	Lapped Cross Section	CCAR	× 3.0
Open Macrocracks in Coarse Aggregate	Lapped Cross Section	OCCA	× 4.5
Coarse Aggregate De-bonded Due To Microcrack Along Aggregate-Paste Interface	Lapped Cross Section	CAD	× 3.0
Cracks in Cement Paste	Thin Section	CCP	× 2.0
Secondary Ettringite Filled Cracks in Cement Paste	Thin Section	ECCP	× 2.5
Secondary Ettringite In Aggregate-Paste Interface	Thin Section	EAP	× 3.0
Secondary Ettringite In Paste	Thin Section	EP	× 3.0
Secondary Ettringite In Air Voids	Thin Section	EAV	× 0.5

- The Damage Rating Index (DRI) is a petrographic method that was developed by Grattan-Bellew (1992) and Dunbar (1995) to evaluate and quantify the extent of damage in concrete caused primarily by alkali-silica reactivity (ASR).
- A lapped cross section of concrete is segmented by a grid of squares that are 0.4 in. x 0.4 in. (1 cm x 1 cm) in size
- The sample is then observed using a stereomicroscope at 15X magnification on a square-by-square basis. A minimum of 200 squares (32 sq. in. area) forms a valid test for a common structural concrete. Alternately, a point-count procedure on an automated motorized stage in a stereo-microscope similar to the procedures of ASTM C 457 for air void measurements can be used to transverse the lapped section at regular intervals, e.g., at 0.4 in. (1 cm) intervals for at least 200 points at 15X magnification covering 32 sq. in. area.
- Alternately, a large-area (50 mm x 75 mm) thin section can be examined in a petrographic microscope with an attached manual or motorized XY stage, e.g., at 1 mm square grids at 4X objective, especially for observations of secondary ettringite. A point-count procedure can also be followed to count all the above features at 1 mm linear translations along an EW traverse with 1 mm distance between the traverses for at least 2000 points.
- The presence of each of the petrographic features listed in the Table is counted in each of the squares examined and those counts are multiplied by "weighing factors".
- These "weighing factors" represent the relative importance of each of the listed features in the deterioration process caused by pyrrhotite oxidation.
- The DRI represents the normalized value [to the area of measurement, e.g., 16 in^2 (100 cm^2)] of the presence of these features once their counts have been weighted and multiplied.
- Although there is no arbitrary value, which will indicate whether the concrete suffers deterioration, nor its severity, DRI values above 50 are generally suggestive of significant damage in case of ASR, which may differ for pyrrhotite oxidation-related distress. For ASR-related distress, Shrimer (2006) proposed the following rating: 0-40 Negligible, 40-125 Minor, 125-300 Moderate, 300-500 Significant, 500-650 Serious, and, > 650 Very Serious.
- The present study is an attempt to quantify the DRI with visible damage and then correlate the DRI values with other parameters of pyrrhotite-oxidation-related distress, e.g., from the proportion of oxidized phases of pyrrhotite to the bulk sulfate content of concrete where sulfate is not only contributed from Portland cement but also from pyrrhotite with its released sulfate in the paste.

Figure 13. Description of damage rating index (DRI) commonly used in assessment of concrete deterioration due to ASR. This rating system can be extended to study the extent of distress from pyrrhotite oxidation, if the characteristic microstructural features of pyrrhotite oxidation can be appropriately assigned with similar weighting factors as the ones used for ASR studies. The study, however, requires not only examinations of lapped cross sections but also of large-area thin sections in an upright microscope with motorized XY-stage and polarized-light facilities as shown in Figure 15.

cracks in aggregates (x 0.75), cracks with ASR gel (x 2.0), open or a fine network of cracks without gel (x 4.0), de-bonded aggregates (x 3.0), reaction rims (x 0.5), cracks in paste (x 2.0), cracks with gel in paste (x 4.0), and gel in air voids (x 0.5). These defects are counted, weighted

at various assigned weighing factors depending on the degree of damage indicated by the feature of interest (shown in parenthesis with the petrographic features), and multiplied. Although there is no defined limiting value which will indicate whether the concrete suffers deterioration due to ASR, nor its severity, DRI values above 50 are generally suggestive of significant damage due to ASR. Though limited by the experience and proper training of the operator, DRI values can provide valuable insights in confirming, or ruling out, if the damage to a questionable structure is primarily an effect of ASR, the degree of severity of damage from ASR, and determining the relative extents of damage between various elements or sections of the structure under evaluation. DRI values usually correlate well with the petrographic features that are directly attributable to ASR.

Similar assessment of quantification and extent of damage from pyrrhotite-oxidation-related distress can be done by recording various petrographic features of interest: (a) first on lapped cross sections during stereomicroscopical examinations with a motorized XY stage during stops at regular intervals of scanning as for the traditional methods, followed by extending the method (b) on multiple thin sections (50 mm x 75 mm size) covering a full-depth longitudinal cross section of core on a transmitted-light stereozoom microscope with polarized light and motorized XY stage facilities, or, on (c) a fluorescent-light or petrographic microscope with motorized XY stage having both fluorescent and polarized light facilities.

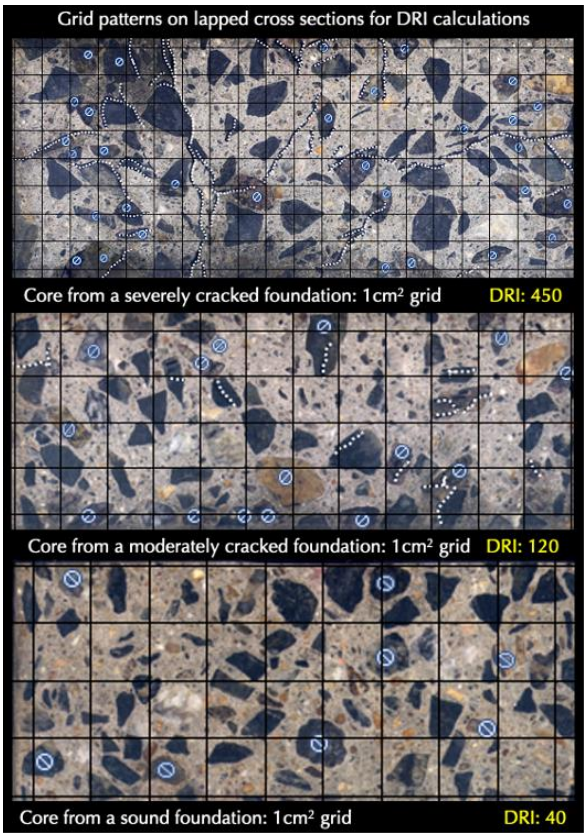

Figure 14. An exercise of assessment of DRI on lapped cross sections of three concrete cores taken from three different locations of a concrete foundation exhibiting various degrees of deterioration where the DRI values show overall good correlations to the extent of distress. Large-area thin sections of the cores were also used in the final calculations of DRI.

Petrographic features of interest and appropriate weighting factors for pyrrhotite oxidation-related distress could be assigned as follows (Figure 13): (a) pyrrhotite-bearing crushed gneiss coarse aggregate particles (x 0.50); (b) cracks in crushed gneiss coarse aggregate particles (x 0.75); (c) cracks with secondary deposits (x 2.0); (d) open cracks in crushed gneiss aggregates (x 4.0); (e) crushed gneiss debonded (x 3.0); (f) oxidation products of pyrrhotite in gneiss (x 1.0); (g) cracks in paste (x 2.0); (h) cracks filled or lined with secondary ettringite in paste (x 4.0); and secondary ettringite deposits in air voids (x 0.5). With such a selection of features and weighting factors, DRI values of cores examined from eastern Connecticut varied from 150 to 300 (Figure 14) where the higher value is consistently obtained from cores collected from severely cracked foundations, indicating the usefulness of DRI in assessing the extent of damage. Figure 15 shows instrument set ups in the author's laboratory for determination of DRIs from lapped cross sections in stereomicroscopes with motorized XY stages, as well as from large-area thin sections in a petrographic microscope with a motorized XY stage.

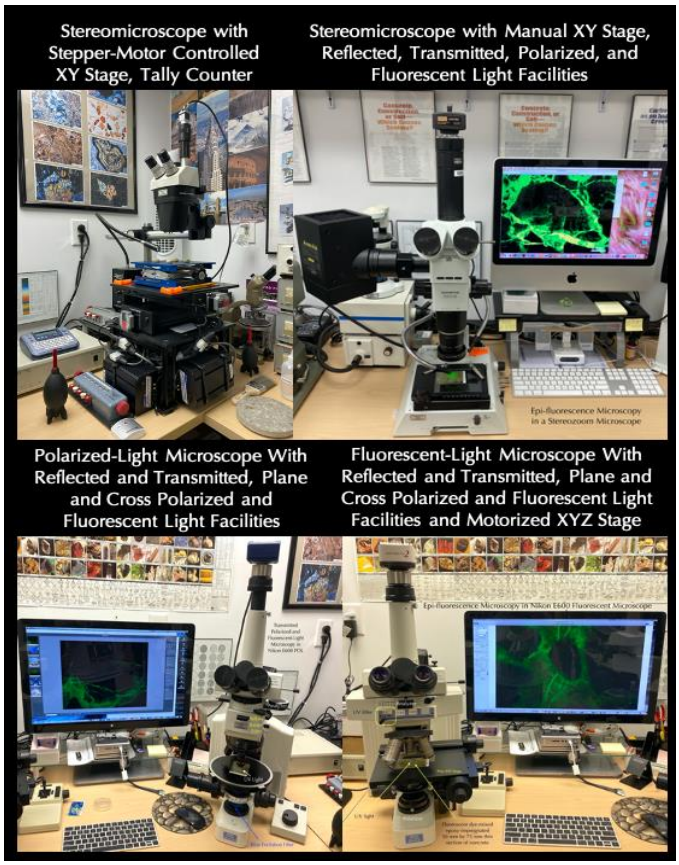

Figure 15. Clockwise from top left: (a) reflected-light stereo microscope; (b) reflected, transmitted polarized and fluorescent light stereozoom microscope; (c) upright (epi) fluorescent and polarizing light microscope with motorized XYZ stage; and, (d) reflected-transmitted-polarized-fluorescent light petrographic microscope with motorized Z-axis. This set-up is used for detailed petrographic examinations, along with calculations of DRIs from lapped cross sections and thin sections of cores collected from various locations of concrete foundations that have exhibited various degrees of deterioration.

Examinations in a Petrographic Microscope

Examinations of polished thin sections in a petrographic microscope detected crushed gneiss coarse aggregates as the host rock, where pyrrhotite occurs as fine, disseminated, dark opaque accessory iron sulfide grains mixed with quartz, potash feldspar (orthoclase), plagioclase (albite and oligoclase), biotite mica, and pyrope garnet. Similar to fine striations on oxidized pyrrhotite seen under a stereo microscope (Figure 9), examinations of polished thin sections in combined transmitted polarized and reflected (epi-illumination) modes show fine striations in more vivid detail consisting of gray bands of oxidized iron in a brighter matrix of iron sulfide (Figure 10). Rusty brown stains are also found around some oxidized pyrrhotite grains. Most oxidized pyrrhotite grains are found in close association with biotite flakes in gneiss (Figures 16 and 17), which is consistent with a prior observation of similar affinity of oxidized pyrrhotite to biotite in the study of Tagnit-Hamou et al. (2005). This indicates a potential for easy migration of moisture and oxygen to the oxidation sites through the weak cleavage planes of biotite. Thin sections show typical schistose textures of parallel alignment of quartz, feldspar, and biotite grains, or gneissose textures of alternating bands of quartzo-feldspathic and micaceous minerals (Figures 16 and 17) where pyrrhotite grains often show elongated shapes arranged in parallel alignment to biotite compared to the cubic or equant shape of pyrite. Mineralogy, texture, gneiss host rocks, and iron sulfide grains in host rock, are compositionally similar to many other distressed foundations from the area confirming the common source of the unsound pyrrhotite-bearing aggregates, which were quarried from the hydrothermal vein in the Becker's quarry situated in Willington, Connecticut.

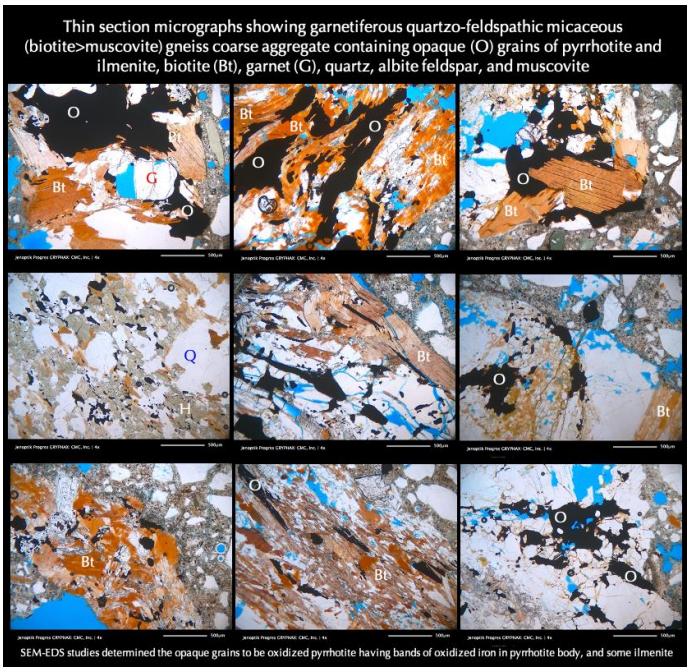

Figure 16. Micrographs of blue dye-mixed epoxy-impregnated thin sections of distressed concrete from eastern Connecticut showing typical parallel alignments of quartzo-feldspathic and micaceous minerals defining schistose and gneissose textures of the garnetiferous quartzo-feldspathic biotitic gneiss crushed stone coarse aggregate particles. The dark opaque grains of pyrrhotite and ilmenite are seen in the plane or cross polarized light views through a petrographic microscope where such grains are present either in finely disseminated forms or in close association with biotite flakes. Scale bars are 0.5 mm.

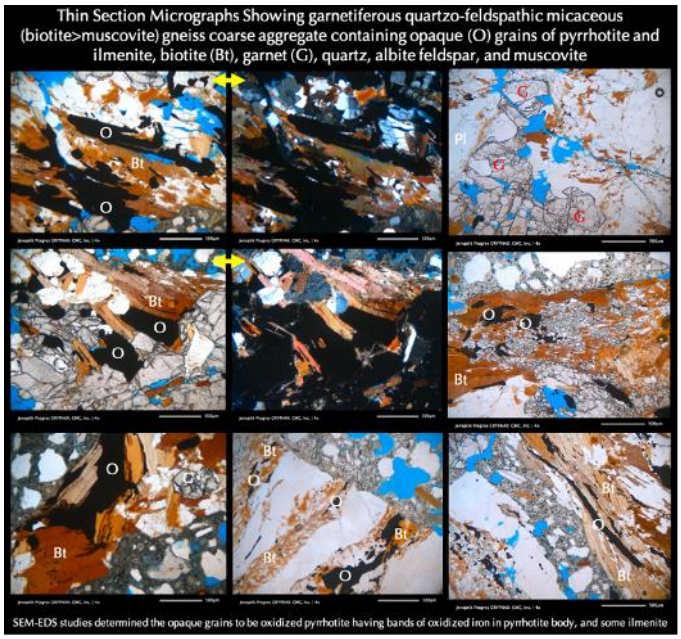

Figure 17. More micrographs of thin sections of distressed concrete from eastern Connecticut showing: (a) garnet porphyroblasts (marked as 'G') typically exhibiting many internal microfractures; (b) parallel alignments of quartzo-feldspathic and micaceous minerals defining schistose and gneissose textures of gneiss coarse aggregate; and (c) deformed elongated opaque ('O') pyrrhotite grains (many with oxidized veins seen only when viewed through both transmitted and reflected light as in Figure 10), preferentially associated and aligned along with pleochroic biotite (Bt) flakes. Scale bars are 0.5 mm.

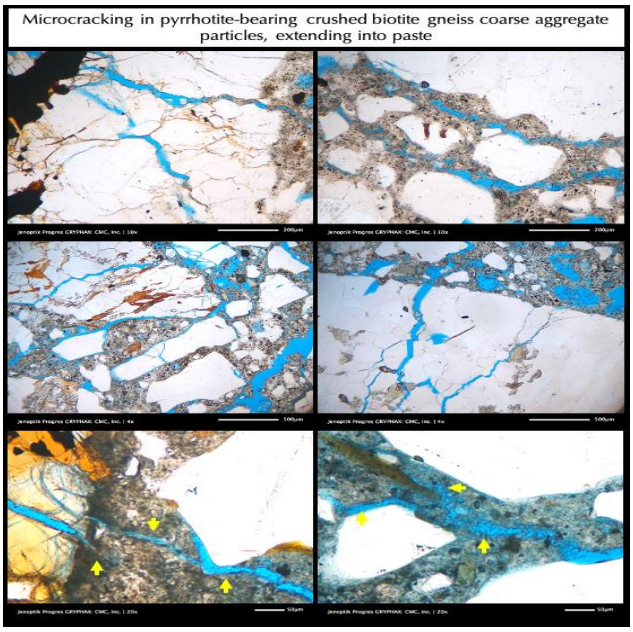

Figure 18. Micrographs of blue dye-mixed epoxy-impregnated thin sections of concrete from eastern Connecticut (Jana, 2022) showing microcracking in unsound pyrrhotite-bearing crushed gneiss coarse aggregate particles where cracks have often extended to the paste. Scale bars are 0.2 mm (top row), 0.5 mm (middle row), and 0.05 mm (bottom row).

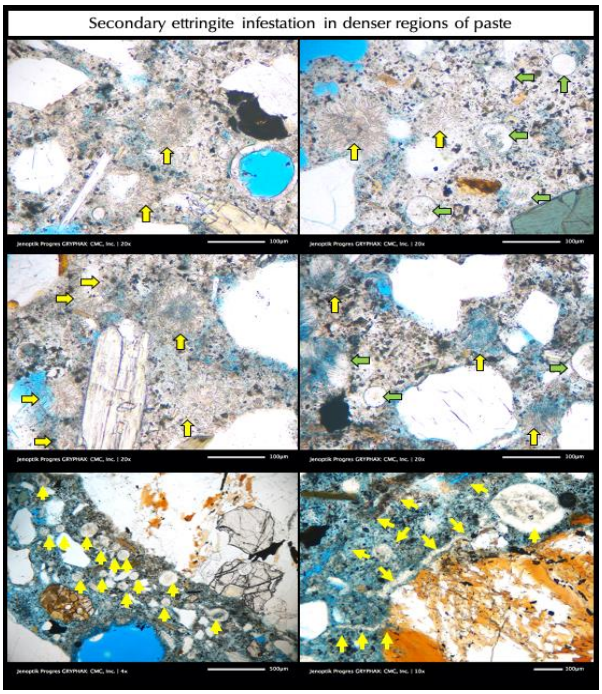

Figure 19. Thin section micrographs showing potentially deleterious ettringite infestation (Jana, 2022) particularly in the denser regions of paste, many of which are marked with yellow arrows. By contrast, green arrows show ettringite precipitations in relatively open spaces as porous regions of paste and in air voids. Scale bars are 0.1 mm.

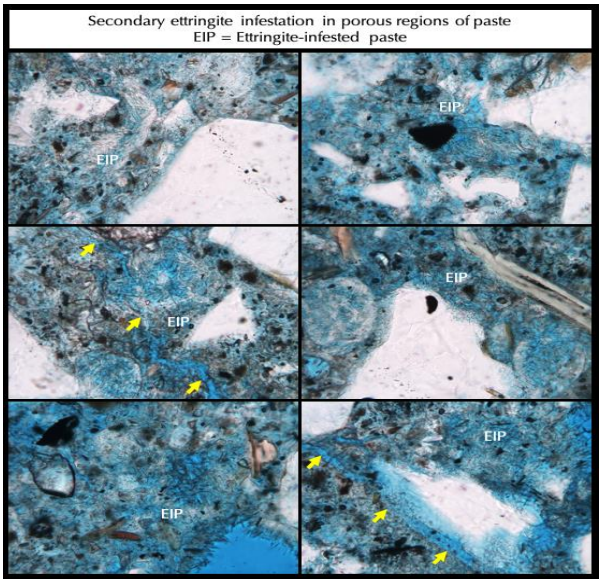

Figure 20. Thin section micrographs showing fine acicular secondary ettringite infestations in the porous regions of paste where ettringite crystals are intermixed with cement hydration products to create ettringite-infested paste (EIP) regions that are responsible for bulk volume increase of paste during moisture absorption and internal sulfate attack to cause additional cracking (shown by arrows) and distress beyond the distress from pyrrhotite oxidation. Field widths are 0.5 mm.

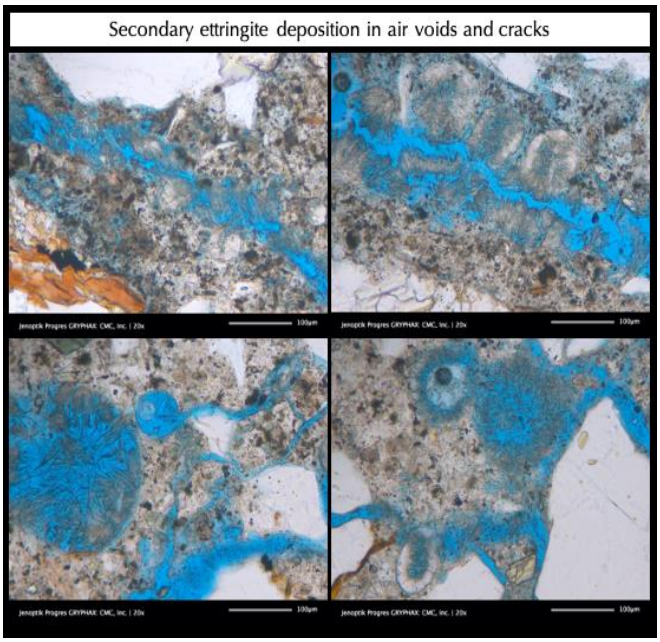

Figure 21. Thin section micrographs (from Jana, 2022) showing relatively innocuous precipitation of secondary ettringite from pore solutions of concrete in the open spaces of air voids and cracks. These are, perhaps, the results of internal sulfate attack of concrete exposed to moisture for prolonged periods, as opposed to being caused by deleterious ettringite formation in the denser more confined regions of paste, as shown in the previous Figure 19. Scale bars are 0.1 mm.

Mortar fractions show characteristic microstructures of pyrrhotite oxidation distress from microcracking to various forms of secondary ettringite products from internal sulfate attack in concrete. Some examples are: (a) Figure 18 shows extensive macro and microcracking, which are highlighted by blue epoxy; (b) Figure 19 shows profuse development of secondary ettringite in the denser regions of paste along with precipitation in cracks, air voids, and along aggregate-paste interfaces; and (c) Figure 20 shows a clustered network of interconnected needles of ettringite in relatively porous regions of paste as *ettringite infested paste* (EIP); and (d) Figure 21 shows general re-precipitation of secondary ettringite after dissolution by moisture in macro and micro cracks, air voids, and capillary pore spaces in paste due to the continued presence of moisture and released sulfates from pyrrhotite oxidation. Although occurrence of secondary ettringite in air voids and a few occasional cracks in an otherwise sound concrete are a common consequence of any concrete exposed to moisture for prolonged periods, profuse development to the extent of large-scale infestation in the denser and porous regions of paste, along aggregate-paste interfaces, along with more common occurrence in air voids, pore spaces, and cracks, as shown in Figures 18 through 21, constitute the telltale evidence of sulfate release and related distress as a byproduct of pyrrhotite oxidation.

Concrete Composition

Similar to compositional similarities of host gneiss coarse aggregates for their common source from Becker's quarry, petrographic examinations of cores collected from different residential concrete foundations across eastern Connecticut showed overall compositional similarities of concretes, in terms of having similar siliceous sand fine aggregates and Portland cement pastes

having various degrees of air entrainments. These findings are consistent with the notion of use of concretes from a single ready-mix concrete supplier in Willington, Connecticut over a period of more than two decades, which has used similar mixes of crushed gneiss from the nearby Becker's quarry, local silica sand, ASTM C 150 Type I/II Portland cement, and water. In all cores examined from eastern Connecticut, concrete contained: (a) crushed gneiss coarse aggregates having nominal maximum sizes of 19 mm; (b) natural siliceous sand fine aggregates having nominal maximum sizes of 9.5 mm (containing major amounts of quartz and quartzite, and subordinate amounts of feldspar, mica, ferruginous rock, and mafic minerals); (c) hardened Portland cement pastes having Portland cement contents estimated to be 6 to $6^1/_2$ bags per cubic yard (without any pozzolans), and water-cement ratios estimated to be in the range of 0.45 to 0.50; and (d) air contents estimated to be 6 to 8%, indicative of air-entrained concrete. Irrespective of the time/year of concrete placement, the same overall composition was found across samples from different foundations built over a period of 20 years.

SEM-EDS

The most characteristic compositional and microstructural evidence of pyrrhotite oxidation revealed from SEM-EDS studies in the eastern Connecticut cores are the oxidized bands or veins of iron in pyrrhotite grains. The iron oxide veins appear in darker shades of gray in BSE and SE images compared to the brighter iron sulfide bodies (Figures 22 and 23). Compositional and X-ray elemental analysis of pyrrhotite show iron and oxygen enrichment of oxidized veins (as > 95% FeO) as compared to iron and sulfur enrichment of pyrrhotite bodies (as 60-65% FeO and 30-35% sulfur expressed as SO_3).

The interstitial mortar fractions show many typical features of pyrrhotite distress, e.g., microcracking, profuse development of secondary ettringite in cracks, voids, and porous areas of paste, and ettringite infestations in denser regions where fine fibrous ettringite is intermixed with Portland cement hydration products. The following list provides the common microstructural features revealed from SEM-EDS studies of deteriorated concrete foundations from eastern Connecticut:

a) Evidence of secondary ettringite crystallization in cracks and gaps along aggregate-paste interfaces (Figure 24);
b) Secondary ettringite crystallization in air-voids (Figure 24);
c) Sulfate contamination of paste from released sulfates from oxidation of pyrrhotite in coarse aggregates where sulfate contents from SEM-EDS analyses showed higher than 'normal' sulfate contributed only from Portland cement (Figure 24);
d) Occasional gaps around coarse aggregates due to expansion of sulfate-contaminated paste, and formation of ettringite in aggregate-paste interfaces (Figure 25);
e) Evidence of fine disseminated iron sulfide inclusions in quarried aggregates, having lower S/Fe ratios (~ 0.8 to 1.5) than pyrite (~ 1.75 to 2.25) to indicate their pyrrhotite compositions (Figures 22, 23 and 24). Due to variable degrees of oxidation, stochiometric S/Fe ratios are slightly different from the ideal atomic ratios of pure non-oxidized pyrrhotite;
f) Evidence of oxidation of pyrrhotite and formation of iron oxide veins or bands within pyrrhotite (Figures 22, 23 and 24);

g) Evidence of unsoundness of pyrrhotite-bearing aggregate from expansion and cracking (Figure 26); and
h) Secondary ettringite infestation in confined areas in paste along with its formation in air voids, cracks, and aggregate-paste interfaces (Figures 25, 26 and 27).

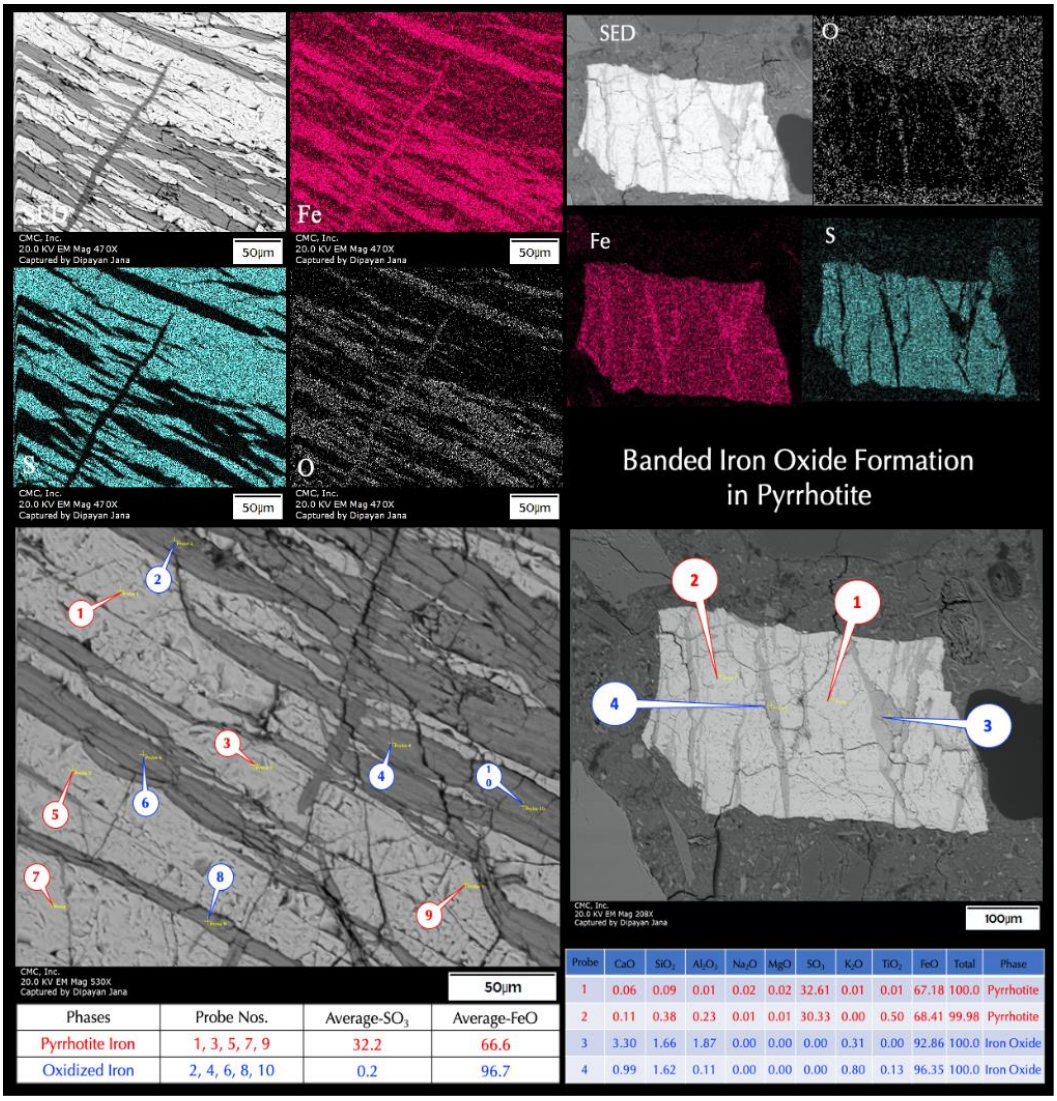

Phases	Probe Nos.	Average-SO_3	Average-FeO
Pyrrhotite Iron	1, 3, 5, 7, 9	32.2	66.6
Oxidized Iron	2, 4, 6, 8, 10	0.2	96.7

Probe	CaO	SiO_2	Al_2O_3	Na_2O	MgO	SO_3	K_2O	TiO_2	FeO	Total	Phase
1	0.06	0.09	0.01	0.02	0.02	32.61	0.01	0.01	67.18	100.0	Pyrrhotite
2	0.11	0.38	0.23	0.01	0.01	30.33	0.00	0.50	68.41	99.98	Pyrrhotite
3	3.30	1.66	1.87	0.00	0.00	0.00	0.31	0.00	92.86	100.0	Iron Oxide
4	0.99	1.62	0.11	0.00	0.00	0.00	0.80	0.13	96.35	100.0	Iron Oxide

Figure 22. Secondary electron image and corresponding X-ray elemental maps of oxidized pyrrhotite grains showing veins of oxidized iron within pyrrhotite bodies that are highlighted by the iron (Fe) and oxygen (O) maps and appeared as dark veins in the S-map. Pyrrhotite is highlighted in the Fe and S maps. Similar compositional and microstructural features of banded appearance of oxidized iron in the iron sulfide bodies are seen in many other oxidized pyrrhotite grains from eastern Connecticut (Jana, 2020, 2022), from Canada, and other regions (Schmidt et al., 2009; Oliveira et al., 2014).

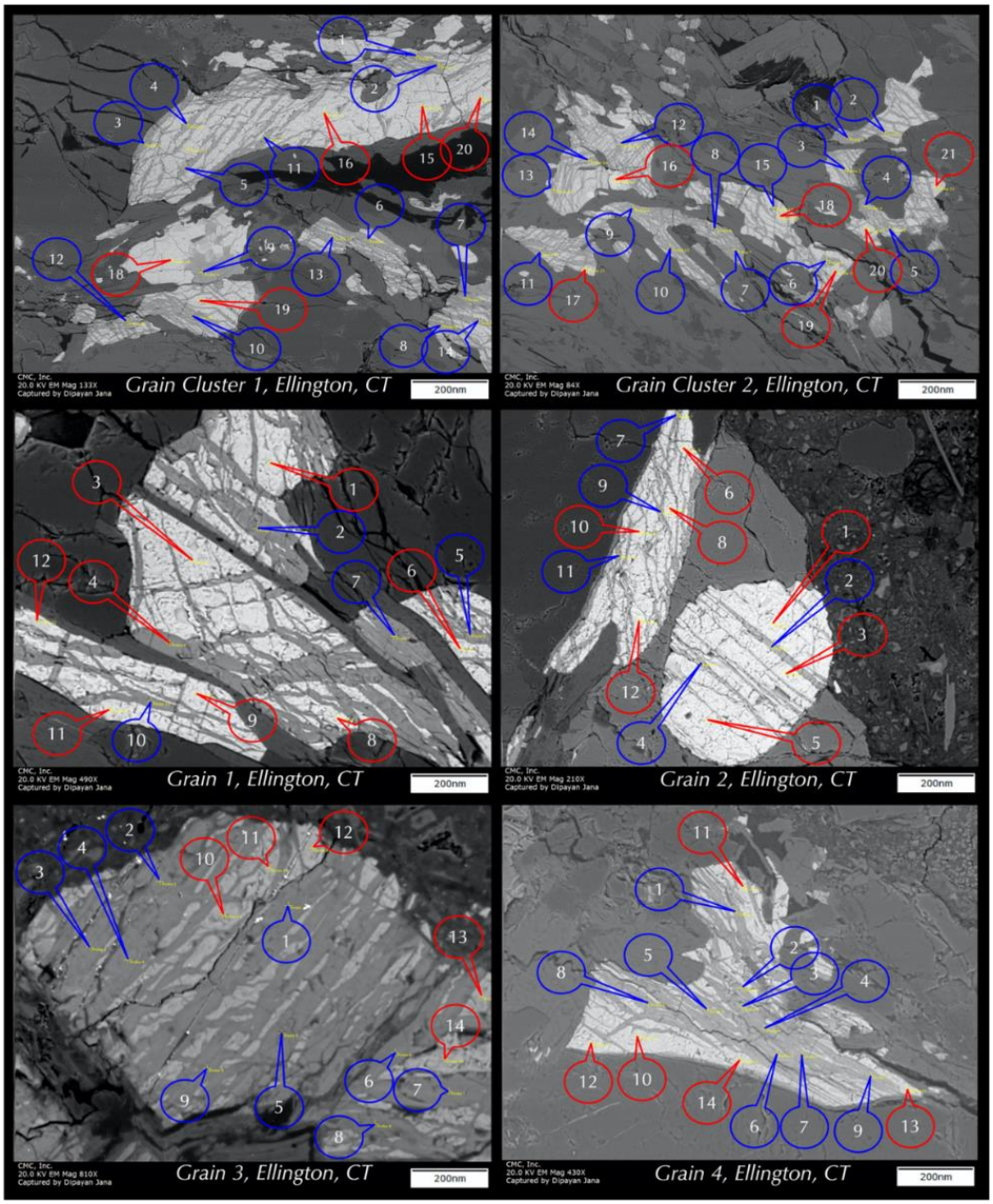

Figure 23. Backscatter electron micrographs of more oxidized pyrrhotite grains across various residential foundations in eastern Connecticut, where dark gray bands of oxidized iron and interstitial brighter iron sulfide matrix are analyzed in SEM-EDS at various locations (sulfide phases are analyzed at the tips of red callouts, and darker gray oxide bands at the tips of blue callouts).

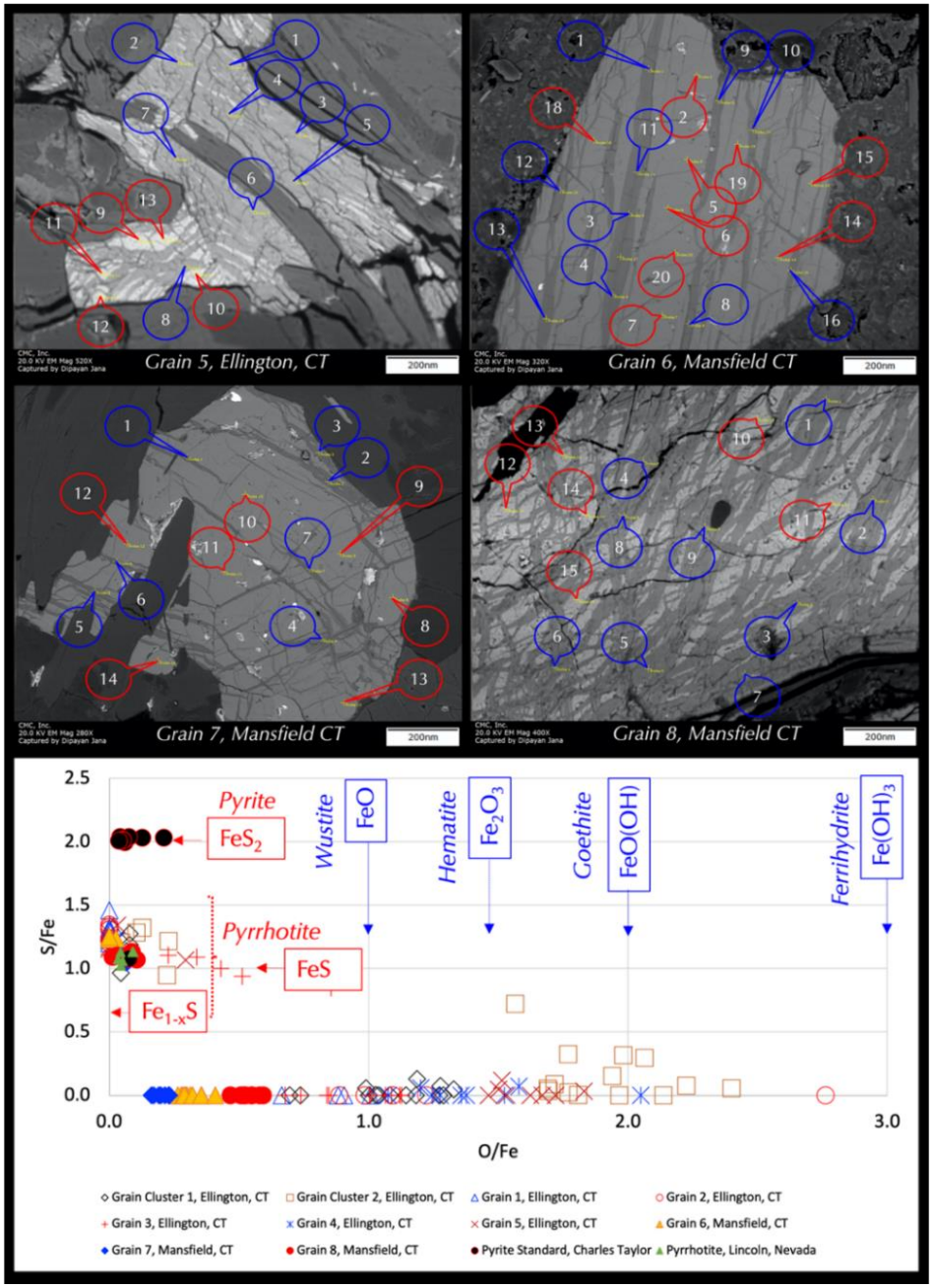

Figure 24. Continued backscatter electron images and EDS X-ray elemental analyses of oxidized pyrrhotite grains across various foundations in eastern Connecticut. Dark gray bands of oxidized iron and interstitial brighter matrix of iron sulfide are analyzed at the tips of blue and red callouts, respectively. Results of EDS analysis of these and previous figure's grains are presented as plots of S/Fe versus O/Fe atomic ratios, showing a large range of O/Fe atomic ratios of oxidized iron bands e.g., from less than 1 through 1 [FeO] to 1.5 [Fe2O3] to 2 [FeO(OH) goethite], to close to 3 [Fe(OH)3 ferrihydrite] (after Schmidt et al., 2009; Oliveira et al., 2014) but a relatively narrow range of S/Fe atomic ratios of interstitial pyrrhotite matrix, e.g., mostly between 0.8 and 1.5. Also plotted are a pyrrhotite mineral from Lincoln, Nevada (green triangles, S/Fe atomic ratio of 1), and a pyrite standard (from CM Taylor, black solid circles, S/Fe atomic ratio of 2 but slightly oxidized).

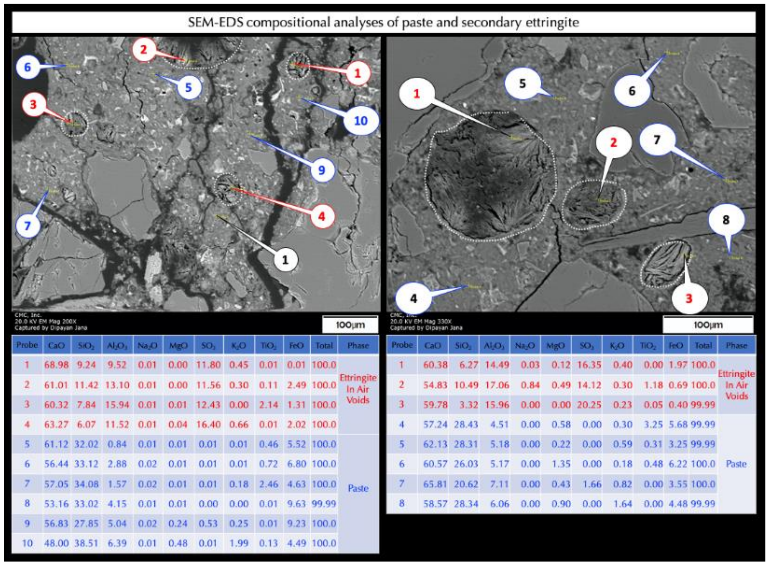

Probe	CaO	SiO_2	Al_2O_3	Na_2O	MgO	SO_3	K_2O	TiO_2	FeO	Total	Phase
1	68.98	9.24	9.52	0.01	0.00	11.80	0.45	0.01	0.01	100.0	
2	61.01	11.42	13.10	0.01	0.00	11.56	0.30	0.11	2.49	100.0	Ettringite In Air Voids
3	60.32	7.84	15.94	0.01	0.01	12.43	0.00	2.14	1.31	100.0	
4	63.27	6.07	11.52	0.01	0.04	16.40	0.66	0.01	2.02	100.0	
5	61.12	32.02	0.84	0.01	0.01	0.01	0.01	0.46	5.52	100.0	
6	56.44	33.12	2.88	0.02	0.01	0.01	0.01	0.72	6.80	100.0	
7	57.05	34.08	1.57	0.02	0.01	0.01	0.18	2.46	4.63	100.0	Paste
8	53.16	33.02	4.15	0.01	0.01	0.00	0.00	0.01	9.63	99.99	
9	56.83	27.85	5.04	0.02	0.24	0.53	0.25	0.01	9.23	100.0	
10	48.00	38.51	6.39	0.01	0.48	0.01	1.99	0.13	4.49	100.0	

Probe	CaO	SiO_2	Al_2O_3	Na_2O	MgO	SO_3	K_2O	TiO_2	FeO	Total	Phase
1	60.38	6.27	14.49	0.03	0.12	16.35	0.40	0.00	1.97	100.0	Ettringite In Air Voids
2	54.83	10.49	17.06	0.84	0.49	14.12	0.30	1.18	0.69	100.0	
3	59.78	3.32	15.96	0.00	0.00	20.25	0.23	0.05	0.40	99.99	
4	57.24	28.43	4.51	0.00	0.58	0.00	0.30	3.25	5.68	99.99	
5	62.13	28.31	5.18	0.00	0.22	0.00	0.59	0.31	3.25	99.99	
6	60.57	26.03	5.17	0.00	0.00	1.35	0.00	0.18	0.48	6.22	100.0 Paste
7	65.81	20.62	7.11	0.00	0.43	1.66	0.82	0.00	3.55	100.0	
8	58.57	28.34	6.06	0.00	0.90	0.00	1.64	0.00	4.48	99.99	

Figure 25. Backscatter electron images (above) and EDS X-ray compositional analyses (below) of distressed concrete in eastern Connecticut showing compositions of secondary ettringite deposits in air voids and various areas in paste at the tips of callouts that are provided in the Table below the image. Secondary ettringite shows high Ca, Al, and S whereas paste shows typical calcium silicate hydrate composition with negligible or variable contamination by sulfates released from pyrrhotite oxidation.

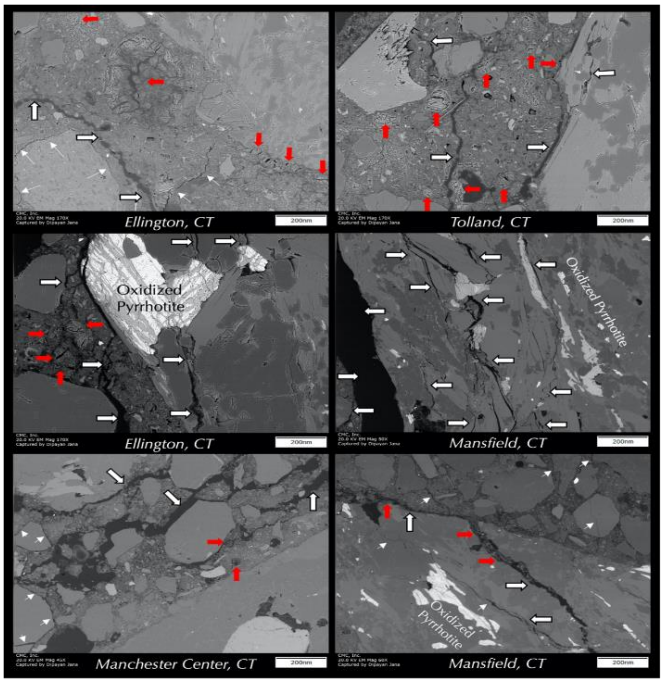

Figure 26. Backscatter electron images of deteriorated concrete across various residential foundations in eastern Connecticut showing extensive cracking in concrete. Some of these cracks are directly associated with oxidized pyrrhotite grains in crushed gneiss. Some major cracks are highlighted in thick white arrows whereas some fine cracks are marked with thin arrows (many of which are seen at aggregate-paste interfaces). Red arrows show secondary ettringite formation in air voids, cracks, at aggregate-paste interfaces, and in paste.

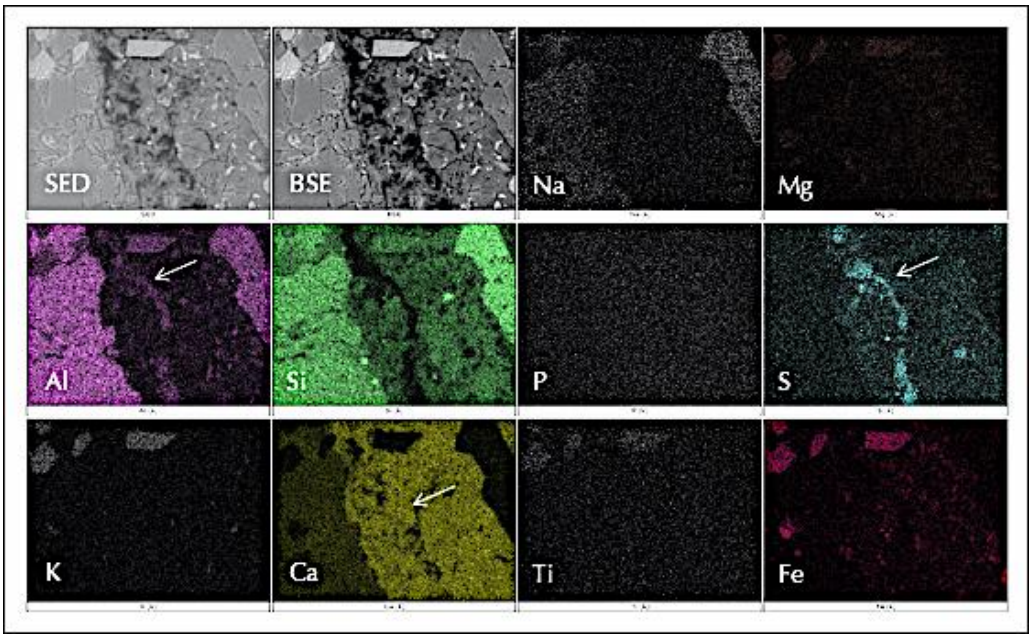

Figure 27. X-ray elemental maps showing secondary ettringite precipitation in a microcrack highlighted by its characteristic elemental compositions in Ca, Al, and S maps. Paste shows overwhelming Ca and Si from calcium silicate hydrate and calcium hydroxide components of Portland cement hydration. Aggregate shows Ca and Al enrichment from a feldspar grain. Some biotite flakes are highlighted in K and Fe maps.

Microstructural Evidence of Distress

Following the macroscopic (field) evidence of distress, e.g., map cracking, reddish-brown stains, efflorescence, pop-outs, spalling, and ultimate crumbling of foundation walls, three telltale microstructural and microchemical evidence of distress are: (a) extensive microcracking of many unsound pyrrhotite-bearing coarse aggregate particles causing fine striations of oxidation products in pyrrhotite to be detected in polished sections during stereomicroscopical observations, or similar microstructure at greater detail in thin sections during observations in a petrographic microscope, or in SEM-EDS; along with (b) detection of extension of cracking from unsound aggregates to the mortar fractions (similar to ASR-related cracking); and (c) compositional analysis of paste in SEM-EDS showing higher-than-normal sulfate contents. Cracks are best seen in lapped/polished sections, and in thin sections, especially after impregnating the sections with a fluorescent dye-mixed low-viscosity epoxy and observing the thin or polished sections in UV light.

Internal microcracks are often associated with reddish-brown iron oxide and hydroxide oxidation products and/or ettringite as deleterious reaction products. External manifestation of such cracks often brings those reaction products to the surface. Upon atmospheric carbonation, many sulfate and carbonate efflorescence deposits may preferentially form along the cracks.

Petrographic examinations of distressed residential foundations across eastern Connecticut also detected abundant secondary ettringite crystallization lining or filling many air voids and occasionally lining some microcracks that are indicative of prolonged presence of moisture in

concretes during service, which is an essential pre-requisite for pyrrhotite oxidation. The presence of moisture also indicates availability of sulfates to be released from pyrrhotite-oxidation and for subsequent ettringite crystallization, which, however, may or may not have necessarily derived from pyrrhotite oxidation, since ettringite-filled air-voids are, in fact, a very common microstructural feature in concrete exposed to moist environments without even any iron sulfide contaminant.

To establish the source of secondary ettringite, i.e., from Portland cement's sulfate and/or from oxidation of pyrrhotite-bearing aggregates, requires determination of sulfate levels in concrete i.e., if the level is higher-than that expected from a typical Portland cement concrete where sulfate (as SO_3) content in cement is around 3% by weight, i.e., giving about 0.45% sulfate in concrete for a common cement content of 15% by mass of a normal-weight concrete. Excess sulfate in concrete, e.g., above 0.45% from cement's contribution would then correspond to the pyrrhotite-aggregate source if no other sulfate source is present. Sulfate levels in concrete, e.g., 2.3% or higher detected from XRF in the author's studies are significantly higher than the sulfate normally contributed from Portland cement, which is due to the contribution from pyrrhotite. Similar to bulk concrete, SEM-EDS studies of sulfate in paste also showed higher values than the contributions from Portland cements, especially in the ettringite-infested regions, which show clustered networks of finely crystalline interlocked fibrous and acicular ettringite crystals.

XRD

XRD analyses of different dark gray and brown coarse aggregate particles extracted from a distressed core as well as XRD analysis of the bulk concrete sliced from the entire length of the core showed overall mineralogical similarities to unsound aggregates and concretes from many other distressed foundations, including detection of pyrrhotite and ferrihydrite type oxidation product (Figures 28 and 29). Detection of pyrrhotite and its oxidation products were possible with slow scans and a Lynxeye silicon drift detector in Bruker's D2 Phaser (2^{nd} generation) benchtop diffractometer. Minerals detected in the extracted crushed gneiss coarse aggregates from cores include quartz, albite, pyrope garnet, biotite, augite, and rutile. Oxidation of pyrrhotite to ferrihydrite released sulfates, which have caused formation of ettringite in cracks, voids, and paste to be detected in XRD analyses of many extracted aggregates (Figure 30).

Wille and Zhong (2016) detected thenardite (sodium sulfate, Na_2SO_4) and mirabilite ($Na_2SO_4.10H_2O$) in the XRD patterns of white efflorescence deposits along cracks on the exposed surfaces, and on spalled surfaces immediately beneath the lost original surfaces of deteriorated foundation walls in eastern Connecticut. These deposits indicate the potential for physical sulfate attack as crypto-fluorescence and salt hydration distress (Hime at al., 2001; Erlin and Jana, 2003) from reversible phase transitions between thenardite and mirabilite due to fluctuations in temperature and/or relative humidity where the solid volume increase from thenardite-to-mirabilite transition can cause a whopping 315% expansion to introduce additional cracking and spalling as an aftermath of pyrrhotite oxidation and internal sulfate attack.

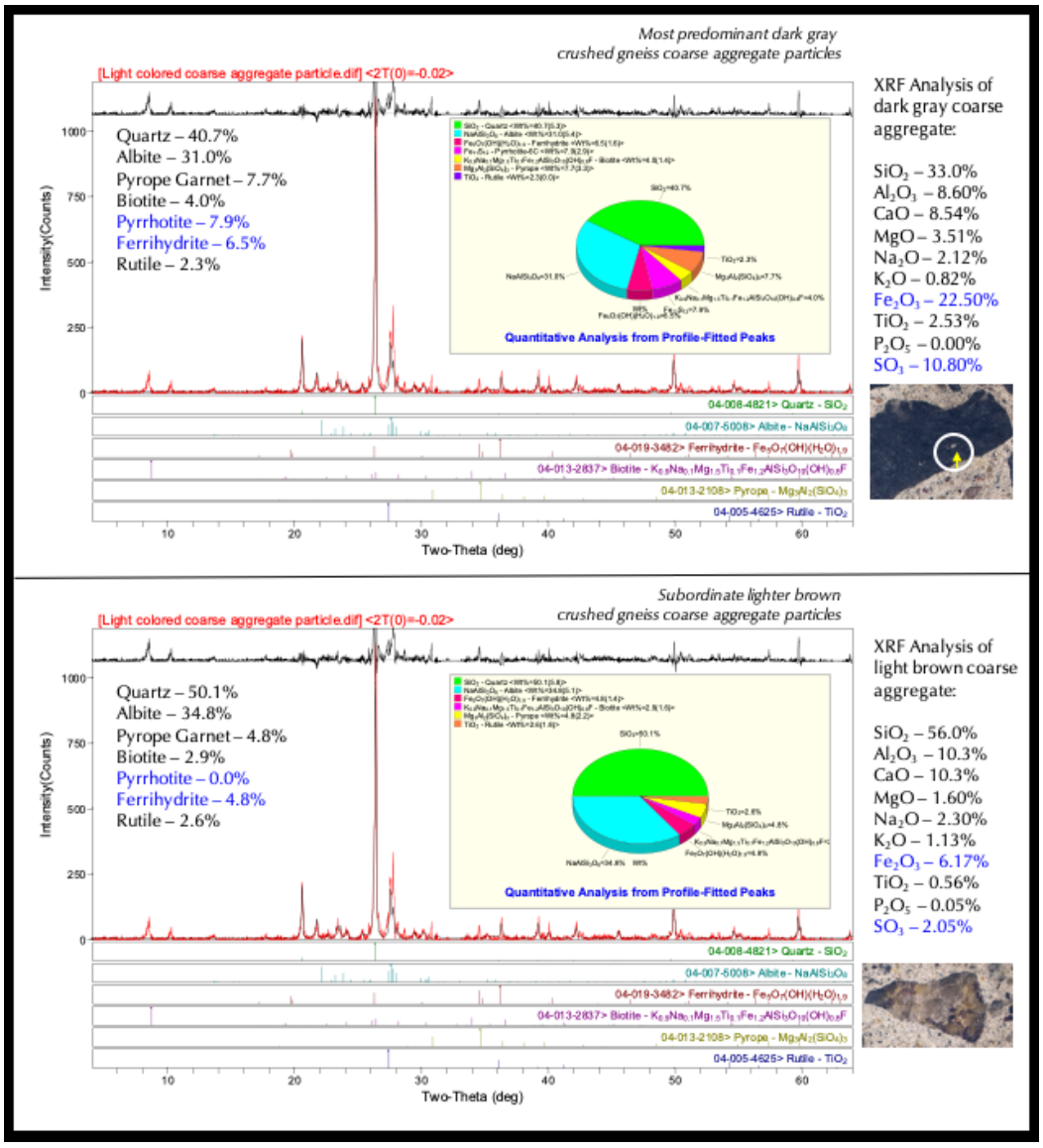

Figure 28. XRF patterns of two different crushed gneiss coarse aggregate particles found in the distressed concrete foundations from eastern Connecticut showing: (a) the predominant dark gray crushed gneiss shown at the top (a finely disseminated pyrrhotite grain in the aggregate is shown with an arrow in the micrograph of lapped cross section of core in the right column), and (b) the subordinate lighter brown crushed gneiss coarse aggregate particles shown at the bottom. Also shown are corresponding major element oxide compositions of aggregates determined from energy-dispersive X-ray fluorescence (ED-XRF) studies.

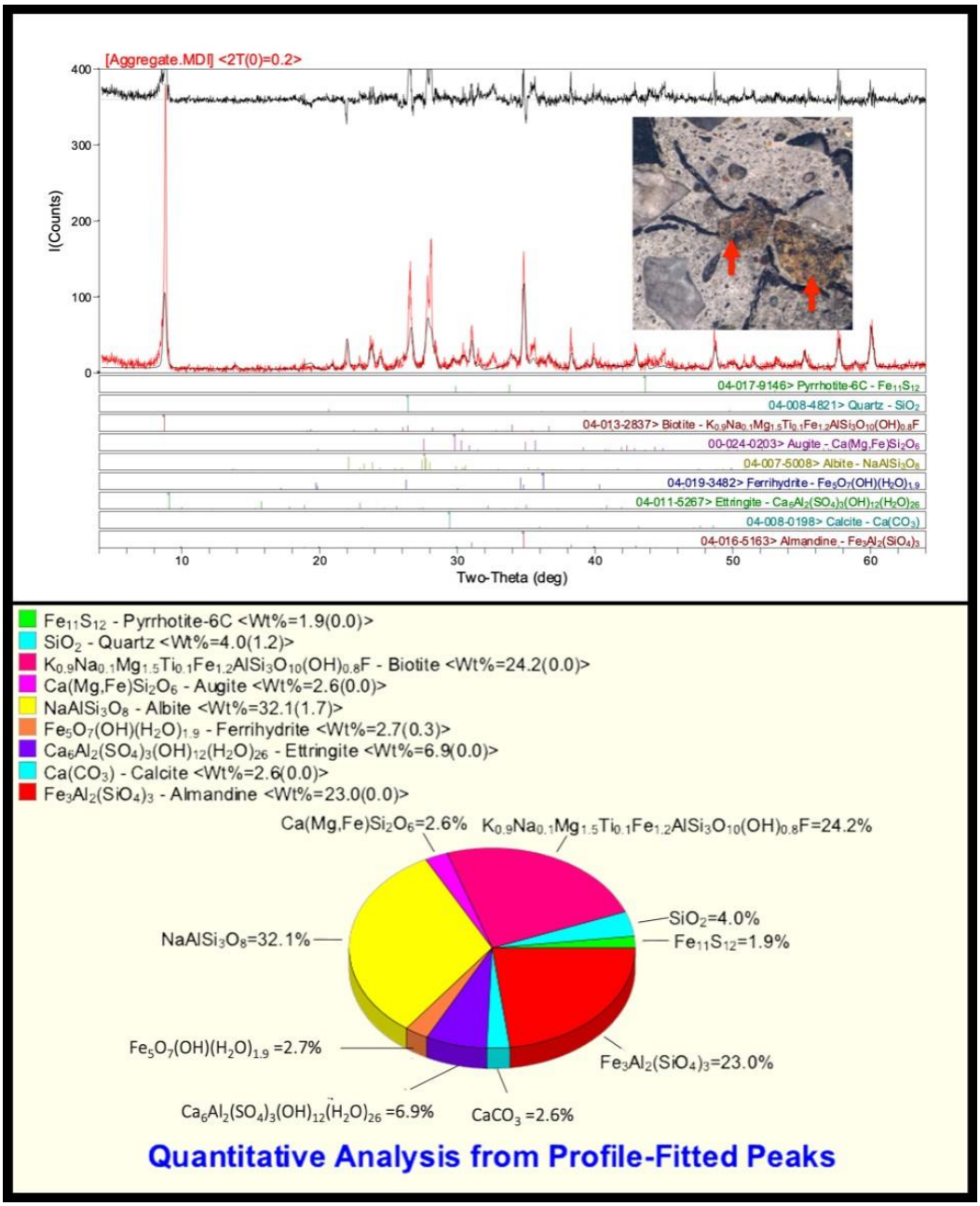

Figure 29. XRD pattern of an unsound crushed gneiss coarse aggregate particle depicting spectacular radial cracking from the aggregate extending into paste, which shows as high as 2.7% ferrihydrite oxidation product from pyrrhotite along with 1.9% pyrrhotite that has not been oxidized. The pie chart shows relative proportions of various phases detected from Rietveld analysis.

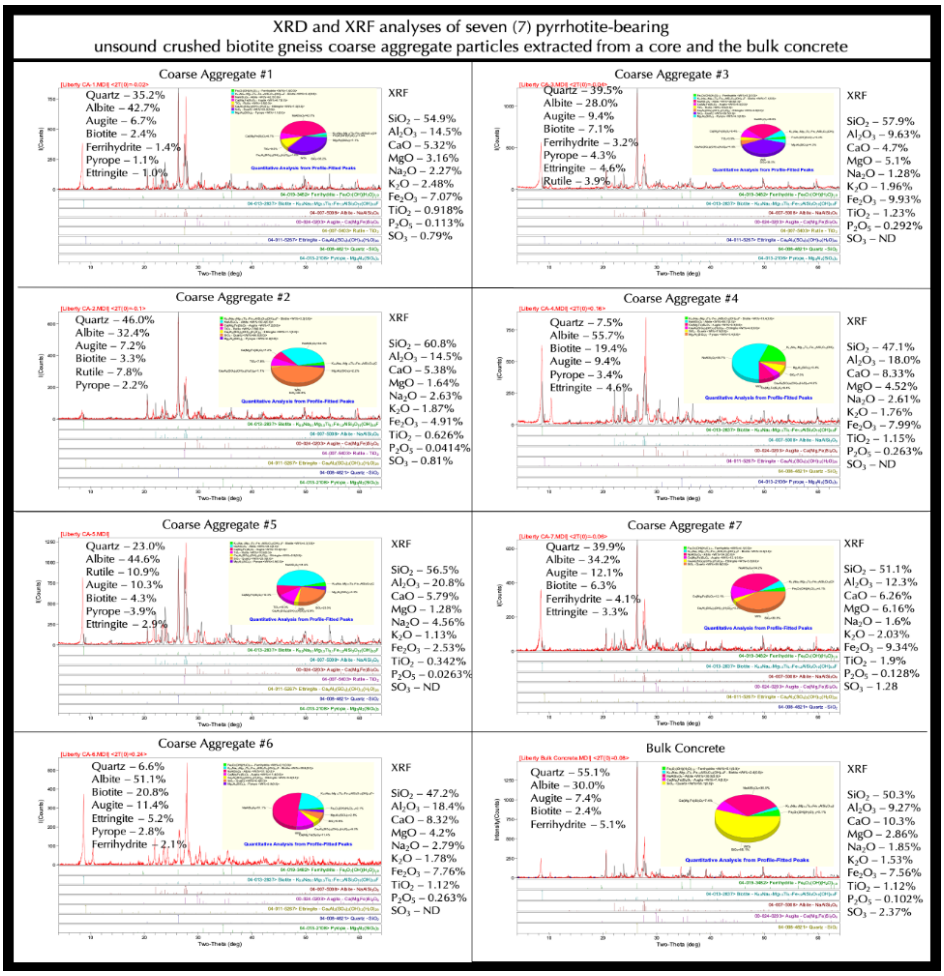

Figure 30. Mineralogical and chemical evidence of pyrrhotite oxidation from seven aggregate particles extracted from cores of distressed foundations in eastern Connecticut (from Jana, 2022), showing: (a) detection of ferrihydrite as the main oxidation product of pyrrhotite; (b) secondary ettringite from the released sulfate from oxidation and internal sulfate attack; along with (c) the host rock mineralogies (e.g., quartz, feldspar, biotite, pyrope garnet, etc.) of coarse aggregates. Right columns show XRF results of the same aggregates and, at the end, of the bulk concrete. High levels of sulfate are detected in some aggregates, and especially in the bulk concrete (2.37%), which is beyond cement's contribution (usually around 0.45%) to indicate additional sulfate released from pyrrhotite oxidation. The pie charts in XRD patterns show relative proportions of various phases detected from Rietveld analyses.

XRF, Sulfur Contents of Aggregates and Concrete

XRF studies of dark gray and brown crushed gneiss coarse aggregates (Figures 28 and 30) showed variable sulfate contents (as SO_3), e.g., from below the detection limit to as high as 10.8%, due to variable pyrrhotite contents in these particles. Bulk concrete showed a noticeable sulfate content of 2.37% as SO_3, which is higher than the amount contributed from Portland cement as the sole source of sulfate. For a concrete having 15% Portland cement by mass and 3% sulfate in cement, cement's SO_3 contribution to concrete is 0.45%. Thus, additional sulfate was released from oxidation of pyrrhotite. Almost all concretes examined in the author's laboratory showed XRF sulfate (SO_3) contents of concretes ranging from 1.5% to 3.5%.

Accelerated Oxidation and Ion Chromatography

In the accelerated pyrrhotite oxidation test (like the test done by Wille and Zhong, 2016 on quarried crushed stones from Connecticut), seven crushed gneiss coarse aggregate particles were extracted from a deteriorated concrete core, cleaned of adhered paste remains, crushed, and then immersed in a strong oxidant of 35% hydrogen peroxide solution for 21 days. Sulfates released from aggregates to the filtrates were measured (as SO_4^{-2}) in a Metrohm anion exchange chromatograph. All particles showed noticeable release of sulfates from aggregates and concretes as opposed to no sulfate release from a control gneiss aggregate containing no pyrrhotite, indicating the potential for continued sulfate release in the field during service in the prolonged presence of moisture (Figures 31 and 32).

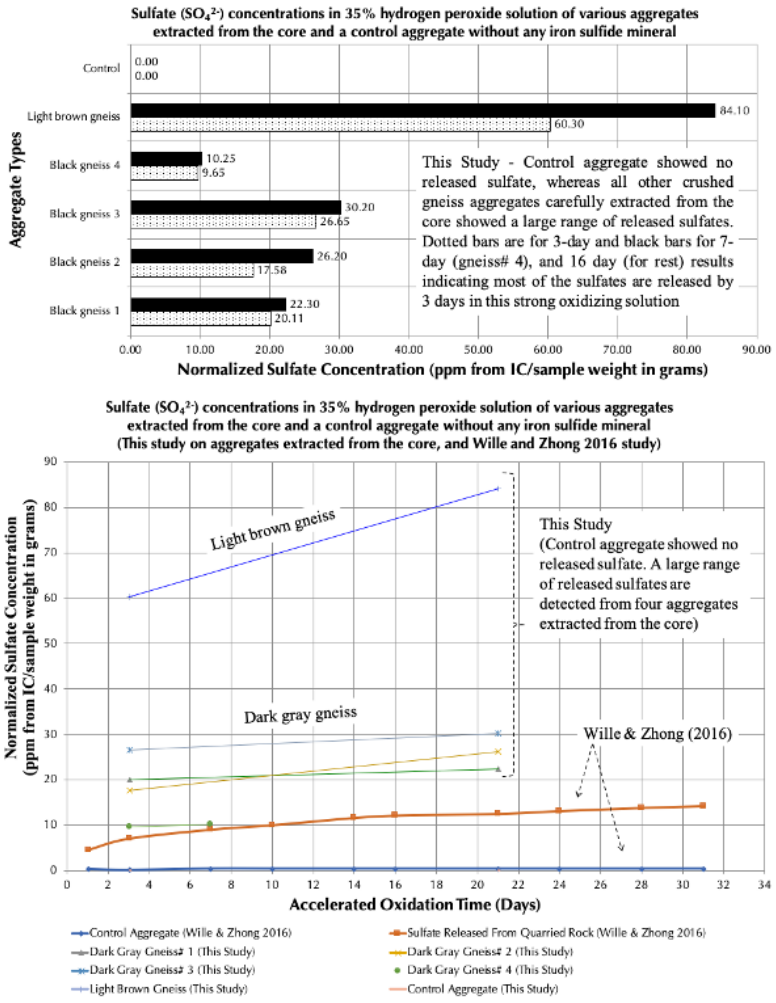

Figure 31. Determination of the amount of sulfates released from accelerated oxidation test of crushed gneiss aggregates extracted from a core from eastern Connecticut, where extracted aggregates were pulverized and immersed in a 35% hydrogen peroxide solution for 3 to 16 days, then filtered through 25-micron filter paper, diluted, and analyzed in an ion chromatogram. Results show increasing sulfate release from all aggregate particles within days of immersion, as also seen in the study of Wille and Zhong (2016). The highest sulfate release was in a light brown gneiss (from Jana, 2020).

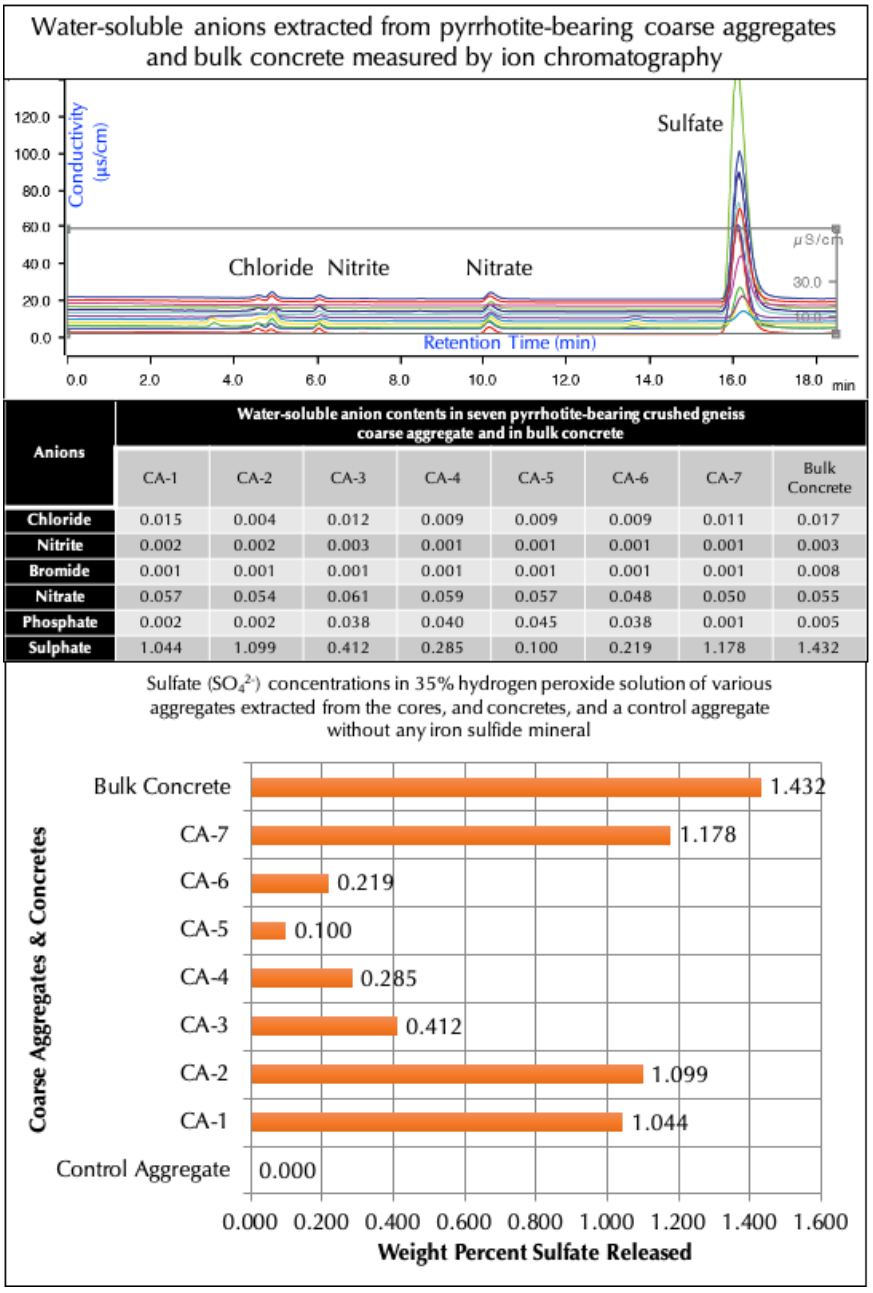

Anions	Water-soluble anion contents in seven pyrrhotite-bearing crushed gneiss coarse aggregate and in bulk concrete							
	CA-1	CA-2	CA-3	CA-4	CA-5	CA-6	CA-7	Bulk Concrete
Chloride	0.015	0.004	0.012	0.009	0.009	0.009	0.011	0.017
Nitrite	0.002	0.002	0.003	0.001	0.001	0.001	0.001	0.003
Bromide	0.001	0.001	0.001	0.001	0.001	0.001	0.001	0.008
Nitrate	0.057	0.054	0.061	0.059	0.057	0.048	0.050	0.055
Phosphate	0.002	0.002	0.038	0.040	0.045	0.038	0.001	0.005
Sulphate	1.044	1.099	0.412	0.285	0.100	0.219	1.178	1.432

Figure 32. Accelerated oxidation tests of seven crushed gneiss coarse aggregate particles extracted from a distressed concrete from eastern Connecticut, along with the pulverized concrete after digestion in 35% hydrogen peroxide solutions for 21 days to determine various levels of sulfates released from oxidation (from Jana, 2022). All samples show noticeable sulfate release, especially the concrete itself compared to a control aggregate with no iron sulfide inclusion. Highest release of sulfate in the bulk concrete sample is due to the contribution from cement's sulfate, along with sulfate released from oxidized pyrrhotite grains in aggregate. Top graph shows superposed anion chromatograms of all samples.

Discussion

Direct and Indirect Detection of Pyrrhotite in Aggregates

Of all the tests mentioned under the methodologies sections, direct detection of the presence of pyrrhotite in a suspected aggregate is done from: (a) petrographic examinations by Tagnit-Hamou et al. (2005), Araugo et al. (2008), Schmidt et al. (2011), Oliveira et al. (2014), Rodrigues et al. (2012 a, 2013), and Jana (2018 a, 2018 b, 2019 a, 2019 b, 2019 c, 2020, 2022); (b) SEM-EDS and electron probe by Schmidt et al. (2011), Rodrigues et al. (2012), Duchesne et al. (2021), Jana (2018 a, 2018 b, 2019 a, 2019 b, 2019 c, 2020, 2022), and Wille and Zhong (2016); (c) XRD by Rodrigues et al. (2012 a), Araugo et al. (2008), Jana (2020, 2022), Wille and Zhong (2016), and Tagnit-Hamou et al. (2005); (d) XPS by Chinchón-Paya et al. (2015); (e) magnetic susceptibility by Geiss and Gourley (2019); (f) DTA by Jensen (2018), and Haugen and Lindgard (2018) if > 0.1% S; and (g) NMR relaxometry by Balachandra (2020). Table 2 provides various methods of pyrrhotite detection, including some rapid identification methods in field concrete and aggregate.

Indirect assessments of pyrrhotite contents in aggregates are determined from: (a) staining (Midgley, 1958; Mielenz, 1963); (b) wet chemical analysis, e.g., acid-solution and the gravimetric method for total sulfur content (Jensen, 2018; Haugen and Lindgard, 2018); (c) micro-XRF (Chinchón-Paya et al., 2015); (d) acid leaching (Marcelino et al., 2016); (e) infrared combustion (Leco) method for total sulfur (Duchesne et al., 2018; Haugen and Lindgard, Jensen, and others in the Oslo workshop, 2018); and (f) WD-XRF (Cruz-Hernandez et al., 2020).

Table 2. Proposed scheme of various laboratory testing methods for assessment of pyrrhotite oxidation and related distress in existing concrete structures, and aggregates for new construction

Phase I: Laboratory Testing of Field Concrete Cores, Sawn Samples, or Broken Chunks	
Petrographic Examinations	• Identify pyrrhotite-bearing aggregates and aggregates having oxidized pyrrhotite grains from stereomicroscopical examinations of lapped/polished sections, and examinations of thin sections in a petrographic microscope • Trace cracks on core surfaces as received, as well as on the sectioned surfaces • Diagnose oxidized pyrrhotite grains, the oxidation products, and banded nature of oxidized products in pyrrhotite matrix in polished thin sections from reflected and transmitted polarized light in a petrographic (ore) microscope • Diagnose internal sulfate attack products and microstructures from examinations of thin sections in a petrographic microscope • Assess damage rating index (DRI) from proportions of oxidized and non-oxidized pyrrhotite-bearing aggregates, and cracks from stereomicroscopical examinations of lapped cross sections. Correlate DRI values with strength data, if available. • Select areas on polished thin sections to be examined further in SEM-EDS
SEM-EDS and Micro-XRF	• Determine products of oxidation of pyrrhotite from EDS elemental analyses • Determine microstructures and products of internal sulfate attack in concrete from BSE images and EDS analyses of polished thin sections from areas selected from prior petrographic examinations • Determine compositions of efflorescence salts from EDS compositional analysis • Scan a polished cross section of concrete in a micro-XRF to spot distribution of pyrrhotite and other sulfide grains in aggregates from the sulfur map

Phase I: Laboratory Testing of Field Concrete Cores, Sawn Samples, or Broken Chunks	
Chemical Analysis	• Determine the bulk sulfur content of concrete (as SO_3) content from a well-calibrated set of standards in an ED-XRF and compare the concrete-SO_3 results between samples to investigate a relationship with the pyrrhotite contents determined separately • Determine the total sulfur content of concrete from an elemental analyzer (Combustion) • Determine sulfate-sulfur from gravimetry, and sulfide-sulfur from the difference
Thermo-magnetic study	• Determine drop in magnetic susceptibility across the Curie temperature of pyrrhotite (325°C), and determine pyrrhotite content from a well-calibrated susceptibility drop versus total sulfur content plot on a set of pyrrhotite-mortar mixes incorporating pyrrhotite standard of similar crystallinities as the field pyrrhotite
XRD	• Determine oxidation products of pyrrhotite, and perform Rietveld analysis for proportions of pyrrhotite and oxidation products • Determine products of internal sulfate attack • Determine efflorescence salts on exposed surface
WD-XRF	• Determine proportions of sulfide-sulfur and sulfate-sulfur in concrete from S Kβ line peak shift in a sequential high-resolution curved crystal WD-XRF by using the fine collimator
IC	• Determine soluble sulfate from digestion of pulverized concrete in deionized water
Phase II: Laboratory Testing of Aggregates Extracted from Field Concrete	
Chemical analysis	• Determine total sulfur from an elemental analyzer (combustion method)
XRD	• Determine oxidation products of pyrrhotite, and perform Rietveld analysis on a slow-scanned pattern for proportions of pyrrhotite and oxidized products
Thermo-magnetic study	• Determine drop in magnetic susceptibility across the Curie temperature of pyrrhotite (325°C), and determine pyrrhotite content from a well-calibrated susceptibility drop versus total sulfur content plot on a set of pyrrhotite-mortar mixes incorporating pyrrhotite standard of similar crystallinities as the field pyrrhotite
WD-XRF	• Determine proportions of sulfide-sulfur and sulfate-sulfur in concrete from S Kβ line peak shift in a sequential high-resolution curved crystal WD-XRF by using the fine collimator • Prepare a set of standard mixes having varying proportions of a sulfide (e.g., FeS, S^{2-}) and a sulfate (e.g., $CaSO_4$, S^{6+}) phase to measure intensities at different S contents for both phases, as well as calibration of total S contents in standards versus total S from WD-XRF
Phase III: Laboratory Testing of Crushed Stone and Loose Aggregate to be used in New Construction	
Chemical Analysis	• Determine total sulfur from Elemental analyzer (Combustion)
Petrographic Examinations	• For aggregates having total sulfur content between 0.1 and 1% by mass, determine non-oxidized and oxidized pyrrhotite grains on a slab of lapped cross section of multiple aggregate particles of a sieve fraction encapsulated in epoxy
Micro-XRF	• Spot pyrrhotite grains across an epoxy-encapsulated sectioned and polished block of compacted aggregate particles in a micro-XRF
XRD	• Determine oxidation products of pyrrhotite, and pyrrhotite content from Rietveld analysis
Thermo-magnetic study	• Determine drop in magnetic susceptibility across the Curie temperature of pyrrhotite (325°C), and determine pyrrhotite content from a well-calibrated susceptibility drop versus total sulfur content plot on a set of pyrrhotite-mortar mixes incorporating pyrrhotite standard of similar crystallinities as the field pyrrhotite
WD-XRF	• Determine proportions of sulfide-sulfur and sulfate-sulfur in concrete from S Kβ line peak shift in a sequential high-resolution curved crystal WD-XRF by using the fine collimator • Prepare a set of standard mixes having varying proportions of a sulfide (e.g., FeS, S^{2-}) and a sulfate (e.g., $CaSO_4$, S^{6+}) phase to measure intensities at different S contents for both phases, as well as calibration of total S contents in standards versus total S from WD-XRF
Accelerated Oxidation, or Oxygen Consumption Tests	• For aggregates providing positive detection of pyrrhotite from petrography or XRD, determine sulfate release potential of aggregates after digestion in an oxidizing (35% H_2O_2) solution for 4 weeks and determine diluted (10x) filtrates selectively collected over the test period for change in sulfate concentration by ion chromatography • Perform oxygen consumption test of a 10 cm thick layer of compacted pulverized aggregate (< 150-micron particle size) in a sealed container at 40% saturation degree for 3.5 h at 22°C

Table 2. (Continued)

Phase III: Laboratory Testing of Crushed Stone and Loose Aggregate to be used in New Construction	
Mortar bar expansion test	• For aggregates releasing high sulfate or showing >5% oxygen consumption, conduct mortar bar expansion test following ASTM C 157 of 25 x 25 x 285 mm mortar prims made using the aggregate in question at size fractions similar to that used for the ASTM C 1260 test, and Portland cement at cement-to-aggregate ratio of 1:2.75, at a water-cement ratio of 0.65; bars are subjected to a 90-day storage period at 80°C (176°F) and 80% RH with two 3-hour soaking periods in a 6% sodium hypochlorite solution
Phase IV: Rapid Identification of Pyrrhotite in Field Concrete and Loose Aggregate	
Portable XRF	• Determine sulfur content of concrete or aggregate powder in a handheld portable XRF unit in the field from a calibrated set of standards, and estimate pyrrhotite content from the elemental sulfur with an assumption that pyrrhotite is the only source of sulfur
Magnetic Sensors	• Due to its weakly magnetic nature (unlike pyrite), pyrrhotite can be detected in the field with many compact portable commercial magnetometers or highly sensitive magnetic sensors either non-destructively or on pulverized concrete; even a semi-quantitative estimate can be obtained from prior use of those devices on a set of calibrated standards of concrete/aggregate powders mixed with various dosages of pyrrhotite
NMR Relaxometry	• Nondestructive identification of pyrrhotite in field concrete or aggregate from NMR relaxation by a compact portable unilateral NMR system

Problems in Determining Pyrrhotite Contents in Aggregates

Assessment of expansion potential of an aggregate due to pyrrhotite oxidation is complicated due to heterogeneous distribution of pyrrhotite, even in aggregates from the same quarry. This heterogeneity is often related to variations within the rock body subjected to the quarrying operations, which may contain areas richer than others in iron sulfides. The sampling method can also contribute to the observed variability. This effect is well documented as the "nugget effect" to reflect the substantial differences that may be found between neighboring samples. Due to this variability in pyrrhotite contents, total sulfur contents of aggregates calculated from the measured total sulfur contents of several concrete cores extracted even from the same foundation in Trois-Rivières (Québec, Canada) showed significant variability (Duchesne et al., 2018). This was despite the fact that a good correlation was observed between the monitoring of cracks and development of expansion in several hundred foundation walls of different initial degrees of damage, which were largely influenced by the exposure and relative humidity conditions within the concrete. Average median sulfur contents in unsound aggregates varied from 6% in Norway to as low as 0.3 to 2.9% in Canada, 1.5 to 2% in Spain to 2.5% in the US. Pyrrhotite contents in the unsound aggregates showed even more variation, e.g., from less than 5% to higher than 75% by volume of all iron sulfides. Geiss and Gourley (2019) recommended analyzing multiple cores per structure, as varying pyrrhotite concentration was found while evaluating the Connecticut samples for magnetic susceptibility measurements. Due to such variability, application of a chemical threshold, e.g., the sulfur content of an aggregate or total sulfur content of concrete (to estimate the amount of sulfide phases in aggregate, after subtracting sulfate contribution from cement) are usually recommended for a quick overview of the presence or absence of sulfide, before proceeding with other screening tests, even though significant variability of sulfur contents is reported between field samples even from the same foundation.

Besides variability in distribution, quantitative detection of pyrrhotite can also be difficult if the amount is 1% or less, which is often below the detection limit (2 to 3%) of XRD. Geiss and Gourley (2019) suggested the use of the drop in magnetic susceptibility across the curie temperature (325°C) of pyrrhotite, which can detect pyrrhotite content as low as 0.1% from a set of well-calibrated standards of similar pyrrhotite crystallinities.

Factors Influencing Pyrrhotite Oxidation

Due to variability in chemical compositions, crystal structures, and specific surface areas, oxidation reactions of pyrrhotite are not only rapid but highly variable. Due to the *deficiency of Fe atoms* in the pyrrhotite structure, oxidation proceeds via formation of a sulfur-rich layer (Chirita and Rimstidt, 2014), whereas in the Fe-rich layer of pyrite, ferric oxyhydroxide forms during initial oxidation (Duchesne et al., 2021). Janzen et al. (2000) studied oxidation kinetics of 12 well-crystallized pyrrhotite specimens of variable specific surfaces from pure hexagonal to monoclinic crystal structures and concluded that neither pyrrhotite crystal structure nor trace metal content had a consistent or systematic effect on oxidation rates. By contrast, Belzile et al. (2004) found a trend of decreasing oxidation rate with increasing trace metal contents. Most studies confirmed the importance of surficial and adsorptive reactions in the oxidation mechanisms, which could explain why crystal structure and surface defects, the presence of catalysts such as bacteria, and to a lesser extent, temperature can be considered as the most important factors in pyrrhotite oxidation studies (Belzile et al., 2004). According to Multani et al. (2018), the 4C magnetic pyrrhotite is more reactive to surface oxidation than its 5C non-magnetic counterpart. Other associated sulfides (e.g., pentlandite, chalcopyrite) may enhance galvanic interactions and accelerate pyrrhotite oxidation. The higher oxidation rate of the 4C type compared to 5C is not only because of higher percentages of vacancies (12.5% in 4C compared to 10% in 5C) and higher proportion of Fe^{3+} (29% of total iron compared to 22% for 5C) but also because of its common occurrence with pyrite to accelerate its oxidation by galvanic interactions in the electrolytic pore solution of concrete having noticeably lower rest potential for pyrrhotite compared to pyrite. Moreover, the higher specific surface area (smaller particle size) of pyrrhotite compared to that of pyrite or other sulfides and higher alkalinity, higher porosity of concrete and moisture condition also enhances its oxidation kinetics (Nicholson and Scharer, 1994). According to Divet and Davy (1996) high pH conditions, such as those found in concrete, enhance iron sulfide oxidation. Oxidation of iron sulfide minerals is exothermic, e.g., pyrite oxidation produces about 1410 kJ of heat by mole of oxidized pyrite, which contributes to locally increasing the temperature and thus accelerating the oxidation reaction of pyrite (Bérubé, 1997).

Mechanisms of Two-Stage Expansions from Pyrrhotite Oxidation and Internal Sulfate Attack

Worldwide occurrences of oxidation of iron sulfide minerals in concrete aggregates have unequivocally confirmed concrete deterioration by two-stage expansions associated with: (a) oxidation of pyrite or pyrrhotite in the presence of oxygen and moisture during service with

formation of iron oxide, hydroxide and oxyhydroxide phases, e.g., goethite, limonite, and ferrihydrite causing the first expansion of the unsound aggregates and formation of cracks within the aggregates and from unsound aggregates to paste, which was then followed by (b) second expansions in the paste from reactions between sulfates released from sulfide oxidation and cement hydration products (internal sulfate attack) and formation of gypsum (from calcium hydroxide), ettringite (from calcium aluminate hydrate phases), or, thaumasite in the presence of carbonate and silicate ions in cold weather conditions, affecting the calcium silicate hydrate framework of paste.

As seen in the previous section, crystal structure, surface defects, presence of catalysts, presence of other iron sulfides such as pyrite for galvanic interactions, higher proportions of vacancies in crystal structures, higher proportion of Fe^{3+}, higher specific surface area, moisture conditions, and various other factors enhance pyrrhotite oxidation. Due to such variabilities, pyrrhotite grains from the same structure may show very different rates of oxidation.

From the SEM-EDS studies of oxidized pyrrhotite grains, Oliveira et al. (2014) proposed three distinct stages of pyrrhotite oxidation starting from (a) the non-oxidized form having very low or no oxygen (S/Fe atomic ratio around 1, O/Fe close to 0) to (b) initiation of oxidation and restructuring of the pyrrhotite into pyrite due to the diffusion of iron through the pyrrhotite surface causing an increase in S/Fe atomic ratio towards pyrite (e.g., S/Fe around 1.5, and O/Fe between 0 and 1), and finally (c) formation of the products of oxidation of pyrrhotite having a large range of O/Fe ratios from wustite (O/Fe = 1) through hematite (O/Fe = 1.5) and goethite (O/Fe = 2) to ferrihydrite (O/Fe = 3), all having a S/Fe ratio of 0. Similar results are found in the SEM-EDS studies of Jana (2022) as also shown here in Figure 24 with a larger database.

Rimstidt and Vaughan (2003) mentioned three distinct steps in the electrochemical oxidation of pyrite involving (a) a cathodic reaction, which transfers electrons from the surface of pyrite to the aqueous oxidant species, usually O_2 or Fe^{3+} ($^1/_2\ O_2 + 2H^+ + 2e^- = H_2O$; $Fe^{3+} + e^- = Fe^{2+}$); then (b) electron transport from the sulfur atoms at the site of an anodic reaction to replace the electron lost from the cathodic site; and finally (c) an anodic reaction where the oxygen atom of a water molecule interacts with a sulfur atom to create a sulfoxy species, which releases an electron into the solid and one or two hydrogen ions to solution ($>S + H_2O = >S\text{-}OH + H^+ + e^-$). The balanced cathodic reactions, $FeS_2 + 3.5O_2 + H_2O = Fe^{2+} + 2H^+ + 2SO_4^{2-}$, and $FeS_2 + 14Fe^{3+} + 8H_2O = 15Fe^{2+} + 16H^+ + 2SO_4^{2-}$, show that the oxidation process does not oxidize iron (it is Fe^{2}+ in the mineral and remains Fe^{2}+ as it is released into the solution), but rather, it oxidizes sulfur. The unique semiconductor nature of pyrite, unlike pyrrhotite, influences electron transfer as an important intermediate step in oxidation. Sulfide mineral oxidation removes seven electrons from disulfide sulfur or eight electrons from sulfide sulfur to form sulfate, which indicates that the sulfur atoms must pass through several oxidation states during the complex oxidation process (since only one or at most two electrons can be transferred at a time), so many different sulfur compounds might be involved.

A number of mechanisms have been proposed over the past five decades to explain the classical external sulfate attacks in concrete. These range from (a) *in situ*, topochemical formation of ettringite by reaction of calcium monosulfoaluminate hydrate and/or calcium aluminate hydrate phases in the cement paste with the external sulfate ions that have entered into concrete from adjacent high sulfate soil or groundwater, and where the reaction products occupy noticeably larger volumes than the reactants causing expansion and cracking (Day, 1992); to (b) moisture absorption and swelling of a colloidal form of ettringite (Mehta, 1973,

1992). Sulfates from the external sources cause the classical external sulfate attack resulting in cracking, spalling, and softening of paste by decomposition of cement hydration products.

Sulfates can also be released from the internal sources, such as in heat-treated concrete where high temperature during steam curing prevents normal formation of ettringite during Portland cement hydration. This can appear at the hardened state if the concrete is exposed to moisture during service (Heinz and Ludwig, 1987; Heinz et al., 1999; Collepardi, 1999; Diamond, 1996; Fu and Beaudoin, 1996; Johnson and Thaulow, 1999). Concrete made using cements having excess alkali sulfate phases in the clinker (Hime, 1996; Hime and Marusin, 1999) can also contribute sulfate to cause internal sulfate attack. Sulfates released after heat treatment in steam-curing or from cement in non-heat-treated concrete can cause *delayed ettringite formation* (DEF) at the hardened state in the presence of moisture during service. Concrete deteriorated by DEF develops cracks, spalls, and gaps around the aggregates due to direct expansion of paste relative to aggregates, where widths of the gaps are usually proportional to the size of the aggregates. Many deteriorated paste microstructures in distressed concretes from eastern Connecticut shared some of these features of DEF, e.g., gaps around aggregates and formation of ettringite in gaps.

Therefore, mechanisms of deterioration from the released sulfate after pyrrhotite oxidation is somewhat similar in terms of expansion at the hardened state to that of DEF even though gaps around aggregates and the presence of 'secondary' ettringite in the gaps (the common characteristic microstructural feature of DEF) may not always be present in the internal sulfate attack from pyrrhotite (or pyrite) oxidation. For example, widths of the gaps around aggregates may not always correlate with the size of aggregates, which is indeed common in DEF-related distress for the bulk volume expansion of paste around aggregates. Besides, primary ettringite formation was not 'delayed' during cement hydration in the cast-in-place pyrrhotite-bearing concretes, hence there is no occurrence of DEF *per se* here. Nevertheless, as in the cases of classical external sulfate attack and DEF, contrary to the mere filling of voids and cracks by the products of sulfate attack, it is rather their formation in the confined spaces in paste, as well as along aggregate-paste interfaces, perhaps associated with moisture absorption of their poorly crystalline form or perhaps in colloidal forms, which cause the second-stage deleterious expansions and related distress.

Relative Expansions from Iron Sulfide Oxidation and Internal Sulfate Attack

To evaluate which of the two stages of expansions causes the most deterioration, Schmidt et al. (2011) found that in their study of the 1970s deteriorated concrete dam in Switzerland, oxidation of iron sulfide grains containing 80% pyrrhotite and 20% pyrite by volume have caused significant cracking from unsound biotite-muscovite-schist aggregate to paste, rust staining, and abundant secondary ettringite formation in cement paste. Image analysis of micrographs of polished and thin sections have revealed that only about 30% to 40% by volume of the total iron sulfides of the extracted aggregates had reacted after more than 40 years in the dam concrete. Pyrrhotite grains showed oxidation of about 60% by volume as opposed to oxidation of only about 4% by volume of pyrite, indicating a significantly higher rate of oxidation in the alkaline environment and expansion potential of pyrrhotite, especially at the earlier stages of concrete distress than pyrite. Studies of deteriorated concrete foundations in the Trois-Rivières area, Canada by Rodrigues et al. (2015) also found deep oxidation of

pyrrhotite, whereas only traces to almost sound condition of associated pyrite. Calculated theoretical solid volume increase of pyrrhotite and pyrite from oxidation are 1.7 and 1.3 times, respectively (Schmidt et al., 2011). For a hypothetical 100% oxidation of both iron sulfides producing half goethite and half ferrihydrite, the calculated maximum expansion of aggregate was 0.07%, which was higher than the intrinsic strain limits of alkali-silica reactive aggregates (usually between 0.016% and 0.018% from Ben Haha et al., 2007) to develop stresses leading to cracking. For (a) the determined amounts of iron sulfides in the dam concrete (i.e., 80% pyrrhotite and 20% pyrite), (b) degree of oxidation (i.e., 60% oxidation for pyrrhotite and 4% oxidation for pyrite), (c) a total 30 to 40% oxidation of iron sulfides after 40 years of weathering for their slow reaction kinetics, and (d) a reasonable 75% aggregate content in their dam concrete, the resulting volume increase and strain of dam concrete was calculated to be in the range of 0.04 to 0.05%, which was reportedly about twice the actual expansion of the dam concrete recorded. This indicated that iron sulfide oxidation could be the main mechanism of expansion and distress with only a minor role, if any, of expansion from internal sulfate attack. In their calculations, 60% oxidation of pyrrhotite released about 4.5 kg/m^3 of SO_3 into the paste, which was correlated to an increase of SO_3 content of paste (having a cement content of 280 kg/m^3) by 1.6%. Assuming an original sulfate content of cement around 2.5%, the total sulfate level was calculated to be around 4.1% after release of sulfate from iron sulfides, which was reportedly still below the amount needed to cause deleterious expansion. Reactions between released sulfates and calcium hydroxide or monosulfate cause expansions from submicroscopic formation of gypsum and ettringite in the confined areas of paste, sometimes resulting in gaps around aggregates. However, the absence of that evidence in their investigation of dam concrete or their calculated lower-than-threshold sulfate content for expansion, did not necessarily lead them to entirely discard the sulfate expansion scenario. Instead, they mentioned the difficulty of determining its relative role when aggregate expansion has clearly played the major role according to their calculations, at least in their investigation of dam concrete, causing cracking within unsound aggregates extending into the paste.

However, many authors believe expansion from internal sulfate attack as the major if not the main mechanism of expansion. According to Casanova et al. (1996), and Duchesne et al., (2021) internal sulfate attack, e.g., causing more than two times solid volume expansion from gypsum formation are, by far, the most expansive reactions compared to oxidation reactions. According to Casanova et al. (1996), pyrrhotite oxidation forming iron sulfate may generate a solid volume increase in the order of 187 cm^3 per mole of sulfide but only *at maximum expansion at reaction completion*, whereas volume changes of 42, 183, and 172 cm^3 per mole of sulfide occurs during formation of gypsum, calcium aluminate monosulfate, and ettringite, respectively, from the internal sulfate attack. As in the case of a study of a 40-year-old distressed dam (Schmidt et al., 2011), or in the distressed concrete from eastern Connecticut, 100% oxidation of iron sulfides is unlikely. Moreover, in the alkaline pore solution of concrete, ferrihydrite is more stable than goethite, hence XRD analyses of aggregates extracted from distressed cores in studies by Jana (2018, 2019, 2020, 2022) showed ferrihydrite as the only oxidation product (although Wille and Zhong (2016) found some goethite with ferrihydrite in quarried stones). The 0.016% to 0.018% intrinsic strain limit of aggregates in calculations by Schmidt et al. (2011) are based on alkali-silica reactive aggregates of Ben Haha et al. (2007), which may not be applicable to the pyrrhotite-bearing gneiss from Connecticut where no evidence of ASR was found. In addition, in the case of pyrrhotite, concrete expansion is not homogeneous, hence aggregate oxidation alone is unlikely the main cause of significant

cracking in Connecticut foundations without contributions from subsequent involvement of internal sulfate attack from the sulfates released from oxidation with cement paste hydrates. Development of profuse fine, microcrystalline, fibrous secondary ettringite deposits, intimately intermixed with cement hydration products were identified in many ettringite-infested confined regions of paste in several case studies by Jana (2008 a, b, 2018 a, b, 2019 a, b, c, 2020, 2022). This was different to the more common precipitation of secondary ettringite in cracks, voids, and porous areas of paste, and are indications of independent expansion in paste regions along with oxidative expansions of aggregates without necessarily creating gaps around aggregates as found in other deleterious ettringite-induced paste expansion cases, e.g., in DEF-related distress of many railroad ties. Products of both pyrrhotite oxidation (iron oxide/hydroxide/oxyhydroxide) and internal sulfate attack (gypsum, ettringite, thaumasite) are found in the studies of deteriorated concrete foundations, both in eastern Connecticut by Jana (2020, 2022) and in the Trois-Rivières area, Canada by Rodrigues et al. (2012 a, 2013). Absorption of moisture by these ettringite-infested regions of paste can induce additional expansion, which is beyond and often more than the expansion simply from secondary ettringite formation, which is similar to the expansion in classical external sulfate attack from moisture-absorption of gelatinous or colloidal ettringite (Mehta, 1973). Hence, internal sulfate attack creates more volume increase in paste than the increase from aggregate oxidation. Abundance of white efflorescence deposits of sulfates, e.g., thenardite and aphthitalite (Wille and Zhong, 2016) in many cracked foundations in Connecticut, indicates leaching of sulfates not only as the product of oxidation of aggregate but also from paste. Additionally, precipitation of profuse secondary ettringite in air voids may also reduce the effectiveness of air voids to hold moisture and prevent freezing-related stresses in concrete. Most residential foundations in Connecticut are exposed to a harsh, moist outdoor environment with freezing at critically saturated conditions.

Therefore, it is the combinations of initial expansions from oxidation of aggregate forming goethite and ferrihydrite, followed by expansion from internal sulfate attack in paste by the released sulfates forming secondary ettringite, which has aggravated most of the pyrrhotite-oxidation distress. Exposures to moist outdoor environment of subfreezing temperatures with limited to no protection against moisture ingress have further aggravated the distress from deeper penetration of moisture and continued reactions. Pyrrhotite in anorthositic gabbro intrusive igneous rocks in the Trois-Rivières area were often surrounded by a thin layer of iron carbonates (siderite) which has promoted thaumasite formation along with oxidation 'rust' of goethite, limonite, and ferrihydrite and sulfate attack products of gypsum and ettringite (Rodrigues et al., 2012). Although Jana (2018, 2019, 2020, 2022) did not find any thaumasite, Wille and Zhong (2016) reported some questionable thaumasite formation along aggregate-paste interfaces in their SEM images (without any elemental or XRD data, or the carbonate source) from distressed foundations from eastern Connecticut.

Assessment of Aggregates for Pyrrhotite Oxidation Potential

Standardization of the amount of iron sulfide minerals considered acceptable in concrete aggregates is not well-established. American, Canadian, British, and French standards for concrete aggregates mention potential problems from use of aggregates containing iron sulfide in concrete but have not established acceptable limits of iron sulfide contents. Limits have been established for total sulfur (S_T) by mass in the French standard at 0.4%, and European standard

at 1%, or 0.1% if pyrrhotite is present [NF EN 12620 "Aggregates for concrete," and also in Annex P of the Canadian Standard, CSA A23.1:19 (CSA, 2019), "Concrete materials and methods of concrete construction/Test methods and standard practices for concrete"]. The European Standard NF EN 12620 (2002) specified that the total sulfur content of the aggregate must not exceed 1% S by mass; if pyrrhotite is present, a maximum total sulfur content of 0.1% S by mass should be applied. Norwegian Standard NS-EN 12620:2002 +A1:2008+NA:2016 also requires analysis of total sulfur according to the test method NS- EN 1744-1 Clause 11. In cases where the aggregate contains pyrrhotite, the limit for total S is 0.1%, or else the limit can be raised to 1%. The threshold value for pyrrhotite-containing aggregates is 10 times smaller than the limit usually accepted for aggregates containing other iron sulfides.

In the Follo Line project for the longest railway tunnel in the Nordic region, approximately 300 crushed Precambrian gneiss and amphibolite aggregates were tested for total sulfur where 30% of the samples did not fulfill the 0.1% sulfur requirements of NS-EN 12620+NA when pyrrhotite was identified in 60% of the samples. The testing performed did not reveal any clear correlation between rock type and the presence of pyrrhotite. Rock types containing pyrrhotite with total S of more than 0.1% S from Norwegian aggregate quarries are (Jensen, 2018) mafic rock (gabbro, amphibolite, greenstone); gneiss; granite; greywacke; sandstone; silt - claystone; limestone; felspathic rock (rhomb porphyry); and volcanic rock (rhyolite). Nevertheless, according to the Norwegian researchers, cases of concrete deterioration due to pyrrhotite have not yet been reported in Norway indicating pyrrhotite in aggregates is not as much of a concrete durability problem in Norway as a requirement driven by the standard (Jensen, 2018).

According to Chinchón-Payá et al. (2011), the 0.1% limit is considered extremely small by many engineers and may have caused the unnecessary rejection of aggregates that could be suitable for producing concrete. The limits as to the amount of pyrrhotite that would lead to damage has not been identified to date. This may be quite difficult to do because the reactivity of pyrrhotite may vary according to its crystallographic characteristics, while many factors are involved in this deleterious mechanism. No precise guidelines or methods have been proposed at the time of this chapter to evaluate the potential reactivity of sulfide containing aggregates. Since pyrite is generally a more common iron sulfide and more stable in concrete than pyrrhotite, it is important to identify the different types of sulfides present in the aggregates before rejecting an aggregate based only on the total sulfur content.

Rodrigues et al. (2016) proposed a three-phase testing program mentioned below, including (a) measurement of total sulfur, (b) oxygen consumption determination, and (c) accelerated mortar bar expansion testing. Limits are proposed for each phase of the protocol but are in need of additional validation. The US Army Corps of Engineers have proposed similar short (1-2 years) to long-term (8+ years) testing protocols for aggregate regulations and structural assessments. Significant research is still needed to identify appropriate limits.

All testing protocols indicate additional evaluation of a quarry is needed for use as a source of concrete aggregate beyond the physical requirements and limits of potentially deleterious constituents mentioned in ASTM C 33.

Multi-Step Laboratory Testing Protocols for Screening of Aggregates

The highly heterogeneous distribution of pyrite and pyrrhotite in aggregates even from the same quarry, along with non-stoichiometric compositional variations of naturally occurring

pyrrhotite having variable chemical compositions, crystallographic structures, and specific surface areas, causes variability in reactivity of pyrrhotite. Both these factors pose challenges in quality control of aggregates for potential pyrrhotite oxidation-related unsoundness (Duchesne at al., 2021).

Rodrigues et al. (2016) proposed a three-phase evaluation protocol, which was subsequently incorporated into the Canadian Standard as Annex P (CSA, 2019), for predicting the damaging potential of aggregates containing iron sulfide minerals prior to their use in concrete. These are described below.

Proposed Canadian Protocol

a) Phase 1 - Determination of *total sulfur content* (S_T % by mass) of 0.3 to 1 gram of aggregate selected by coning and quartering from a representative 4 kg (8.8 lb.) aggregate sample (5 to 20 mm particle size), followed by successive splitting to 2 kg subsets, and then progressive crushing, splitting, and pulverizing until all the particles pass the 80 µm (0.003 in.) sieve. The final stage was splitting the 80 µm material into four subsamples to be used for the S_T determination in three different laboratories, by carbon/sulfur induction arc furnace where the sample is melted in a pure oxygen atmosphere, causing sulfur to react to form sulfur dioxide (SO_2). The SO_2 content is determined by infrared absorption, from which the S_T is calculated. The values obtained and considering existing standards lead to proposing: (a) an $S_T > 1\%$ as the value for rejecting the aggregate; (b) $0.1\% < S_T \leq 1.0\%$ as the interval value for proceeding to the second phase of the protocol; and (c) the $S_T \leq 0.10\%$ as the limit value for acceptance.
b) Phase 2 - *Oxygen consumption test*. The aggregates ($0.1\% < S_T \leq 1.0\%$) that are directed to Phase 2 are ground to produce a particle size less than 150 µm and then exposed to the oxygen consumption test described before (Rodrigues et al. 2016). The tests are conducted in sealed methyl methacrylate columns 200 mm (7.87 in.) in height and 142 mm (5.59 in.) in internal diameter. The compacted ground aggregate lies in the bottom part of the container, while a galvanic-cell oxygen sensor (able to measure 0 to 100% oxygen) is inserted through the methyl methacrylate cover at the top of the column and connected to a data-logger. Different parameters were evaluated to find the optimum testing conditions, such as the particle size (mortar bar size fractions 150 µm to 5 mm [0.006 in. to 0.20 in.], < 1.18 mm [0.046 in.], or <150 µm [0.006 in.]) of the aggregate; the ground material thickness (2.5, 5, and 10 cm [0.98, 1.97, and 3.94 in.]); its saturation degree (40% and 60%); and headspace for oxygen consumption measurements (2.5, 5, 10, 15, and 17.5 cm [0.98, 1.97, 3.94, 5.91, and 6.89 in.]). Optimized parameters comprised a 10 cm compacted layer of aggregate material with particle size <150-µm, kept at 40% saturation, and with a 10-cm headspace left at the top of the cell. The consumption of the O_2 present in the headspace is monitored over a 3-h testing period at 22°C. The test was able to discriminate sulfide-bearing aggregates from a control one when using a threshold limit of 5% O_2 consumed. All the measurements were performed at atmospheric pressure, at room temperature (22°C [71.6°F]) and using a 3.5-h test duration (30 minutes for the probes to stabilize plus 3 h of effective oxygen consumption measurements). Considering the limited number of aggregates tested, the tentative acceptance limit was set at lower than 5.0% of consumed oxygen, which has effectively separated sulfide-bearing aggregates from

non-sulfide control ones, while aggregates inducing values equal to or higher than 5.0% should be tested in Phase 3 of the protocol.

c) Phase 3 consists of a *two-part mortar bar test*. Mortar bars 25 x 25 x 285 mm (0.98 x 0.98 x 11.22 in.) in size, were manufactured using a general-use high-alkali (0.95% Na_2Oeq) Portland cement, a cement-to-aggregate ratio of 1:2.75, with the proportions of the various aggregate size fractions similar to those used in the accelerated mortar bar test for ASR (ASTM C 1260). A water-cement ratio of 0.65 was used to simulate the characteristics of concrete used for housing foundations in the Trois-Rivières area. In Part I, mortar bars are subjected to a 90-day storage period at 80°C (176°F) and 80% RH with two 3-h soaking periods in a 6% sodium hypochlorite solution. It was found that expansions in excess of 0.10% at 90 days could be caused by ASR and/or the oxidation of sulfide phases within the aggregate. The exact reason for this excessive expansion should be clarified before deciding whether to use or reject the aggregate. If the values are lower than 0.10%, the samples should be transferred to 4°C (39.2°F) and 100% RH for another 90-day period. If, at the end of those 90 days, the sample expansion remains stable, the aggregates could be accepted. However, if the expansion continues, the aggregate should be rejected. The proposed protocol and preliminary test limits, although based on the results of an extensive test program, will need to be further validated through the testing of a larger number of aggregates.

Jana (2020) described a five-step laboratory testing protocol for aggregates (after being found satisfactory according to ASTM C 33) to evaluate any potentially deleterious reactions from oxidation of iron sulfide minerals, an updated version of which is summarized below and in Figure 33. Additionally, Table 2 provides a scheme for various laboratory testing of existing concretes, aggregates extracted from existing concretes, crushed stone and loose aggregates for new construction, and rapid identification of pyrrhotite in field concrete and aggregate.

Jana Protocol

a) Step 1 - Aggregates in conformance to the ASTM C 33 specification should first undergo *petrographic examinations* according to ASTM C 295, on representative portions of crushed stone, gravels, or preferably on rock cores drilled from a quarry to represent different depths e.g., stratigraphic formations, to examine the presence of iron sulfide minerals. Rock core should be examined on cylindrical surfaces as well as on cross sections by using a low-power stereomicroscope, followed by preparing thin sections for further examinations in a petrographic microscope to determine the depth and abundance of various iron sulfide minerals. Reflected-light (ore) microscopy of polished rock sections, micro-XRF, or SEM-EDS of sulfide grains detected on lapped cross sections from stereo microscopical examinations and in thin sections, can also be done to determine the composition and speciation of iron sulfides, including potential detection of pyrrhotite and pyrite. A positive identification of pyrrhotite in aggregate separate from other sulfides, e.g., from Fe/S atomic ratio in SEM-EDS, is essential at this stage before proceeding to the chemical analysis of total sulfur content in Step 2.

b) Step 2 - *Total sulfur contents* (S_T) of the portions of rock core that have revealed the presence of iron sulfide minerals by petrography should then be determined by various methods, e.g., by portable handheld XRF on core sections; micro-XRF of core; bench top ED-XRF on pressed pellets of pulverized rock; fused beads of pulverized rock in WD-XRF; or by the more conventional combustion IR method. A sulfur content of less than 0.1% will be considered as the safe limit for acceptance, greater than 1% should be rejected unless aggregate has a prior satisfactory performance record or will not be incorporated in concrete for moist environments, whereas amounts between 0.1 and 1% ST should be examined further before acceptance for concrete in moist environments.
c) Step 3 - Aggregates that showed $0.1\% < S_T \leq 1.0\%$ should then be examined by X-ray diffraction and magnetic susceptibility drop during heating across the Curie temperature of pyrrhotite (325°C) to determine the types and abundances of iron sulfide minerals, particularly including pyrrhotite, quantification of pyrrhotite by both studies, as well as detection of the oxidation products of pyrrhotite from XRD.
d) Step 4 - Aggregates showing positive detection of pyrrhotite in Step 3 should then be subjected to an oxygen consumption test. Either the Rodrigues et al. (2016) oxygen consumption test should be done, or the Wille and Zhong (2016) and Jana (2020) method of digestion of pulverized aggregate in a strong oxidizing solution of 35 to 40% hydrogen peroxide for several days to a month, should be done to determine the amount of released sulfate in the diluted filtrate by ion chromatography (ASTM D 4327).
e) Step 5 - Aggregates that do not meet the acceptance criterion, i.e., > 5.0% oxygen consumption from Rodrigues et al. (2016)'s test should be further evaluated in the accelerated mortar bar expansion test, e.g., according to the Phase 1 method of Rodrigues et al. (2015) (unless the concrete also shows evidence of thaumasite attack, in which case Phase 2 should also be done). Aggregates showing expansions in excess of 0.1% will be rejected.

Petrography, chemical (total sulfur content), pyrrhotite quantification (XRD, thermo-magnetic study), oxygen consumption rate, and mortar bar expansion tests are the five fundamental categories of tests that should effectively screen sound aggregates from the potentially unsound ones. However, care must be exercised before rejecting an aggregate because of its failure in one test unless pyrrhotite is positively identified as the main sulfide phase and showing a high oxidation potential for incorporation in concrete for a moist environment. There are cases, such as described in the Nordic Workshop (contrary to the historical damage from pyrrhotite in alum shale in Oslo concrete) where detection of pyrrhotite, even at amounts in excess of the 0.1% total sulfur threshold (range of 0.01 to 0.26% S_T) did not cause any distress in concrete (Haugen and Lindgard, 2018; Jensen, 2018; however, which could possibly be due to prior oxidation of aggregates before incorporation in concrete, which may not be the case for freshly quarried crushed stone).

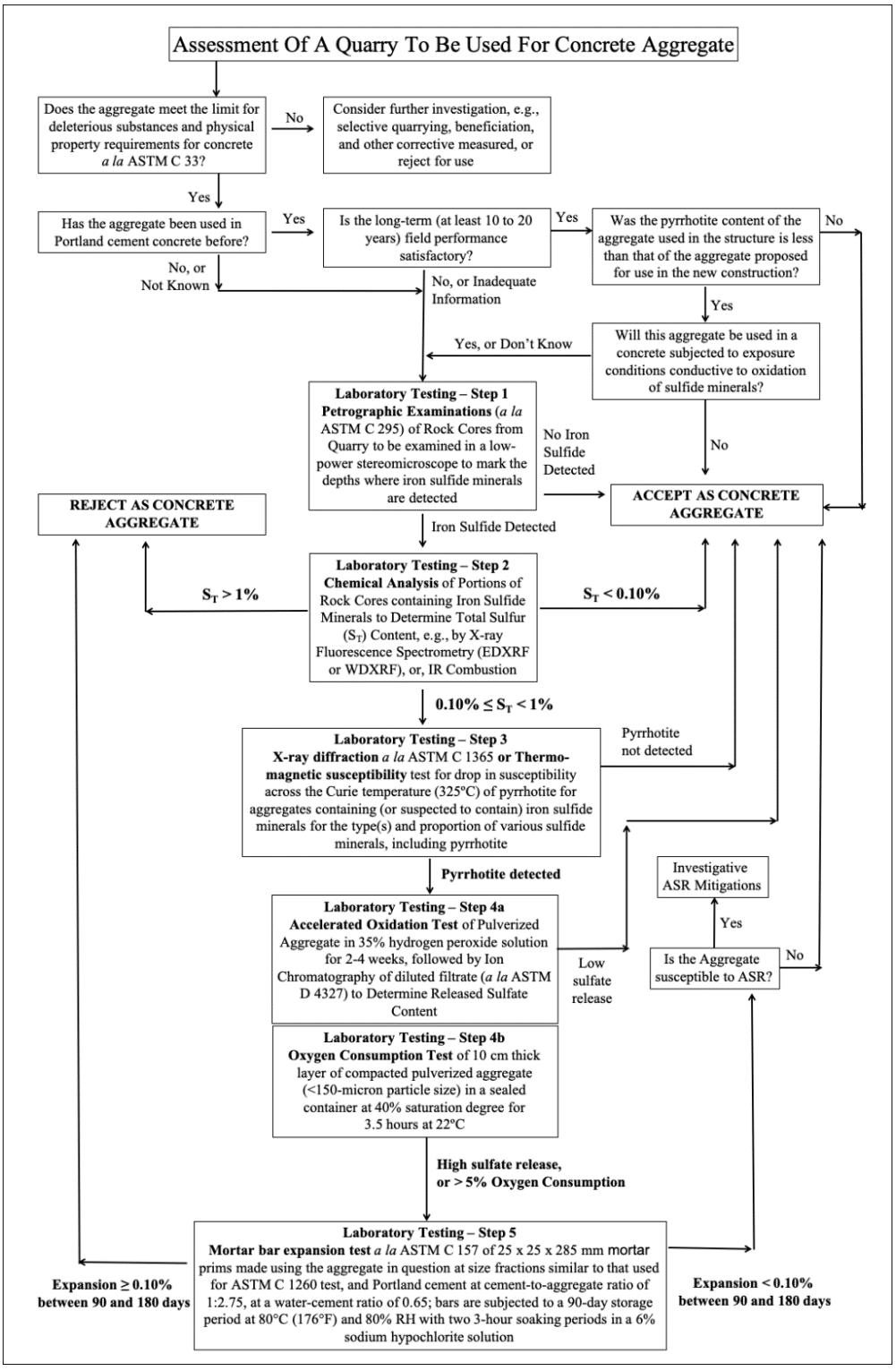

Figure 33. Assessment of a quarry through a five-step laboratory testing protocol for use as concrete aggregate to mitigate pyrrhotite-related deterioration (modified from Jana, 2020).

Conclusion

Oxidation of pyrite, or pyrrhotite in the presence of hydroxyl ion causes formation of ferrous sulfate, ferric hydroxide, and sulfuric acid as a preliminary step, followed by hydrolysis of ferrous sulfate to ferric hydroxide and sulfuric acid. Interaction of the sulfuric acid with the calcium hydroxide component of Portland cement hydration in concrete produces calcium sulfate, which, in turn, produces calcium sulfoaluminate by interaction with aluminates in the cement paste. The resultant substantial increase in solid volumes, first from oxidation and then from internal sulfate attack cause respective expansion and cracking in unsound aggregates and the paste fraction of concrete. Concrete deterioration across tunnels, dams, houses, and residential foundations across many parts of the world has not only confirmed the presence of disseminated pyrrhotite inclusions in unsound aggregates, but also evidenced pyrrhotite oxidation-related distress, e.g., from reddish brown stains to cracking, and associated internal sulfate attack from the sulfuric acid released from pyrrhotite oxidation. Perhaps, the epicenter of this distress is found in the eastern Connecticut region of the US where crushed gneiss coarse aggregates from a local quarry with significant pyrrhotite crystallization showed variable concentrations of pyrrhotite in the quarried stone, as well as varying degrees of oxidation and resultant deterioration, e.g., from no distress in some foundations despite having pyrrhotite in crushed gneiss to severe cracking in others. Even from the same foundation in Connecticut, concrete having a greater proportion of dark gray and brown crushed granite gneiss in the coarse aggregate showed more distress due to a noticeable amount of coarsely disseminated pyrrhotite grains, than the off-white gneiss coarse aggregate particles which contain finely disseminated pyrrhotite. Extensive macro and micro cracking in thousands of foundations are testament of the severity of the deleterious actions of pyrrhotite oxidation. Very high sulfate (as SO_3) contents in the distressed concretes (e.g., as high as 2.7% SO_3 in Connecticut compared to ~ 0.45% SO_3 in normal Portland cement concrete) indicates additional sulfate sources beside Portland cement, which was confirmed to be from pyrrhotite in the aggregates. Cracking, high sulfate, and resultant sulfate products are, in fact, similar to other types of concrete deteriorations, e.g., in the chimney or sewer environments (Jana, 2008), or, in the cases of delayed ettringite formation (Jana, 2008). However, pyrrhotite-related distresses can be distinguished by (a) direct detection of the products of oxidation, e.g., goethite, limonite, ferrihydrite, etc., from the definitive occurrences of pyrrhotite in unsound aggregates, and (b) the source of high sulfur from pyrrhotite oxidation, e.g., either in the total sulfur content in concrete from combustion IR or XRF, or, higher sulfate (as SO_3) in the paste than that contributed from Portland cement from SEM-EDS studies. Due to the limitation of XRD studies on pyrrhotite detection, e.g., usually only above 1% concentration, XRD studies may not detect pyrrhotite in concrete or even in extracted unsound coarse aggregates (despite its positive detection from optical/ore microscopy, and SEM-EDS) but the oxidation products, e.g., goethite and ferrihydrite can be detectable from XRD. Jana (2020) found unreacted pyrrhotite during slow scans in XRD studies of aggregates extracted from cracked concrete cores. SEM-EDS studies detect veins of oxidized iron in iron sulfide bodies in pyrrhotite, and sulfate contamination in paste from sulfates released from pyrrhotite oxidation. Micro-XRF studies can separate various sulfide species in aggregates on a large-area lapped section. Therefore, a combined approach of optical microscopy, SEM-EDS, XRD, XRF, micro-XRF, and chemical analysis (total sulfur content) are essential for investigation of a pyrrhotite-

bearing aggregate for its potentially deleterious role if intended for use in a concrete, or, the extent of distress in a deteriorated concrete from pyrrhotite oxidation. Ion chromatography of filtrates of potentially unsound aggregates digested in a highly oxidizing solution (35% hydrogen peroxide), or the oxygen consumption test of a gravel or a quarried pyrrhotite-bearing aggregate showing > 5% consumption are two follow-up tests to measure potentially deleterious release of sulfate in the alkaline pore solution of concrete in the presence of oxygen and moisture to contribute to internal sulfate attack. Accelerated length change measurements of concrete prisms or mortar bars made using suspected aggregates are also beneficial to filter aggregates showing high expansion potentials. All these screening tests are indeed very effective when used together rather than relying only on a threshold sulfur value for screening potentially unsound pyrrhotite-containing aggregate. Many pyrrhotite and pyrite-bearing aggregates are performing satisfactorily in concrete even in moist outdoor environments, whereas many others are showing similar distress mechanisms from both iron sulfide types in concrete. Satisfactory field performance of an iron sulfide bearing aggregate can only be assessed when oxidation, expansion, and sulfate release potentials of quarried stone or gravels are verified with the laboratory tests discussed in this review.

Not all concrete containing pyrrhotite-bearing aggregates showed distress, as the author has seen in a school from eastern Connection (Jana, 2019 b) where construction dating back to 1998 showed severe deterioration, whereas a 2001 addition using the same pyrrhotite-bearing crushed gneiss aggregates, reportedly supplied by the same contractor, showed no damage. In the case of the newer wall with a dense 1-mm thick cementitious protective coating on the concrete, showed no distress at the time of investigation except some minor localized internal cracking in some crushed gneiss particles. Clearly, availability of moisture during service and the means to prevent its penetration into concrete, played an important role in preventing pyrrhotite oxidation-related distress in concrete.

Relevant questions still left to be addressed are: (1) methods of rapid, in-situ, field detection of pyrrhotite in aggregates and concrete, where non-destructive techniques such as NMR, portable XRF units, or thermomagnetic susceptibility studies are promising; (2) the threshold pyrrhotite content in aggregates to cause expansion and associated distress, which can be investigated by measuring sulfur content in aggregate, pyrrhotite content, and studies of expansion potentials of aggregates of variable sulfur (pyrrhotite) contents in accelerated laboratory tests; (3) how long it takes for the reactions to cause damage, which are essentially controlled by the reaction kinetics (which, in turn, are controlled by pyrrhotite crystal structure, Fe-vacancies, crystal size, etc.), moisture availability, abundance of unsound pyrrhotite grains in aggregates, and influence of other sulfide species on pyrrhotite oxidation; and (4) how moisture control can prevent or slow down oxidation damage. This is similar to controlling other moisture-induced damage like ASR, perhaps by improving the overall impermeability of concrete to moisture ingress by improving the concrete mix design (lower water-cementitious materials ratio, incorporating reactive pozzolans, etc.) to improving curing, degree of consolidation and other design and construction aspects to improve the overall durability of concrete in a moist environment so that any potential future distress from oxidation of pyrrhotite can be mitigated.

Acknowledgments

The author extends his thanks to his wife for reviewing an early version of this manuscript and coping with his time away from family during preparation of the manuscript. Sincere thanks are also due to Dr. Donald Campbell, the world-renowned concrete petrographer and clinker microscopist for reviewing an early version of this manuscript. The author is privileged to have learned concrete petrography from the founding fathers, Rich Mielenz to Bryant Mather and worked closely with Bernie Erlin for many decades with many exciting discussions on iron sulfide oxidation, sulfate attack, and many other issues addressed in this chapter. This work is dedicated to thousands of homeowners in Connecticut, Massachusetts, and across the world who have lost their homes from this distress.

References

Anderson, W. H. (2008). Foundation Problems and Pyrite Oxidation in the Chattanooga Shale. *Geological Survey Report of Investigation*. Estill County, Kentucky: Kentucky Geological Survey, Series XII, Report of Investigations 18.

Araujo, G. S., Chinchón, J. S. and Aguado, A. (2008). Evaluation of the Behavior of Concrete Gravity Dams Suffering from Internal Sulfate Attack. Ibracon, *Structures and Materials Journal*, Vol. 1, No. 1, pp. 84-112.

ASTM C 33. (2016). Standard Specification for Concrete Aggregates. Vol. 4.02, *Concrete and Aggregates*, ASTM International, West Conshohocken, PA.

ASTM C 114. (2018). Standard Test Methods for Chemical Analysis of Hydraulic Cement. Vol. 4.01, *Cement; Lime; Gypsum*, ASTM International, West Conshohocken, PA.

ASTM C 150. (2007). Standard Specification for Portland Cement. Vol. 4.01, *Cement; Lime; Gypsum*, ASTM International, West Conshohocken, PA.

ASTM C 157. (2014). Standard Test Method for Length Change of Hardened Hydraulic-Cement Mortar and Concrete. Vol. 4.02, *Concrete and Aggregates*, ASTM International, West Conshohocken, PA.

ASTM C 295. (2018). Standard Guide for Petrographic Examination of Aggregates for Concrete. Vol. 4.02, *Concrete and Aggregates*, ASTM International, West Conshohocken, PA.

ASTM C 856. (2020). Standard Practice for Petrographic Examination of Hardened Concrete. Vol. 4.02, *Concrete and Aggregates*, ASTM International, West Conshohocken, PA.

ASTM C 1260. (2014). Standard Test Method for Potential Alkali Reactivity of Aggregates (Mortar-Bar Method). Vol. 4.02, *Concrete and Aggregates*, ASTM International, West Conshohocken, PA.

ASTM C 1365. (2018). Standard Test Method for Determination of the Proportion of Phases in Portland Cement and Portland-Cement Clinker Using X-Ray Powder Diffraction Analysis. ASTM International, West Conshohocken, PA.

ASTM C 1723. (2016). Standard Guide for Examination of Hardened Concrete Using Scanning Electron Microscopy. Vol. 4.02, *Concrete and Aggregates*, ASTM International, West Conshohocken, PA.

ASTM D 4327. (2017). Standard Test Method for Anions in Water by Suppressed Ion Chromatography. Vol. 11.01, *Water*, ASTM International, West Conshohocken, PA.

Ayora, A., Chinchón, J. S., Aguado, A. and Guirado, F. (1998). Weathering of Iron Sulfides and Concrete Alteration: Thermodynamic Model and Observation in dams from Central Pyrenees, Spain. *Cement and Concrete Research*, Vol. 28, Issue 4, pp. 1223-1235.

Balachandra, A. (2020). Novel pyrrhotite detection method in concrete aggregate. Research grant from US Department of Defense, personal communication, US Patent Pending, Metna Co., Lansing, Michigan.

Bastow, T. J. and Hill, A. J. (2018). ^{57}Fe NMR characterization of pyrrhotite. *Journal of Magnetism and Magnetic Materials*, Vol. 447, pp. 58-60.

Belzile, N., Chen. Y., Cai, M. and Li, Y. (2004). A review on pyrrhotite oxidation. *Journal of Geochemical Exploration*, Vol. 84: pp. 65-76.

Belzile, N., Maki, S., Chen, Y. W. and Goldsack, D. (1997). Inhibition of pyrite oxidation by surface treatment. *Science of the Total Environment*, Vol. 196(2): pp. 177-186.

Ben Haha, M., Gallucci, E., Guidoum, A. and Scrivener, K. L. (2007). Relation of expansion to alkali silica reaction to the degree of reaction measured by SEM image analysis. *Cement and Concrete Research*, Vol. 37, pp. 1206–1214.

Berard, J. (1970). Black Shale Heaving at Ottawa, Canada: Discussion. *Canadian Geotechnical Journal*, Vol. 7(2), pp. 113-114.

Bérubé, M. A., Locat, J., Gelinas, P., Chagon, J. Y. and Lefrancois, P. (1986). Heaving of Black Shale in Québec City. *Canadian Journal of Earth Sciences*, Vol. 23, pp. 1774-1781.

Bérubé, M. A. (1997). Les shales pyriteux et les problèmes de gonflement: La situation actuelle au Québec [Pyritic shales and swelling problems: The current situation in Québec]. *Colloquium of Association of Engineering Geologists*, Montréal section, Laval, Québec, pp. 40.

Bruker Lab Report XRF 145, *S8 Tiger Series 2*. (2022). The determination of sulfur species (sulfide-sulfate) in cement by WDXRF, pp. 1-4.

Casanova, I., Agulló, L. and Aguado, A. (1996). Aggregate expansivity due to sulfide oxidation - I. Reaction system and rate model. *Cement and Concrete Research*, Vol. 26 (7): pp. 993-998.

Chinchón, J., Lopez, A., Querol, X. and Ayora, C. (1990). La Cantera de Mont Palau I: influéncia de la mineralogía de los áridos en la durabilidad del hormingón [The Mont Palau I Quarry: influence of aggregate mineralogy on concrete durability]. *Ing. Civil*, Vol. 72 pp. 79–88.

Chinchón, J., Lopez, A., Soriano, J. and Vazquez, E. (1990). La Cantera de Mont Palau II: Formacion de Compuestos Expansivos Generados en la Reaccion Arido-Hormingon [The Mont Palau II Quarry: Formation of Expansive Compounds Generated in the Aggregate-Hormingon Reaction]. *Ing. Civil*, Vol. 72 pp. 109–113.

Chinchón-Paya, S., Aguado, A. and Chinchón, S. (2012). A Comparative Investigation of the Degradation of Pyrite and Pyrrhotite Under Simulated Laboratory Conditions. *Engineering Geology*, Vol. 127, pp. 75-80.

Chinchón-Paya, S., Aguado, A., Coloma, F. and Chinchón, S. (2015). Study of aggregate samples with iron sulfides through micro-X-ray fluorescence (μXRF) and X-ray photoelectron spectroscopy (XPS). *Materials and Structure*, Vol. 48: pp. 1285-1290.

Chinchón, J. S., Ayora, C., Aguado, A. and Guirado, F. (1995). Influence of Weathering of Iron Sulfides Contained in Aggregates on Concrete Durability. *Cement and Concrete Research*, Vol. 25, No. 6, pp. 1264-1272.

Chirita, P. and Rimstidt, J. D. (2014). Pyrrhotite dissolution in acidic media. *Appl. Geochem*, Vol. 41: pp. 1-10.

Chuvarov, V., Aisueva, T. and Finkelshtein, A. (2016). Determination of Sulfide and Total Sulfur in Ore by Wavelength-Dispersive X-ray Fluorescence. *Analytical Letters*, Vol. 49, pp. 2099-2107.

Collepardi, M. (1999). Damage by Delayed Ettringite Formation. *Concrete International*, January, pp 69-74.

Cruz-Hernandez, Y., Chrysochoou, M. and Willie, K. (2020). Wavelength dispersive X-ray fluorescence method to estimate the oxidation reaction progress of sulfide minerals in concrete. *Spectrochim Acta*, Part B Vol. 172: 105949.

CSA Research Group. (2019). *Multi-laboratory study of proposed new test for determination of Sulphide sulphur content of concrete aggregates*. CSA-Research-Sulphide-Sulphur-Content-of-Concrete-Aggregates.pdf (csagroup.org).

CSA. (2019). *Concrete materials and methods of concrete construction/Test methods and standard practices for concrete*, CSA A23.1:19/CSA A23.2:19, CSA Group, Toronto.

Day, R. L. (1992). The Effect of Secondary Ettringite Formation on the Durability of Concrete: A Literature Analysis. *Research and Development Bulletin RD108T*, Portland Cement Association, Skokie, Illinois. 130p.

Deer, W. A., Howie, R. A. and Zussman, J. (2013). *An Introduction to the Rock-Forming Minerals 3rd Edition*. UK: Berforts Information Press, pp. 696.

Diamond, S. (1996). Delayed Ettringite Formation – Processes and Problems. *Cement and Concrete Composites*, Vol. 18, pp. 205-215.

Divet, L. and Davy, J. P. (1996). Étude des risques d'oxydation de la pyrite dans le milieu basique du béton [Study of the risks of oxidation of pyrite in the basic environment of concrete]. *Bull. Lab. Ponts et Chaussées* 204, pp. 97–107.

Duchesne, J. and Fournier, B. (2013). Deterioration of Concrete by the Oxidation of Sulphide Minerals in the Aggregate. *Journal of Civil Engineering and Architecture*, Vol. 7(8), pp. 922-931.

Duchesne, J. and Fournier, B. (2011). Petrography of Concrete Deteriorated by Weathering of Sulphide Minerals. *International Cement Microscopy Association Conference*.

Duchesne, J., Fournier, B. and Francoeur, J. (2018). Study of the Deterioration of Concrete Incorporating Sulfide-Bearing Aggregates. *Sixth International Conference on Durability of Concrete Structures*, pp. 273-280.

Duchesne, J., Rodrigues, A. and Fournier, B. (2021). Concrete damage due to oxidation of sulfide-bearing aggregate: a review of recent advances and limitations. *RILEM Technical Letters*, Vol. 6: pp. 82-92.

Dunbar, P. and Grattan-Bellew, P. (1995). Results of damage rating evaluation of condition of concrete from a number of structures affected by AAR. Proceedings *CANMET/ACI Workshop on Alkali-Aggregate Reactions in Concrete*, Dartmouth, NS, pp. 257 – 265.

EN 12620 (2002). *Norme européenne; granulats pour béton* [*European Standard: aggregates for concrete*], Comité européen de normalization, Brussels, Belgium.

Elberling, B., Nicholson, R. V., Reardon, E. J. and Tibble, P. (1994). Evaluation of sulfide oxidation rates: a laboratory study comparing oxygen fluxes and rates of oxidation product release. *Can. Geotech. J.*, Vol. 31 pp. 375-383.

Elberling, B. and Nicholson, R. V. (1996). Field determination of sulphide oxidation rates in mine tailings. *Water Resour. Res.*, Vol. 32 (6) pp. 1773-1784.

Erlin, B. and Jana, D. (2003). Forces of hydration that can cause havoc in Concrete – May the force not be with you. *Concrete International*, American Concrete Institute, pp. 51-57.

Fu, Y. and Beaudoin, J. J. (1996). Mechanism of Delayed Ettringite Formation in Portland Cement System. *ACI Materials Journal*, V 93, No. 4, July/August, pp 327-333.

Gazulla, M. F., Gomez, M. P., Orduna, M. and Rodrigo, M. (2008). New methodology for sulfur analysis in geological samples by WD-XRF spectrometry. *X-ray Spectrom*, Vol. 38, pp. 3-8.

Geiss, C. E. and Gourley, J. R. (2019). A thermomagnetic technique to quantify the risk of internal sulfur attack due to pyrrhotite. *Cement and Concrete Research*, Vol. 115: pp. 1-7.

Gomides, M. (2009). *Investiga ç ão de Agregados contendo Sulfetos e seus efeitos sobre a durabilidade do concreto* [*Investigation of Aggregates containing Sulfites and their effects on the durability of concrete*]. Universidade Federal do Rio Grande do Sul, Brazil (PhD. Thesis).

Gourley, J. (2018). Trinity College Environmental Science Program, Hartford, Connecticut, and Margaret Thomas, Connecticut State Geologist.

Grattan-Bellew, P. E. and Eden, W. J. (1975). Concrete deterioration and floor heave due to biogeochemical weathering of underlying shale. *Can. Geotech. J.* 12 pp. 372–378.

Guirguis, B., Shehata, M. H., Duchesne, J., Fournier, B., Durand, B. and Rivard, P. (2018). The application of a new oxidation mortar bar test to mixtures containing different cementing systems. *Construction and Building Materials*. Vol. 173, pp. 775-785.

Hagerman, T. and Roosaar, H. (1955). Kismineralens Skadeinwarkens pa Betong [The damaging effect of the silica mineral on concrete]. *Betong*. 2: pp. 151-161.

Hawkins, A. B. and Pinches, G. M. (1987). Cause and Significance of Heave at Llandough Hospital, Cardiff - A Case History of Ground Floor Heave due to Gypsum Growth. *Quarterly Journal of Engineering Geology and Hydrogeology*, Vol. 20, pp. 41-57.

Haugen, M. and Lindgard, J. (2018). Determination of Total Sulfur Content in Aggregates (2004-2018) – Results from SINTEF. Workshop *Impact of sulphide minerals (pyrrhotite) in concrete aggregate on concrete behavior*. 15th – 16th November, Oslo, Norway.

Heinz, D. and Ludwig, V. (1987). Mechanism of Secondary Ettringite Formation in Mortars and Concretes Subjected to Heat Treatment, Concrete Durability. *Katharine and Bryant Mather International Symposium, SP-100*, American Concrete Institute, Farmington Hills, Michigan, pp. 2059-2071.

Heinz, D., Kalde, M., Ludwig, U. and Ruediger, I. (1999). Present State of Investigation on Damaging Late Ettringite Formation (DLEF) in Mortars and Concretes. *Ettringite: The Sometimes Host of Destruction*, Bernard Erlin (ed), ACI SP-177, pp. 1-13.

Hime, W. G. (1996). Clinker Sulfate: A Cause for Distress and a Need for Specification. *Concrete in the Service of Mankind, Concrete for Environment, Enhancement, and Protection*, E & FN., Spon, pp. 387-395.

Hime, W. G. and Marusin, S. L. (1999). Delayed Ettringite Formation: Many Questions and Some Answers. *Ettringite: The Sometimes Host of Destruction*, Bernard Erlin (Ed), ACI SP-177, pp. 199-206.

Hime, W., Martinek, R. A., Backus, L. A. and Marusin, S. L. (2001). Salt Hydration Distress. *Concrete International*, V. 23, No. 10, pp. 43-50.

Hoover, S. E. and Lehmann, D. (2009). The Expansive Effects of Concentrated Pyritic Zones within the Devonian Marcellus Shale Formation of North America. *Quarterly Journal of Engineering Geology and Hydrogeology*, Vol. 42(2), pp. 157-164.

Impact of Sulphide minerals (pyrrhotite) in concrete aggregate on concrete behavior. (2018). *Workshop Proceedings No. 14, Nordic Workshop*, Oslo, Norway, pp. 180.

Jana, D. (2006). Sample Preparation Techniques in Petrographic Examinations of Construction Materials: A State-of-the-art Review. *Proceedings of the 28th Conference on Cement Microscopy*, ICMA, Denver, Colorado, pp. 23-70.

Jana, D. (2008a). Concrete Deterioration from Pyrite Staining, Sewer Gases, and Chimney Flue Gases - Case Studies Showing Microstructural Similarities. *Proceedings of the 30th Conference on Cement Microscopy*, ICMA, Reno, Nevada, pp. 1-23.

Jana, D. (2008b). DEF and ASR in Concrete - A Systematic Approach from Petrography. *Proceedings of the 30th Conference on Cement Microscopy*, ICMA, Reno, Nevada, pp. 1-17.

Jana, D. (2018a). Investigation of Presence of Pyrrhotite in a residential Concrete Foundation in Mansfield Center, Connecticut. Unpublished Research Report of Construction Materials Consultants, Inc. pp. 1-55.

Jana, D. (2018b). Investigation of Pyrrhotite Oxidation-Related Distress in a Residential Concrete Foundation in Ellington, Connecticut. Unpublished Research Report of Construction Materials Consultants, Inc. pp 66, pp. 1-86.

Jana, D. (2019a). Investigation of Possible Pyrrhotite-Related Deterioration in a Residential Concrete Foundation in Mansfield, Connecticut. Unpublished Research Report of Construction Materials Consultants, Inc. pp. 1-95.

Jana, D. (2019b). Laboratory Analyses of Concrete Cores from Birch Grove School, Tolland, Connecticut. Unpublished Research Report of Construction Materials Consultants, Inc. pp 66, pp. 1-239.

Jana, D. (2019c). Investigation of Possible Pyrrhotite-Related Deterioration in a Residential Concrete Foundation in Mansfield, Connecticut. Unpublished Research Report of Construction Materials Consultants, Inc. pp. 1- 66.

Jana, D. (2020). Pyrrhotite Epidemic in Eastern Connecticut: Diagnosis and Prevention. *ACI Materials Journal*, Vol 117, No. 1, 1-20.

Jana, D. (2022). Cracking of Residential Concrete Foundations in Eastern Connecticut, USA From Oxidation of Pyrrhotite. *Case Studies in Construction Materials*, Elsevier, Vol 16, pp. 1-18.

Janzen, M. P., Nicholson, R. V. and Scharer, J. M. (2000). Pyrrhotite reaction kinetics: reaction rates for oxidation by oxygen, ferric iron, and for nonoxidative dissolution. *Geochim et Cosmochim Acta.* Vol. 64: pp. 1511-1522.

Jeffrey, M. L. (2020). New USGS map helps identify where pyrrhotite, a mineral that can cause concrete foundations to fail, may occur. *United States Geological Survey*, https://www.usgs.gov/news/new-usgs-map-helps-identify-where-pyrrhotite-a-mineral-can-cause-concrete-foundations-fail-may

Jensen, V. (2018). Total S and Pyrrhotite in Norwegian concrete aggregate deposits Statistical assessment from NBTLs database over projects. Workshop *Impact of sulphide minerals (pyrrhotite) in concrete aggregate on concrete behavior*. 15th – 16th November, Oslo Norway.

Johnson, R. H., Blowes, D. W., Robertson, W. D. and Jambor, J. L. (2000). The hydrogeochemistry of the Nickel Rim mine tailings impoundment, Sudbury, Ontario. *Journal of Contaminant Hydrology* Vol. 41(1-2): pp. 49-80.

Johansen, V. and Thaulow, N. (1999). Heat Curing and Late Formation of Ettringite. In *Ettringite: The Sometimes Host of Destruction*, Bernard Erlin (ed), ACI SP-177, pp. 47-64.

Jones, C. F., Lecount, S., Smart, R. and White, T. (1992). Compositional and structural alteration of pyrrhotite surfaces in solution: XPS and XRD studies. *Appl. Surf. Sci*., Vol. 55, pp. 65–85.

Legrand, D. L., Bancroft, G. M. and Nesbitt, H. W. (2005). Oxidation/alteration of pentlandite and pyrrhotite surfaces at pH 9.3: Part I - assignment of XPS spectra and chemical trends. *Am. Mineral*., 90, pp. 1042–1054.

Lorenzen, L. (1995). Some guidelines to the design of a diagnostic leaching experiment. *Miner Eng* Vol. 8 (3): pp. 247-256.

Mahanta, P. L., Singh, A. K., Radhamani, R. and Prasad Rao, D. (2017). Determination of total sulfur and sulfate sulfur in geological materials of rocks, soils, and sediments by ICP-OES after sample digestion using alkali flux. *Atomic Spectroscopy*, Vol. 38 No. 4, pp. 99-105.

Marcelino, A., Calixto, J. M., Gumieri, A. G., Ferreira, M. C., Caldeira, C., Silva, M.V. and Costa, A. L. (2016). Evaluation of pyrite and pyrrhotite in concretes. *Rev Ibracon Estrut Mater* Vol. 9: pp. 484-493.

Marcelino, A. P., Calixto, J. M., Gumieri, A., Caldeira, C. L. and Ferreira, M. C. (2019). Long-term behavior of mortars produced with sulfide-bearing aggregates. *Revista Matéria*, Vol. 24, No. 4.

Marcelino, A. P., Calixto, J. M., Gumieri, A., Caldeira, C. L., Delbern, I. D. and Ferreira, M. C. (2020). A feasible evaluation protocol to determine the most reactive sulfide-bearing aggregate for use in concrete. *Construction and Building Materials*, Vol. 242, No. 10 pp. 1-8.

Mauk, J. L., Crafford, T. C., Horton, J. D., San Juan, C. A. and Robinson Jr., G. R. (2020). Pyrrhotite distribution in the conterminous United States, 2020. *U.S. Geological Survey Fact Sheet* 2020-3017.

Mehta, P. K. (1973). Mechanism of expansion associated with ettringite formation. *Cement and Concrete Research*, Vol. 3: pp. 1-6.

Mehta, P. K. (1992). Sulfate Attack on Concrete – A Critical Review. In, *Materials Science of Concrete*, III, J. Skalny, ed., American Ceramic Society, pp. 105-130.

Midgley, H. G. (1958). The Staining of Concrete by Pyrite. *Mag. Concrete Research*, Vol. 10: pp. 75-78.

Mielenz, R. C. (1963). Reactions of Aggregates Involving Solubility, Oxidation, Sulfates, or Sulfides. *Highway Research Record*, No. 43, pp. 8-18.

Mielenz, R. C., Marusin, S. L., Hime, W. G. and Jugovic, Z. T. (1995). Investigation of Prestressed Concrete Railway Tie Distress. *Concrete International*, V17, No. 12, December, pp. 62-68.

Moum, J. and Rosenqvist, I. Th. (1959). Sulfate Attack on Concrete in the Oslo Region. *Journal of the American Concrete Institute*. Vol. 56, No. 18, pp. 257-264.

Multani, R. S. and Waters, K. E. (2018). A Review of the physicochemical properties and flotation of pyrrhotite superstructures (4C - Fe_7S_8 / 5C - Fe_9S_{10}) in Ni-Cu Sulphide Mineral Processing. *Can J Chem Eng*. Vol. 96 (5): pp. 1185-1206.

Mycroft, J. R., Nesbitt, H. W. and Pratt, A. R. (1995). X-ray photoelectron and Auger electron spectroscopy of air-oxidized pyrrhotite: Distribution of oxidized species with depth. *Geochimica et Cosmochimica Acta*., Vol. 59, pp. 721–733.

Nagashima, S., Yoshida, M. and Ozawa, T. (1972). The determination of sulfide- and sulfate-sulfur in igneous rocks with tin(II)-strong phosphoric acid and strong phosphoric acid. *Bulletin of the Chemical Society of Japan*, Vol. 45, No. 11, pp. 3446-3451.

Nicholson, R. V. and Scharer, J. M. (1994). Laboratory studies of pyrrhotite oxidation kinetics. in Environmental Geochemistry of Sulfide Oxidation. *ACS Symposium Series*, Vol. 550: pp. 14-30

Oberholster, R. E. and Krüger, J. E. (1984). Investigation of alkali-reactive, sulphide-bearing and by-products aggregates. *Bull. Int. Assoc. Eng. Geol*. Vol. 3, pp. 273–277.

Oberholster, R. E., Du Toit, P. and Pretonius, J. L. (1984). Deterioration of concrete containing a carbonaceous sulphide-bearing aggregate. International Cement Microscopy Association (ICMA) (Ed.) *Sixth International Conference on Cement Microscopy*, Albuquerque, New Mexico, USA.

O'Neill, S. J. (2018). Pyrrhotite Contaminated Concrete – A call for collaboration. *AIA Western Massachusetts Newsletter*, pp. 11-14.

Oliveira, I., Chinchón-Paya, S., Aguado, A. and Chinchón, S. (2011). Pyrrhotite oxidation kinetics: host rock influence and the effect of aggregate size on a concrete dam. *XIII ICCC - International Congress on Chemistry of Cement*, Madrid, Spain, ISBN: 84-7292-399-7.

Oliveira, I., Cavalaro, S. H. P. and Arguado, A. (2014). Evolution of Pyrrhotite Oxidation in Aggregates for Concrete. *Materiales De Construccion*. 038, Vol. 64, pp. 316.

Penner, E., Eden, W. J. and Grattan-Bellew, W. J. (1972). Expansion of Pyritic Shales. NRC Publication archive, *Canadian Building Digest*, CBD, Vol. 152.

Pratt, A. R., Muir, I. J. and Nesbitt, H. W. (1994). X-ray photoelectron and Auger electron spectroscopic studies of pyrrhotite and mechanism of air oxidation. *Geochimica et Cosmochimica Acta*., Vol. 58, 827–841.

Powers, L. J. and Shrimer, F. H. (2007). Quantification of ASR in Concrete: An Introduction to the Damage-Rating Index Method. Presented at *International Cement Microscopy Association meeting*, Montréal, QC.

Quigley, R. M. and Vogan, R. W. (1970). Black Shale Heaving at Ottawa, Canada. *Canadian Geotechnical Journal*, Vol. 7(2), pp. 106-112.

Ramos, V., Rodrigues, A., Fournier, B. and Duchesne, J. (2015). Development of a quick screening staining test for detecting the oxidation potential of iron sulfide-bearing aggregates for use in concrete. *Cement and Concrete Research*, Vol 81, PP. 49-58.

Rimstidt, J. D. and Vaughan, D. J. (2003). Pyrite Oxidation: A state-of-the-art assessment of the reaction mechanism. *Geochimica et Cosmochimica Acta.*, Vol. 67, No. 5, pp. 873-880.

Rivard, P., Fournier, B. and Ballivy, G. (2002). The Damage Rating Index Method for ASR Affected Concrete – A Critical Review of Petrographic Features of Deterioration and Evaluation Criteria. *Cement, Concrete and Aggregates*, ASTM, Vol 24 – pp. 81-91.

Rodrigues, A., Duchesne, J. and Fournier, B. (2012a). Mineralogical and chemical assessment of concrete damaged by the oxidation of sulfide-bearing aggregates: Importance of thaumasite formation on reaction mechanisms. *Cement and Concrete Research*, Vol. 42, pp. 1336-47.

Rodrigues, A., Duchesne, J. and Fournier, B. (2012b). Microscopic Analysis of The Iron Sulfide Oxidation Products Used in Concrete Aggregates. *Proceedings of 34th International Conference on Cement Microscopy*, International Cement Microscopy Association. pp 317-335.

Rodrigues, A., Fournier, B. and Duchesne, J. (2013). Petrographic characterization of the deterioration products of a concrete containing sulfide bearing aggregates; A particular case of internal sulfate attack. *Proceedings of 35th International Conference on Cement Microscopy*, International Cement Microscopy Association. pp 317-335.

Rodrigues, A., Fournier, B. and Duchesne, J. (2014). Damage Evaluation of Two Different Concrete Mix Designs Containing Sulfide-Bearing Aggregates. *Proceedings of 36th International Conference on Cement Microscopy*, International Cement Microscopy Association. pp 317-335.

Rodrigues, A., Duchesne, J. and Fournier, B. (2015). A new accelerated mortar bar test to assess the potential deleterious effect of sulfide-bearing aggregate in concrete. *Cement and Concrete Research*, Vol. 73, pp. 96-110.

Rodrigues, A., Duchesne, J. and Fournier, B. (2016a). Quantitative Assessment of the Oxidation Potential of Sulfide-Bearing Aggregates in Concrete Using an Oxygen Consumption Test. *Cement and Concrete Composites*, Vol. 67, pp. 93-100.

Rodrigues, A., Duchesne, J., Fournier, B., Durand, B., Shehata, M. H. and Rivard, P. (2016b). Evaluation Protocol for Concrete Aggregates Containing Iron Sulfide Minerals. *ACI Materials Journal*, Vol. 113, pp. 349-359.

Royal Institution of Chartered Surveyors (RICS). (2016). The Mundic Problem. *RICS guidance note*, UK, 3rd Edition.

Saengsoy, W., Yongchaitrakul, L., Sinlapasertsakulwong, P. and Tangtermirikul, S. (2020). Identification of iron sulfide minerals in aggregate by accelerated mortar bar test. Bridge Maintenance, Safety, Management, Life-Cycle Sustainability and Innovations, *Proceedings of the Tenth International Conference on Bridge Maintenance, Safety and Management* (IABMAS 2020), June 28-July 2, Sapporo, Japan, by Hiroshi Yokota and Dan M. Frangopol.

Schmidt, T., Leemann, A., Gallucci, E. and Scrivener, K. L. (2009). Microstructural investigations of iron sulfide degradation in concrete. *Int. Baustofftagung (IBAUSIL),* Weimar, Germany, pp. 23–26.

Schmidt, T., Leemann, A., Gallucci, E. and Scrivener, K. (2011). Physical and microstructural aspects of iron sulfide degradation in concrete. *Cement and Concrete Research*, pp. 263-269.

Seaton, S. G. (1948). Study of Causes and Prevention of Staining and Pop-Outs in Cinder Concrete. *Amer. Cone. Inst*. Proc., 44: pp. 361-380.

Shayan, A. (1988). Deterioration of a Concrete Surface Due to the Oxidation of Pyrite Contained in Pyritic Aggregate. *Cement and Concrete Research*, Vol. 18, No. 5, pp. 723-730.

Shrimer, F. (2006). Development of the Damage Rating Index Method as a Tool in the Assessment of Alkali-Aggregate Reaction in Concrete: A Critical Review. *Proceedings, Marc-André Bérubé Symposium on Alkali-Aggregate Reactivity in Concrete*, Montréal, Canada, pp. 391 – 412.

Steger, H. F. (1982). Oxidation of sulphide minerals VII. Effect, of temperature and relative humidity on the oxidation of pyrrhotite. *Chem. Geol*. 35 pp. 281–295.

Tagnit-Hamou, A., Saric-Coric, M. and Rivard, P. (2005). Internal Deterioration of Concrete by Oxidation of Pyrrhotitic Aggregates. *Cement and Concrete Research*, Vol. 35, pp. 99-107.

Vlisidis, A. C. (1966). The determination of sulfate and sulfide sulfur in rocks or minerals. *Contributions to Geochemistry, Geological Survey Bulletin 1214-D*, United States Department of the Interior, Geological Survey, pp. D1-D5.

Wille, K. and Zhong, R. (2016). *Investigating the Deterioration of Basement Walls Made of Concrete in Connecticut, Storrs, Connecticut.* University of Connecticut, pp 84.

Zhong, R. and Wille, K. (2018). Deterioration of residential concrete foundations: The role of pyrrhotite-bearing aggregate. *Cement and Concrete Composites*, Vol. 94, pp. 53-61.

Michael L.J. Maher

Editor

Pyrite and Pyrrhotite

Managing the Risks in Construction Materials and New Applications

nova science publishers

www.novapublishers.com

ISBN-13: 979-8-88697-395-2

9 798886 973952